8-31-2021

Rhyolite Stratigraphy Along Succor Creek: Insights into the Eruptive History of the Three Fingers and Mahogany Mountain Volcanic Field

Cassandra Caryl Black
Portland State University

Rhyolite Stratigraphy Along Succor Creek: Insights into the Eruptive History of the Three Fingers and Mahogany Mountain Volcanic Field

by

Cassandra Caryl Black

A thesis submitted in partial fulfillment of the
requirements for the degree of

Master of Science
in
Geology

Thesis Committee:
Dr. Martin Streck, Chair
Dr. Ashley Streig
Dr. John Bershaw

Portland State University
2021

Abstract

The Mahogany Mountain and Three Fingers calderas with their associated tuffs, the tuff of Leslie Gulch and tuff of Spring Creek, respectively, were the centerpiece of a larger rhyolite center that developed in response to Columbia River Basalt volcanism as numerous other mid Miocene rhyolite centers in a corridor from Baker City in the north to northern Nevada. Previous studies suggest a two caldera model, while others advocated for a single large caldera producing solely the tuff of Leslie Gulch. This study refines the eruptive stratigraphy along the northeastern margin of this rhyolite field with important implications for the entire field. Several distinct rhyolitic units are identifiable, these are (from oldest to youngest) the tuff of Leslie Gulch, the Old McIntyre rhyolite, the newly named tuff of Succor Creek, the Young McIntyre rhyolite, and a sequence of thin, non-welded ignimbrites. In addition, intermediate to mafic lavas under- and overlie rhyolites. Stratigraphy in this study area indicates the tuff of Leslie Gulch varies texturally throughout and has an eruptive history that includes multiple phases, with a new $^{40}Ar/^{39}Ar$ age of 15.98±0.05 Ma. This study also uses geochemical and stratigraphic data to distinguish between the Old and Young McIntyre Rhyolite units, providing two new ages for the Old McIntyre, 16.02±0.02 and 15.95±0.03 Ma. A newly named unit, the tuff and rhyolite of Succor Creek have also been described by this study and based on work by Marcy (2013), has an age of 15.74±0.09 Ma. High precision yet overlapping ages and stratigraphic field relationships highlight the explosive history of a 250 ky lasting, prolific explosive silicic rhyolite field.

Acknowledgments

Thank you to my advisor, Martin Streck, for his patience and guidance during my time at Portland State. Martin's advice and vast knowledge helped guide me through graduate school and complete this project. A big thank you to my committee, Dr. Ashley Streig and Dr. John Bershaw for their time, insight, and thoughtful thesis reviews. I thank my wonderful field assistants, Tia Untalan and Michael Biedebach for taking time out of their summers to join me in the hot, Oregon desert. I will forever be grateful for their positivity and efforts in the field. Thank you to Drs. Jon and Linda Fink and the Scion Natural Science Association for providing field work funding assistance. I thank my graduate student cohort for their continued moral support and reassurance. Thank you to the 'Hard rock Group' for their support, suggestions and advice. Lastly, I thank my parents and sister for always supporting and encouraging me in my endeavors, no matter how far from home my crazy ideas might take me.

Table of Contents

List of Tables

List of Figures

1. Introduction

Contemporaneous silicic and basaltic volcanism has played a major role in the volcanic formations of eastern Oregon seen in the field today. The flood basalt lavas of Columbia River Basalt Group began erupting approximately 17 Ma from fissures in eastern and southeastern Oregon, later northeastern Oregon, and finally from fissures in southeastern Washington (Camp *et al.*, 2017). Silicic volcanism also occurred throughout eastern Oregon during the mid-Miocene, and along with flood basalts are often associated with the impingement of the Yellowstone hotspot (Coble and Mahood, 2012).

The Mahogany Mountain and Three Fingers caldera of southeastern Oregon have been known as the source for the tuff of Leslie Gulch (LGT) and tuff of Spring Creek (Vander Meulen, 1989), respectively have been the center of debate for over 20 years. Benson and Mahood (2016) describe the two units as one single ignimbrite erupting at 15.8 Ma and noted that alteration resulted in different mineral compositions leading to seemingly different units. They describe the contacts between the units as gradational as the alteration changes. Consequently, Benson and Mahood (2016) also suggest the existence of only one caldera eruptive center, the Rooster Comb caldera, which encompasses both the Three Fingers caldera and Mahogany Mountain caldera. Others (Marcy *et al.*, 2013, Ferns *et al.*, 2017) argue for two separate major explosive events based on age and compositional data, with the tuff of Spring Creek being younger.

This study focuses on the presumed northeastern margin of the Three Fingers caldera. This is an area where both tuffs appear to be exposed as well as other pre- to

post-caldera rhyolite lavas (Vander Meulen map reference, Benson & Mahood, 2016; Ferns et al., 2017). This study seeks to clarify which units are exposed and their stratigraphic relationships to each other. Field mapping, detailed stratigraphy of selected sections in combination with analytical data provide the necessary information to refine the eruptive stratigraphy along the eastern margin of this rhyolite field with important implications for the entire Mahogany Mountain – Three Fingers rhyolite field.

The McDermitt caldera, located only 62 miles southwest of the study location, is currently thought of as the starting point of the Yellowstone hotspot (Henry et al., 2017). This caldera experienced mid-Miocene silicic volcanism, like what is seen at the project location. Due to the proximity of the Three Fingers – Mahogany Mountain rhyolite field to McDermitt caldera, this study also provides further insight into the history of the Yellowstone hotspot, particularly its early history where rhyolite volcanism coincided with eruptions of the Columbia River flood basalts.

2. Background

2.1 Geologic Setting

Volcanism in the greater area of the Mahogany –Three Finger rhyolite field occurred in three main stages as described by Camp *et al.* (2003). First from Oligocene to early Miocene calc-alkaline lavas and pyroclastic flows were emplaced. The second stage consisted of the eruption of tholeiitic lavas of the Columbia River Basalt. The final stage, from mid-Miocene to Holocene, saw more calc-alkaline lavas, pyroclastic flows, and some felsic extrusions (Camp *et al.,* 2003). The Columbia River Basalt Group (CRBG) was the result of large volume tholeiitic lavas, erupting from dike swarms, lasting over short time periods (Figure 1). Due to the geologically young age of the basalts and no subsequent rifting, the CRBG is the best-preserved flood basalt province in the world (Hooper *et al.,* 2002). There are many different suggestions as to how this volcanism occurred. Some explanations are lithospheric extension, backarc spreading, and a rising mantle plume (Hooper *et al.,* 2002).

The oldest basalt in the CRBG, located in southeastern Oregon, is the Steens Basalt, which erupted between 16.9-16.6 Ma (Barry *et al.,* 2013) and is associated with three main mid-Miocene rhyolite volcanic centers in the La Grande – Owyhee eruptive axis (Figure 1). These centers are the Lake Owyhee volcanic field (LOVF), the McDermitt volcanic field, and High Rock caldera. The volcanic field of most importance to this project is the LOVF, located in the southeastern region of the eruptive axis. Ferns and McClaughry (2013) describe the LOVF as being the second stage in the development

of the La Grande-Owyhee eruptive axis. Between 15.8-14.6 Ma, basaltic activity was occurring in the northern region of the eruptive axis, while contemporaneous ash-flow tuffs and rhyolites were erupting in the LOVF. These rhyolites ranged from Dooley Mountains to 300km south at McDermitt volcanic field.

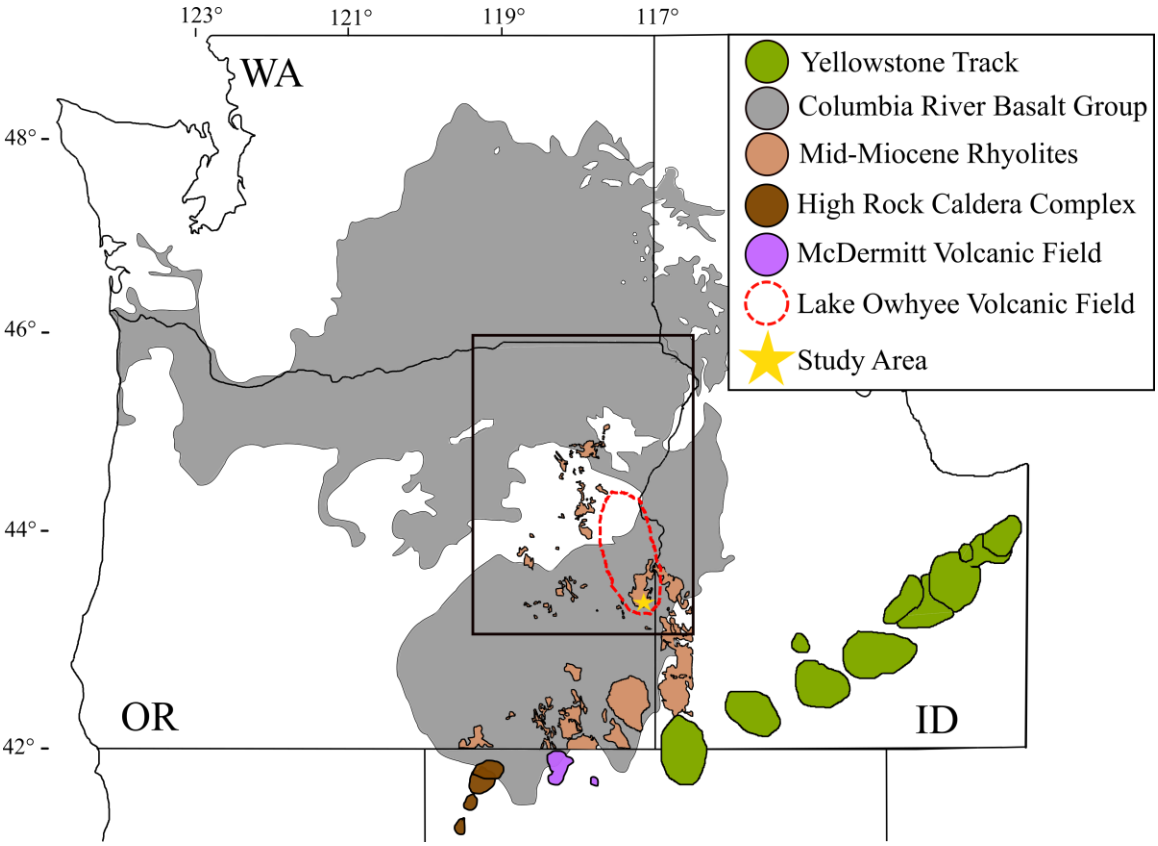

Figure 1. Extent of the volcanism in Oregon. Columbia River Basalt Group in gray (from Reidel et al., 2013), mid-Miocene silicic volcanism in orange (from Webb et al., 2018), and Yellowstone hotspot trend in green (Coble and Mahood, 2012). High Rock Caldera Complex shown in brown, McDermitt Volcanic Field in purple, Lake Owyhee Volcanic Field in dashed red line. Study area location indicated by yellow star. Black box shows area of figure 2.

2.2 Tectonic Setting

Along with volcanism, the tectonics of this region were evolving. Three large north- trending grabens exist in the Lake Owyhee eruptive axes (LOEA), which are the La Grande, Baker, and the Oregon-Idaho graben (OIG) (Figure 2). The La Grande and Baker grabens are located in the northern region of the LOEA, while the OIG is in the southern region (Ferns *et al.,* 2017). Geologic mapping revealed the OIG in the late 1980s to early 1990s. The graben began subsiding after tholeiitic basalt eruptions which were part of the CRBGs approximately 15.5 Ma (Cummings *et al.,* 2000). Formation of the OIG occurred in three stages which resulted in the 50 to 60 km wide by 100 km long graben. The first stage of graben formation occurred from 15.3 to 14.3 Ma and is associated with mid-Miocene rhyolite volcanism. Cummings *et al.,* 2000 describe the intra-graben caldera forming eruptions of the tuff of Leslie Gulch and tuff of Spring Creek as being two eruptions responsible for subsidence during this stage. The graben continued to subside until approximately 11 Ma, indicated by stratigraphic and structural relationships within the OIG (Cummings *et al.,* 2000).

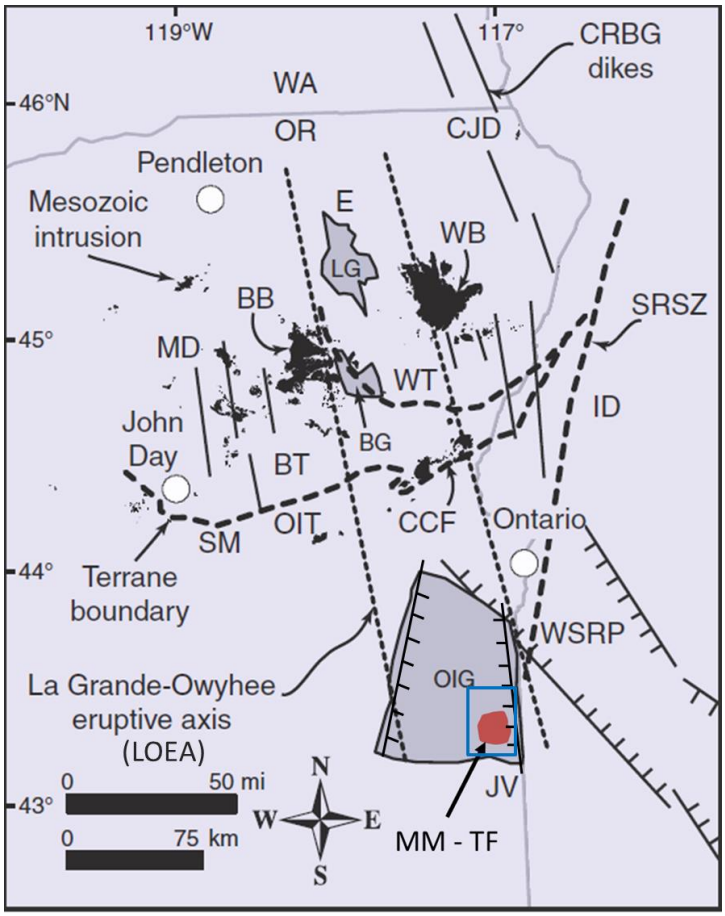

Figure 2. Paleozoic-Mesozoic terrane in eastern Oregon. Black color indicates Mesozoic intrusions. WA – Washington; OR – Oregon; ID – Idaho; LOEA – Lake Owyhee Eruptive Axis; LG – La Grande graben; BG – Baker graben; OIG – Oregon-Idaho graben; MM-TF – Mahogany Mountain and Three Fingers Calderas; SM – Strawberry Mountain; MD – Monument dike swarm; CJD – Chief Joseph dike swarm; CRBG – Columbia River Basalt Group; OIT – Olds Ferry-Izee terrane; BT – Baker terrane; WT – Wallowa terrane; CCF – Connor Creek fault; SRSZ – Salmon River suture zone; BB – Bald Mountain Batholith; WB – Wallowa Batholith; WSRP – Western Snake River Plain. Blue rectangle indicates area of figure 3. Caption and figure modified from Ferns et al., 2013.

2.3 Previous Work in the Mahogany Mountain – Three Fingers Rhyolite Field

Currently a number of geologists have opposing views regarding the source of the tuff of Spring Creek and the tuff of Leslie Gulch. On one side of the controversy is Benson and Mahood (2016) who describe the tuffs as a single eruptive unit, the tuff of Leslie Gulch, and the reasoning for different appearances is the result of secondary alteration. Benson and Mahood (2016) made their conclusions based on work completed within Leslie Gulch. Evidence to support their study consists of physical, stratigraphic, alteration assemblages, and $^{40}Ar/^{39}Ar$ dates. The authors maintain the three different facies described by Vander Meulen (1989) for the tuff of Leslie Gulch, as being an intra-caldera ignimbrite, a crystal poor ash-fall tuff, and outflow sheets. As for the description of the tuff of Spring Creek, Benson and Mahood (2016) do not agree with Vander Meulen (1989), suggesting that instead of being an intra-caldera member, it is a post caldera rhyolitic unit that has interacted with lake sediments.

The contact between the two units is described as gradational, with the tuff of Spring Creek being above the tuff of Leslie Gulch. Mineral assemblages of the tuff of Leslie Gulch are sanidine phenocrysts and glass altered to an assemblage of albite + quartz + minor phyllosilicate, compared to the tuff of Spring Creek groundmass that is composed of clinoptilolite + mordenite + minor smectite. The green color of the tuff of Spring Creek is attributed to the clinoptilolite. Benson and Mahood (2016) plotted trace element data of intra-caldera samples of each tuff, which shows some overlap. Finally, Ar-Ar age dates of sanidine phenocrysts from outflow and intra-caldera samples were obtained. The Leslie Gulch outflow tuff yielded an age of 15.84±0.05 Ma, while Spring

Creek ignimbrite yielded ages of 15.75±0.05 Ma and 15.83±0.05 Ma. From these analyses, Benson and Mahood concluded that the tuff of Leslie Gulch and tuff of Spring Creek are one large eruptive unit, and propose calling this unit the Tuff of Leslie Gulch. They also suggest that this ignimbrite did not erupt from the Mahogany Mountain caldera, but from a larger caldera which they give the name Rooster Comb Caldera (Figure 5). Benson and Mahood (2016) suggest that the eruptive history began with the McIntyre rhyolite, followed by the tuff of Leslie Gulch, and ending with the Three Finger rhyolite and some other units not discussed in this paper (Figure 3).

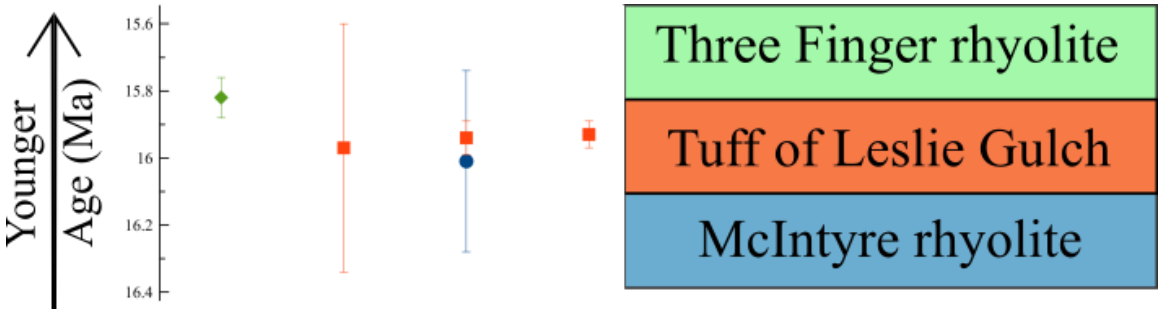

Figure 3. Generalized schematic stratigraphic section with Benson and Mahood (2016) age data and stratigraphic interpretations of eruptive units in study area.

Other researchers, such as (Vander Meulen, 1989; Marcy 2013; Ferns *et al.*, 2017,) suggest that the tuff of Spring Creek and tuff of Leslie Gulch are two eruptive units. Vander Meulen (1989) describes the tuff of Leslie Gulch as explained above. Their explanation of the tuff of Spring Creek is that it is an ash-flow tuff which erupted from the Three Fingers caldera and is younger than the tuff of Leslie Gulch. Ar-Ar age dating was conducted by (Marcy, 2013) and yielded an age of 15.74±0.09 Ma (corrected for FCT of 18.20 Ma) for the Spring Creek outflow facies at Succor Creek, which is approximately 0.11 to 0.19 Ma younger than the ages from Benson and Mahood (2016). This ash-flow tuff was thought to occur in the Mahogany Mountain caldera as well. At

the base of the unit, a light green color is observed with feldspar and quartz phenocrysts. Above this is a layer of lighter green tuff which contains lithic and pumice fragments. Vander Meulen (1989) describes the eruptive history of the Mahogany Mountain – Three Fingers rhyolite field as beginning with pre-caldera lavas. No unit names or ages are given. This is then followed by the tuff of Leslie Gulch and the tuff of Spring Creek. Finally, some post caldera intrusions and lavas complete the eruptive sequence (Figure 4).

Figure 4. Generalized schematic stratigraphic section with Vander Meulen (1989) stratigraphic interpretations of eruptive units in study area.

These differing interpretations of the units and eruptive histories motivated this project. I focused on the northeastern extent of the Three Fingers Caldera, where both tuff of Leslie Gulch and tuff of Spring Creek have been known to crop out (Figure 5).

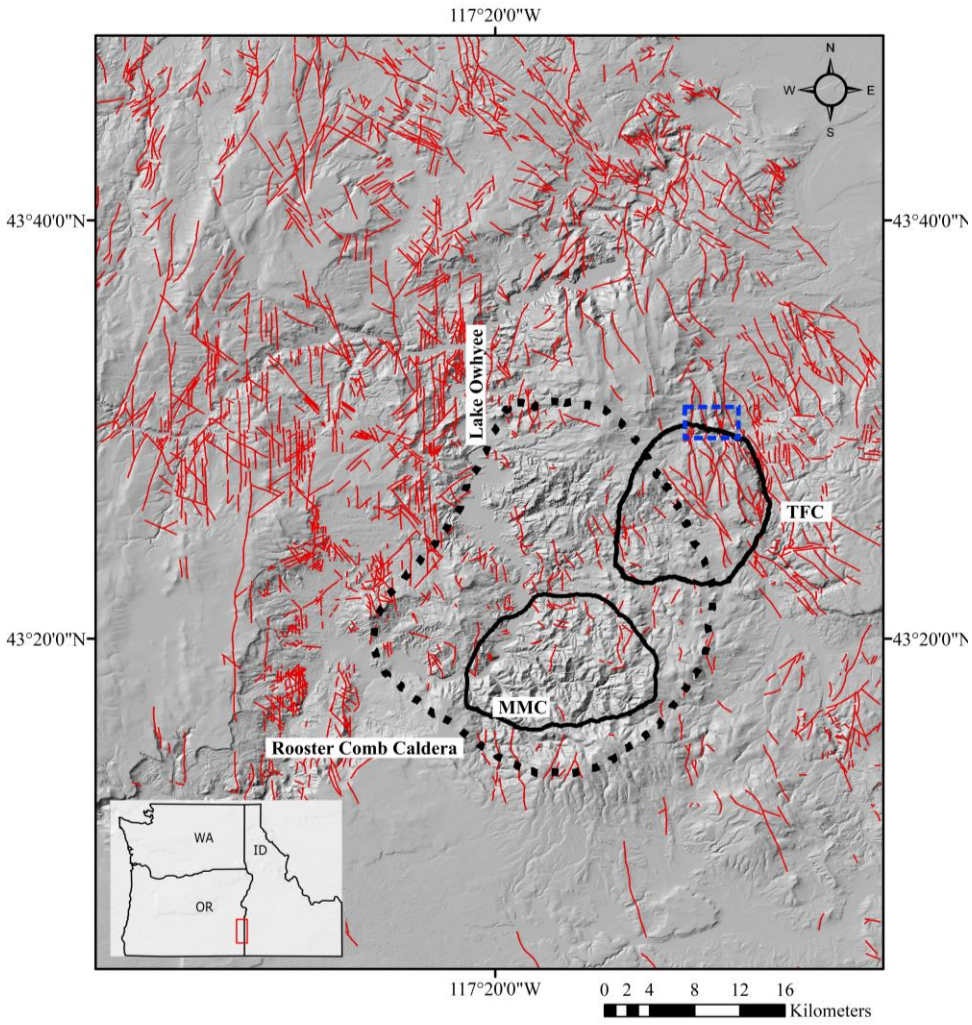

Figure 5. Location map detailing the Mahogany Mountain - Three Fingers Caldera volcanic field, with the Rooster Comb Caldera outlined by dotted line after Benson and Mahood (2016). Solid line for Mahogany Mountain Caldera (MMC) and Three Fingers Caldera (TFC), after Rytuba et al. (1991). Blue dashed box is location of study area, and is the area of figure 17. Red lines show faults in the area, showing an overall N-S trend throughout, fault data from DOGAMI, Oregon Geologic Data Compilation release 6 (ODGC-6). Inset map shows location of study area in Oregon.

3. Methods

3.1 Field Methods and Sample Selection

Fieldwork involved mapping on 1:24,000 scale quadrangles, identifying stratigraphic sections, and sample selection. While collecting samples in the field, stratigraphic relationships and descriptions were documented. Before selecting samples for analysis, the main stratigraphic sections were defined, based on their location in the study area. These sections were selected due to their thickness, sample quality and variability of sample, and distribution over the area selected. A total of nine key stratigraphic sections were selected in the study area (blue rectangle in Figure 5). Once selected, sections were logged for lithology and thickness. Samples were taken to cover lithological variation from bottom to top of each stratigraphic section. Samples were collected when differences in textures were observed, when there was an observable change in abundance of phenocrysts, lithic or other fragments, or other general changes in the outcrops In addition, all encountered rock units were sampled such as rhyolite lavas and mafic lavas in addition to samples from the stratigraphic sections.

3.2 Analytical Methods

Major and trace element compositions of 29 bulk samples were acquired using X-ray fluorescence (XRF) and inductively coupled mass spectrometry (ICP-MS) analyses. After crushing and selecting sample material, samples were sent to Washington State University to be further prepared and analyzed at the GeoAnalytical. Analytical precision

for ICP-MS data is 5% RSD for rare elements and 10% RSD for trace elements (Johnson et al., 1999). These data were used for determining the differences between units and the stratigraphic sections.

Petrographic thin sections were prepared for 14 samples by Spectrum Petrographic. The thin sections were analyzed using a petrographic microscope to determine difference in mineral assemblage, textures and abundance. Overview scans of each thin section were also taken. Three samples were analyzed with the scanning electron microscope (SEM) to determine feldspar compositions. Other SEM analyses was conducted on feldspar crystals mounted in an epoxy plug. This work was conducted at Portland State University. Precise microprobe analysis was completed on three thin sections, one from each main identified unit. This was completed to obtain information on the composition of pyroxene phenocrysts of critical units. Rock slabs of each sample within the stratigraphic sections as well as geochemically analyzed lavas were cut and polished for macroscopic descriptions of each units/ sample.

To obtain better constraints on eruption ages, three samples, two rhyolite lavas and one tuff, were used for age dating by the $^{40}Ar/^{39}Ar$ technique. This was conducted at Ar-Ar Geochronological Laboratory at Oregon State University. The methods as described by Jordan *et al., 2004* and Ford *et al., 2013* were followed for this process.

4. Results

4.1 Stratigraphy

A total of nine stratigraphic sections distributed from south to north across the study area were investigated by field work.

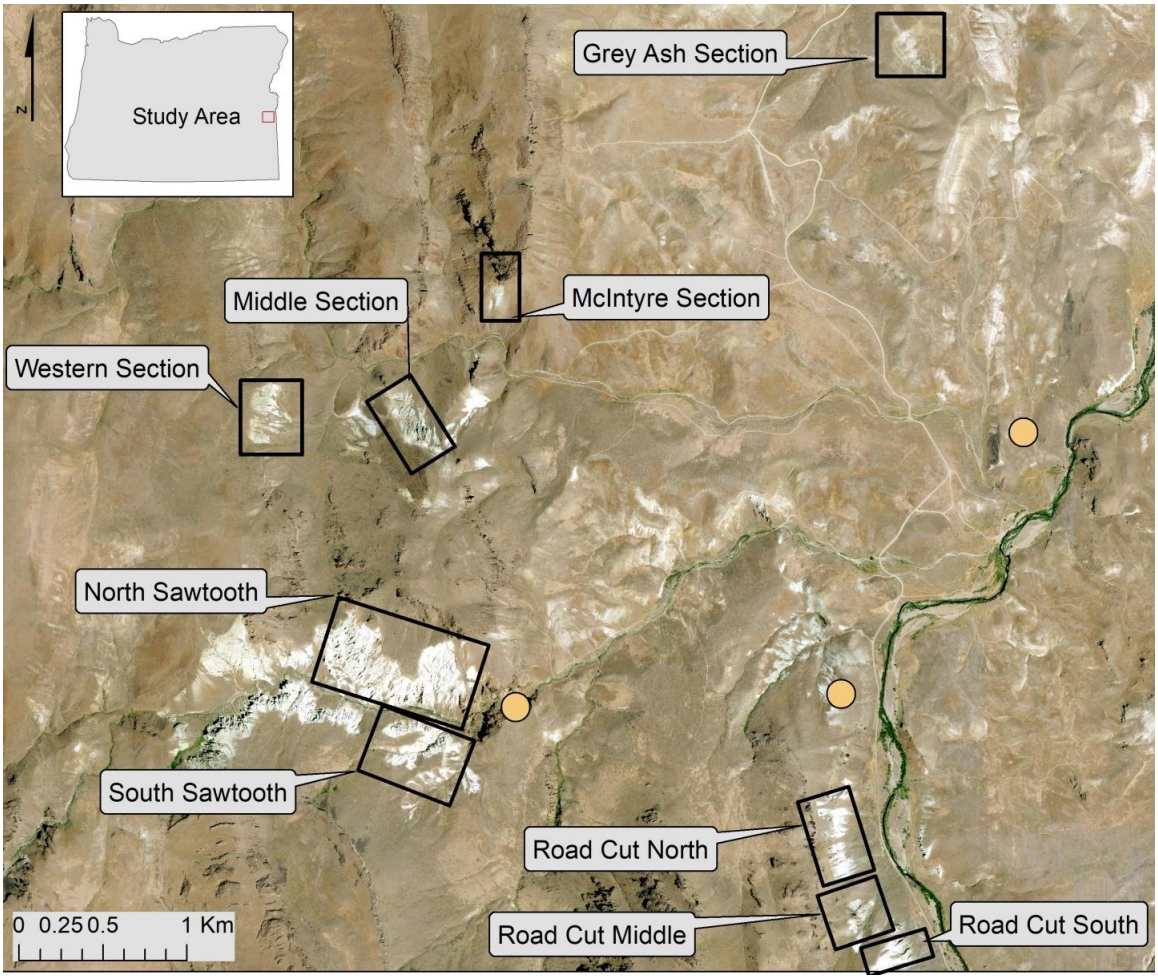

Figure 6. Locations of each stratigraphic section throughout the study area. Yellow circles indicate locations of rhyolite and tuff of Succor Creek rhyolite samples. Orthoimagery from 2017 Oregon Statewide Imagery Program. Inset map shows location of study area outlined in red.

4.1.1 Grey Ash Section

Named for the light grey colored ignimbrite, the Grey Ash section is the most northern stratigraphic section of the study area (Figure 6). This unit has been described as the Top Unwelded Ignimbrite. Of all nine sections, this is the thinnest section, with a total thickness of 3 m. A total of four unwelded ignimbrite samples make up this section. Figure 18 shows this section in the field, with samples CB-19-50 and CB-19-51 in the top half of the outcrop and samples CB-19-53 and CB-19-54 on the bottom.

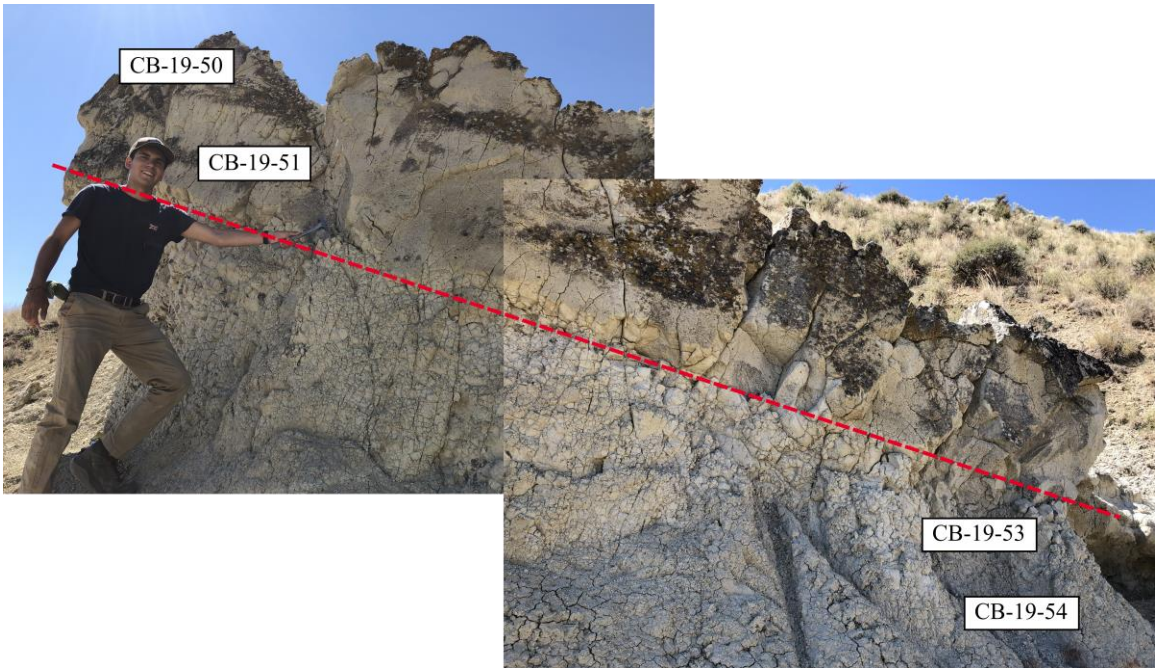

Figure 7. Field photo of the Grey Ash section. Above the red dashed line is where samples CB-19-50 and CB-19-51 are found. Below this line is where samples CB-19-53 and CB-19-54 are found. 1.75 m field assistant for scale. Photo looking south.

The top layer, sample CB-19-50, is a 0.25 m thick fine-grained ignimbrite (Figure 8). This sample has 2% abundance of pumices, crystals, and lithic fragments, around 2% for each. Pumice and lithic fragments are less than 3 mm in size, while phenocrysts are less than 1 mm. Below this top ignimbrite is sample CB-19-51, the coarsest grained ignimbrite. With a thickness of approximately 1 m, a sample of this unit has the highest

abundance of pumices, approximately 15% and ranging from an ash to coarse lapilli. Lithic fragments are coarse ash size, as well as phenocrysts. CB-19-53 is a 0.5 m thick, poorly sorted medium grained sample which has larger and more abundant lithic fragments than the previous samples, ranging from coarse ash to fine lapilli size. The base of the section is sample CB-19-54, with thickness of 0.5 m. This is a lithic rich tuff with poor sorting, as the lithic fragments range from a fine ash to coarse lapilli. Pumice pieces are ash to fine lapilli grain size.

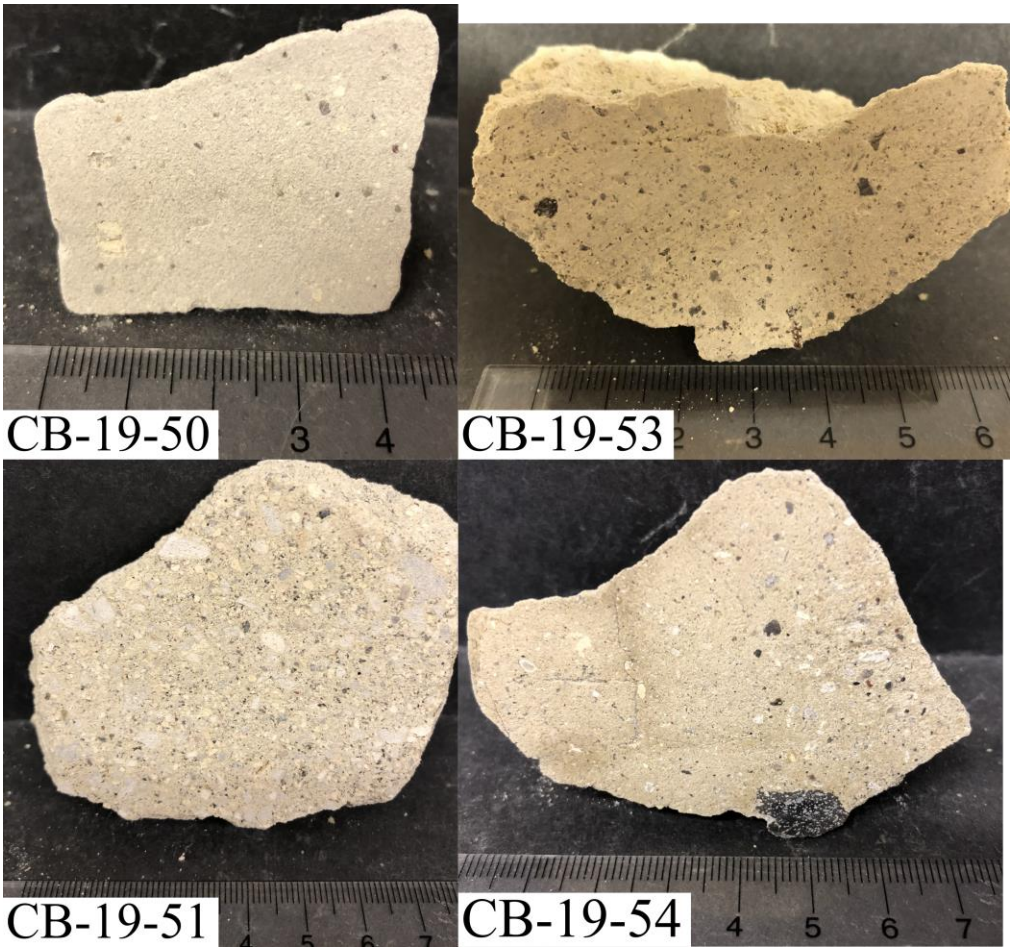

Figure 8. Cut hand samples of Grey Ash stratigraphic section. Sample CB-19-50 was collected from the top of the section and CB-19-54 was collected from the bottom.

4.1.2 McIntyre Section

The McIntyre Section is the second northern most section in the study area (Figure 6) and named for the direct exposure of McIntyre Rhyolite on top. The exposed part of this stratigraphic section that was sampled is approximately 30 m thick, which does not include the capping Old McIntyre Rhyolite unit (Figure 9). A total of six samples were collected from this section.

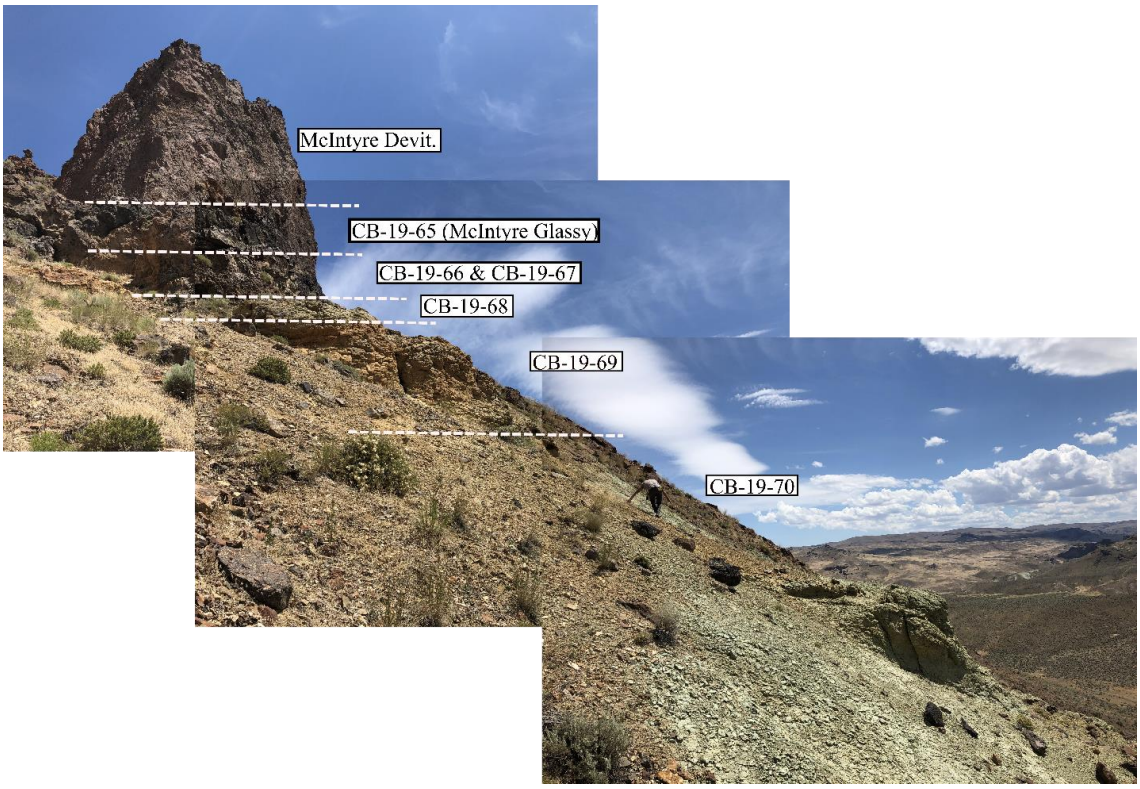

Figure 9. Field photo of the McIntyre Section and relative sample locations. Photo looking east.

Figure 11 shows a more detailed view of the hand samples. The base of the section is a 12 m thick, pumice poor ash layer, sample CB-19-70. Phenocryst content is approximately 2% with sizes of less than 1mm. Lithics in this sample were also small in size, less than 2mm, with a similar percentage as the phenocrysts. Pumices range in size

from 2 to 5 mm. Pumices and shards have similar light greenish color. Above this is sample was the 8m thick partially welded tuff, CB-19-69 which is described in the Lithology of Units section below. Next is sample CB-19-68, another partially welded ignimbrite, though more crystal poor than the layer below. Pumices in this sample are very slightly flattened (less than in the unit below, CB-19-69) and range in size from 1mm to 3cm. Sample CB-19-66 and sample CB-19-67 are both welded ignimbrites but are texturally strikingly different. Both are approximately 1.5 m thick. The size of dense glassy lithic fragments increases from 1 mm in CB-19-67 to up to 8 cm in CB-19-66. In other words, CB-19-67 is fined grained throughout, while CB-19-66 is poorly sorted with much coarser fragments (Figure 10). The size difference is also seen in the glass shards with CB-19-67 having smaller glass shards than CB-19-66. The top of the sampled section is the 3 m thick basal vitrophyre of the crystal poor Old McIntyre rhyolite; sample CB-19-65. The devitrified Old McIntyre Rhyolite caps the section.

Figure 10. Samples CB-19-66 and CB-19-67 in the field. The large glassy lithic fragments are within CB-19-66 while smaller glassy lithic fragments are found in CB-19-67.

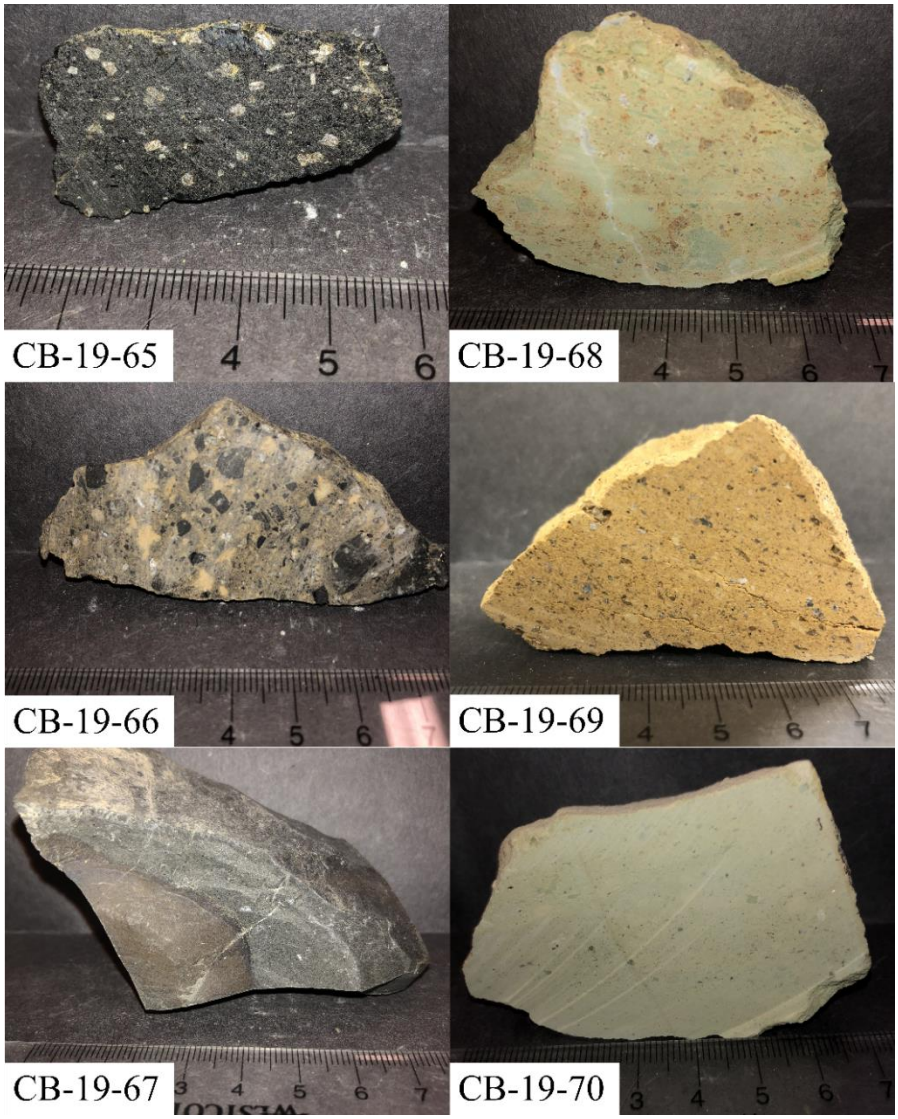

Figure 11. Cut hand samples of the McIntyre Section. CB-19-65 is a sample of Old McIntyre rhyolite, collected from the top of the section and CB-19-70 was collected from the bottom.

4.1.3 Middle Section

The Middle stratigraphic section is directly across a creek drainage from the McIntyre section (Figure 6). Figure 12 shows the 43 m thick section. Though the top of the section was not reached in the field, it appears that near the top, a welded ignimbrite similar to CB-19-69 (Figure 12) is present. This observation is based on the same distinct orange coloration and at same elevation as is observed in the McIntyre section. This is also observed in a small outcrop slightly east of this section. Four samples were collected at this section.

Figure 12. Field photo of Middle Stratigraphic section and relative sample locations. Photo looking south-southwest.

Hand samples cut into polished slabs can be seen in Figure 13. Sample CB-19-09 is found at the base of this section and is 3 m thick. This sample is lithic poor, with phenocrysts and pumices all in the fine to coarse ash size range. It is equally abundant in phenocrysts and pumices, about 3-5%. Above is 13 m thick sample CB-19-10, which has the same abundance and size of lithic fragments, though it does contain slightly larger pumices. These pumices are small lapilli sized, 4 mm. Stratigraphically above is CB-19-

11 which is a 3 m thick layer. Pumices in this sample are similar in size to CB-19-10, but now the lithic fragments are fine lapilli sized. Abundance of lithics is still low, 2%. Phenocryst size and abundance stays relatively the same throughout this unit. The top of this section is the 18 m thick CB-19-12. Once again, the lithic fragments become ash sized, and very low in abundance. Pumices are mainly lapilli size, and are the largest observed in this section with average maximum of about ~1.5cm. Also, phenocrysts slightly increase in abundance (~6%) and size (up to 5 mm) compared to the layers below.

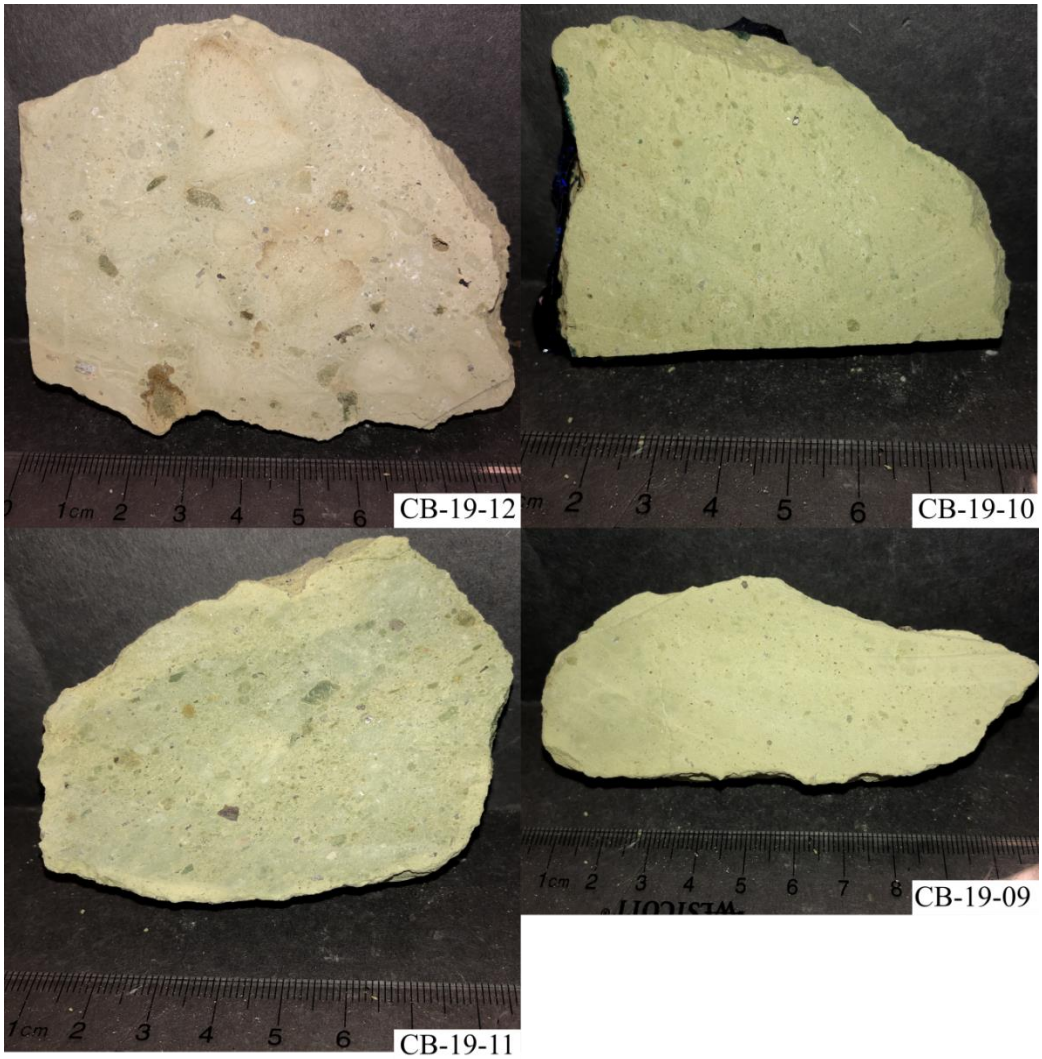

Figure 13. Cut hand samples of the Middle stratigraphic section. CB-19-12 was collected from the top of the section and CB-19-09 was collected from the bottom.

4.1.4 Western Section

The Western stratigraphic section is named for its location as the most western extent of the study area (Figure 6). A total of five samples were taken to represent lithological variations throughout this 38 m thick section (Figure 14). Above and to the right (north) of the section are the basaltic trachyandesitic columnar jointed lavas, and to the left (SSW) of the section is Old McIntyre Rhyolite. These columnar joints appear to be offset, with the portion to the north of the western section being displaced along a fault (Figure 15).

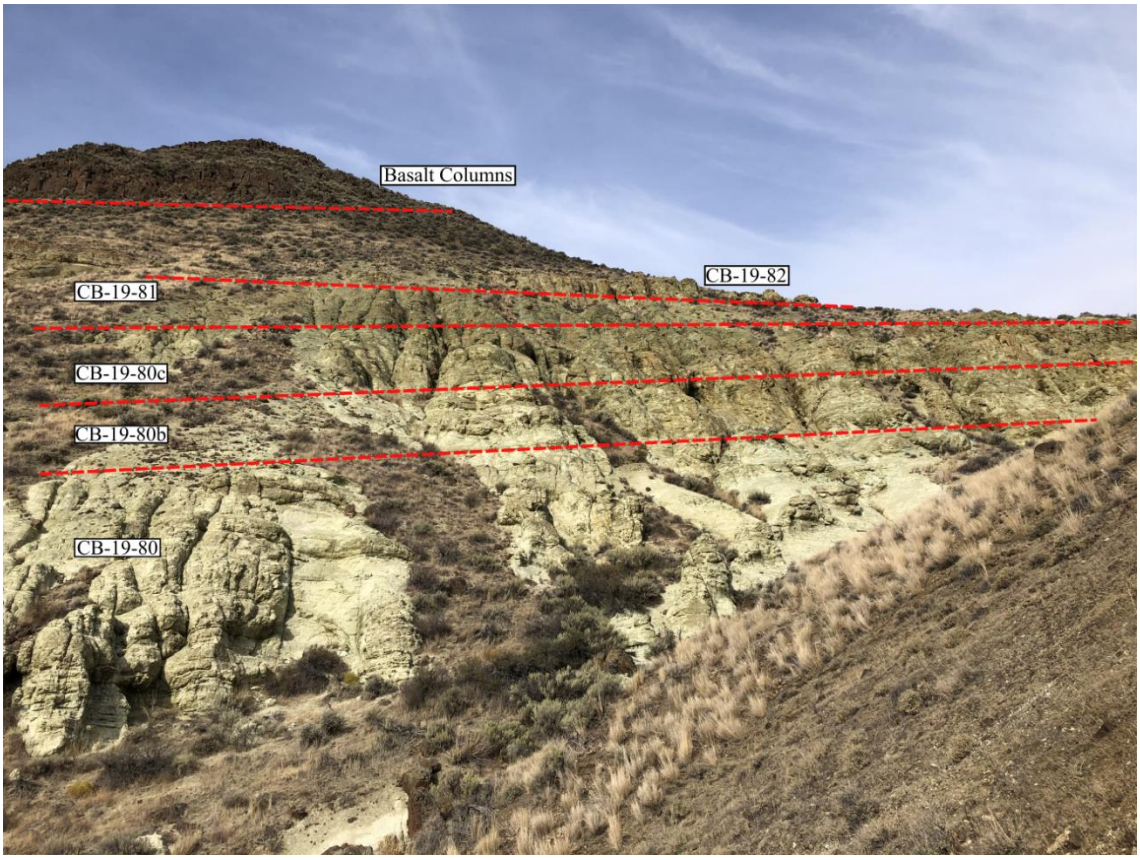

Figure 14. Field photo of Western stratigraphic section and relative sample locations. Photo looking west.

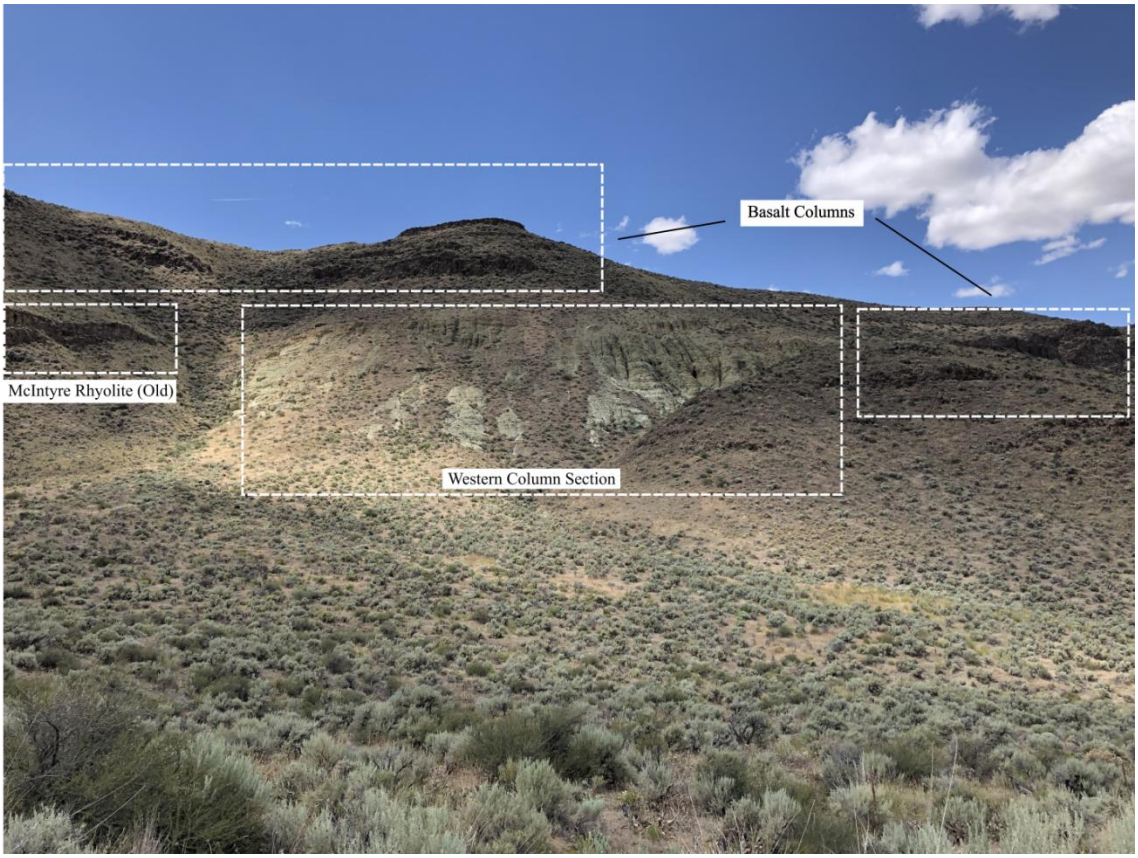

Figure 15. Field photo, looking west towards Western Section. Old McIntyre rhyolite found just south of section and basalt columns just north and stratigraphically above the samples Western section. Basalt columns on the right of the section are offset, displaced along a possible N-S trending fault.

At the base of the section is sample CB-19-80, a 15 m thick lithic and pumice rich tuff. Both pumices and lithics range from ash to fine lapilli size. Abundance of each is ~ 10%. Above this is sample CB-19-80b. This layer is 6 m thick. Pumice sizes in this sample stay between ash to fine lapilli, while the lithic fragments increase to medium lapilli (Figure 16). Phenocryst abundance is around 3% and are no greater than 1 mm. Sample CB-19-80c is above this, with a thickness of 6 m. Lithic abundance and size has significantly decreased in this sample compared to the two before it. The size is primarily fine ash, though some are 1 mm. Sample CB-19-81 is the second from the top. It is a

pumice and phenocryst rich sample. Lithic abundance is 5%, with most having a fine ash size, aside from a few that are 1 cm. Pumices are less than 1 mm to 1 cm sized, i.e. coarse ash to small lapilli. Phenocrysts range from 1 mm to 3 mm in size. Finally, at the top of this section is CB-19-82, the 5 m thick fine ash deposit. Throughout this section, only faint bedding or lamination were observed (Figure 14).

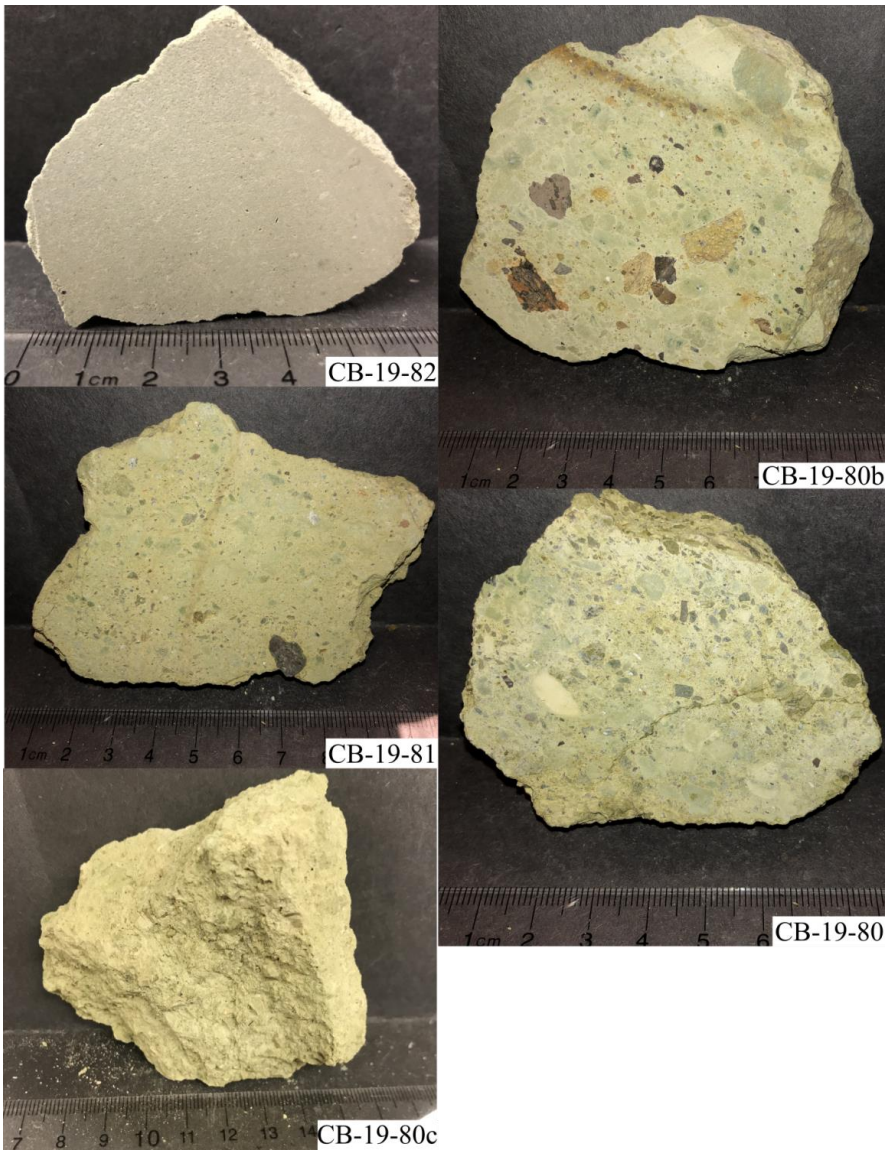

Figure 16. Cut hand samples the Western stratigraphic section. CB-19-82 was collected at the top of the section and CB-19-80 was collected from the bottom.

4.1.5 Sawtooth Stratigraphic Sections

The Sawtooth section is located in the south-center of the study area (Figure 6), and has been divided into the North and South Sawtooth stratigraphic sections. The area of these outcrops is approximately 0.34km^2, making it the largest and most expansive in the study area. Predominant deposits in this section are surge deposits, as seen in Figure 17. These surge deposits are present both in the North and South Sawtooth sections.

Figure 17. Surge deposits in Sawtooth section, 1.75 m field assistant for scale.

4.1.5.1 North Sawtooth Section

The North Sawtooth section is 60 m thick and five samples were collected. At the top of the section is a mafic dike cutting through the tuff (Figure 18). Capping the section is the Old McIntyre Rhyolite.

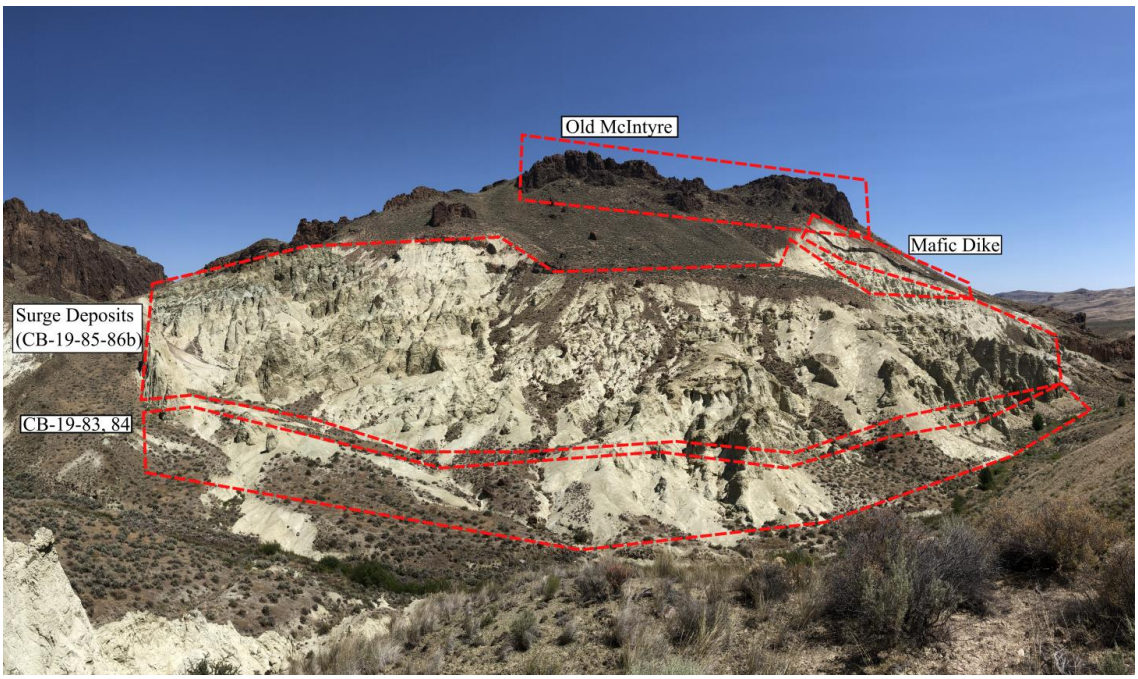

Figure 18. Annotated field photo of layers observed in the North Sawtooth Column. Surge deposits are located in the bottom two thirds, with the pumice rich tuff above. Capping the section is Old McIntyre rhyolite. A mafic dikes cut samples CB-19-86 and CB-19-86b. Photo looking north-northeast.

The base, CB-19-83 is a 3 m thick crystal rich tuff. Above CB-19-84 samples a 6 m thick tuff section. This tuff is very dense, possibly silicified. Pumices are 1 mm to 5 mm in size, and phenocryst and lithic poor. Next is CB-19-85, a sample from the lowest part of the surge deposit. This sample is a fine ash, which is pumice and lithic poor, but contains phenocrysts with 5% abundance and size up to 5 mm. Above this is sample CB-19-86, a 17 m pumice rich lapilli tuff, with poor sorting and no laminations. There are

few lithic and phenocrysts present in this sample. Finally, at the top is the surge deposit CB-19-86b, see Lithology of Units. Figure 19 shows examples of these samples.

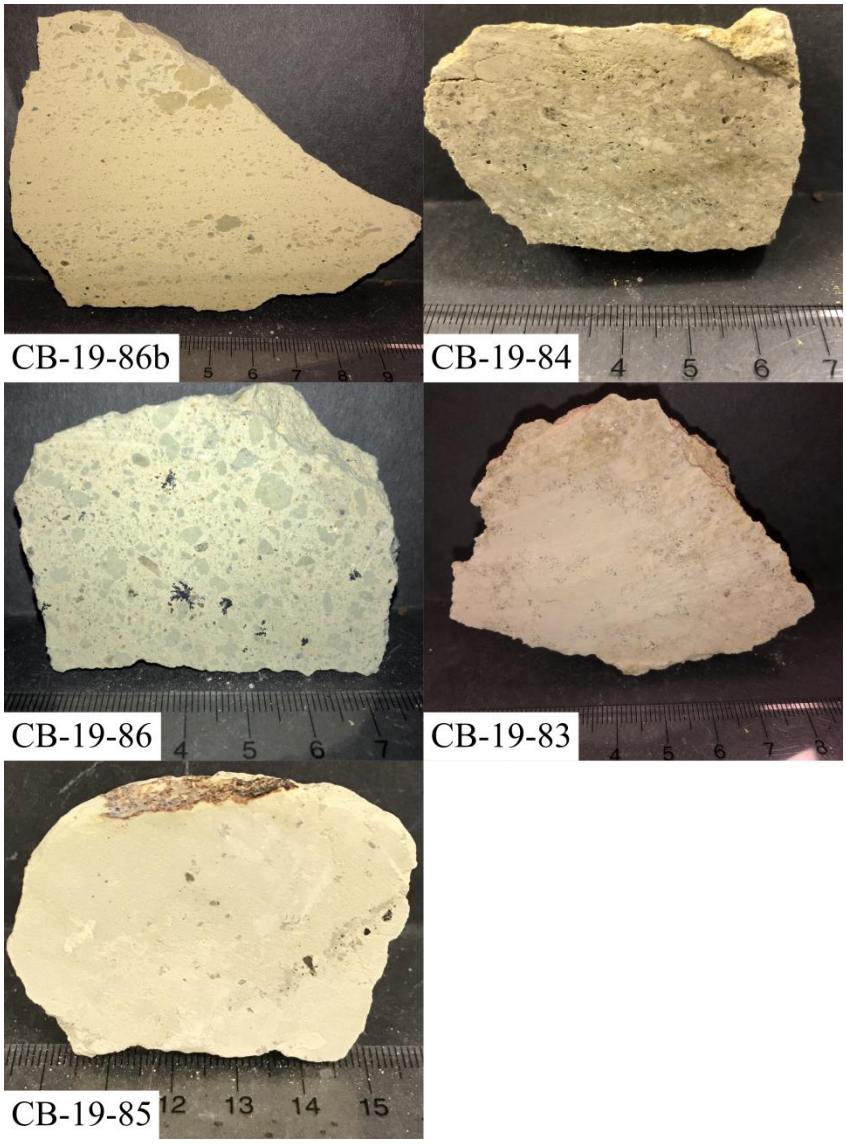

Figure 19. Cut hand samples the North Sawtooth stratigraphic section. CB-19-86b was collected at the top of the section and CB-19-83 was collected from the bottom.

4.1.5.2 South Sawtooth Section

The South Sawtooth stratigraphic section is directly south from the North Sawtooth section (Figure 6). Figure 20 was taken from the base of the North Sawtooth section, looking south towards the South Sawtooth section. Five samples were collected, relative stratigraphic positions of the samples are shown in Figure 20. The total thickness of this section is approximately 60 m. Surge deposits are also present in this section, shown in Figure 20 by the sub-horizontal but irregular texture visible in this photo at the stratigraphic horizons of units 91, 92, and 93.

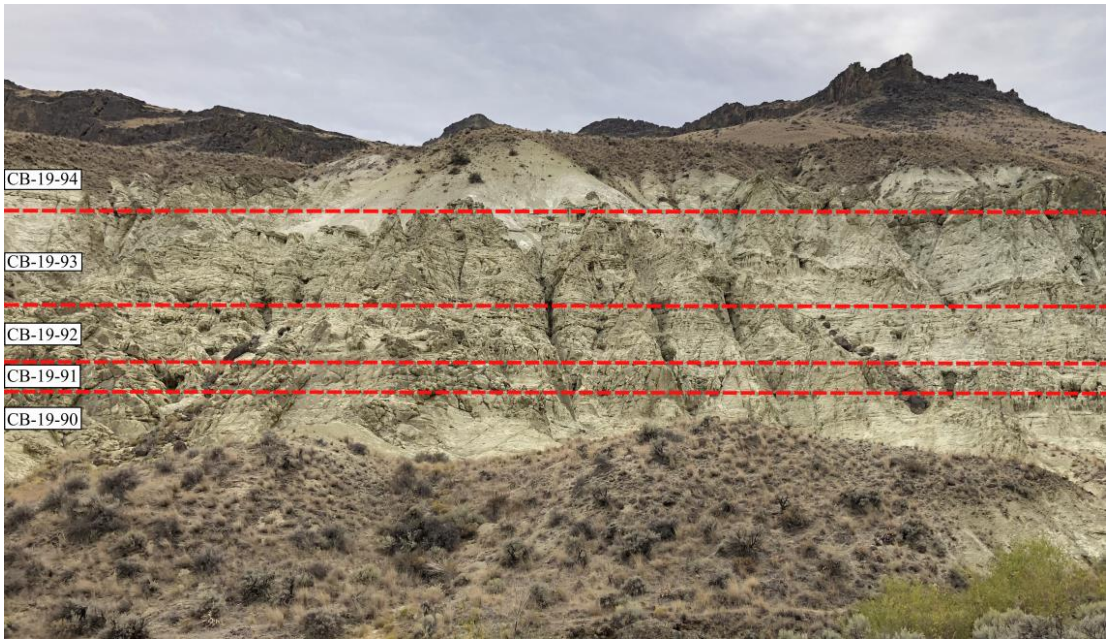

Figure 20. South Sawtooth stratigraphic section and relative sample locations. Photo looking south.

The base of this column is the 10 m thick tuff sampled by CB-19-90, a pumice and lithic poor fine ash layer with 2% phenocrysts of less than 1 mm to 2 mm size. Next section is represented by CB-19-91 and 3 m thick. This sample is crystal and lithic rich, about 10% crystals and 5% lithic fragments. Exemplary surge deposits in a 5 m thick section are found above – and sample CB-19-92 was taken from there. Similar to the

surge deposit in North Sawtooth, this contains 10% pumices ranging in size from ash to medium grained lapilli. Similar normally graded layers are observed as well (Figure 21). Above this is a 10 m thick section represented by sample CB-19-93. Equal percentage ~5% of lithic, pumice and phenocrysts are observed. The final sample collected in this section is CB-19-94. This sample represents the top and thickest layer, at approximately 30 m thick. Lithic poor, this sample contains 5% ash sized phenocrysts and 8% ash to fine lapilli pumices.

Figure 21. Cut hand samples the South Sawtooth stratigraphic section. CB-19-94 was collected at the top of the section and CB-19-90 was collected from the bottom.

4.1.6 Road Cut - North

Three separate sections make up the Road Cut exposures in this field area (Figure 6). These exposures are found at the southernmost extent of the study area along the western side of Succor Creek Road. As its name suggests, the Road Cut North section is the most northern of the three sections. This is section also has the greatest horizontal outcrop extent, approximately 300 m with an approximate thickness of 70 m. A total of five samples were collected throughout this section (Figure 22).

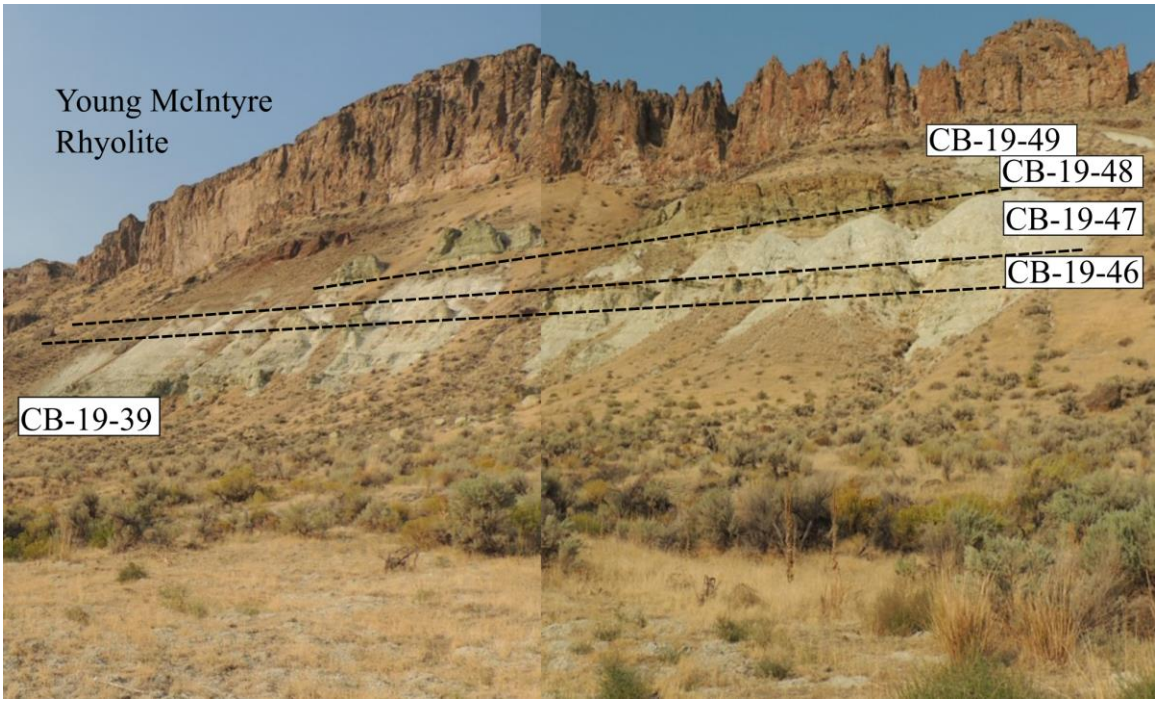

Figure 22. Photograph of Road Cut North section, showing location of samples collected. Photo looking south-southwest.

The base of this section, CB-19-39, is also found at the base of the Road Cut Middle and top of Road Cut South sections. A fine groundmass with 2-3% abundance of ash sized pumice, lithics and phenocrysts. Next was a fine ash sample, CB-19-46, 4m thick. This sample is well sorted and very lithic, pumice, and phenocryst poor. Above this is the 10 m thick pumice rich lapilli tuff, CB-19-47. A few of the pumice fragments

displayed a degree of flattening, and pumice size ranged from 1 mm to 5 mm. Sample CB-19-48 is the pumice and lithic rich ignimbrite described in the lithology section above. This is a 4 m thick layer. Finally, at the top of the section is CB-19-49, which is 8 m thick. Like the layer below, it was a pumice and lithic rich ignimbrite, though with lesser abundance of each pumices and lithics. Figure 34 shows each of these samples in polished slab form. The McIntyre rhyolite outcrop above this section was not reached due to slope, though a rhyolite lava sample was collected from the ground near to this section.

Figure 23. Cut hand samples the Road Cut North Sawtooth stratigraphic section. CB-19-49 was collected at the top of the section and CB-19-39 was collected from the bottom.

4.1.7 Road Cut - Middle

The middle of the Road cut columns is 75 m thick. At the base of this section is the 50 m thick sample CB-19-39. Above this is CB-19-43, a 2 m thick dense sample with a phenocryst abundance of 5%, similar to the phenocrysts in the sample above. No lithic fragments were found in this sample. The top layer in the stratigraphic section is CB-19-44, one of the rhyolite lava samples described in Lithology of Units. This sample is phenocryst poor, about 5% abundance of feldspar crystals. The devitrified rhyolite outcrop that capped the section was not accessible as the cliff face became too steep.

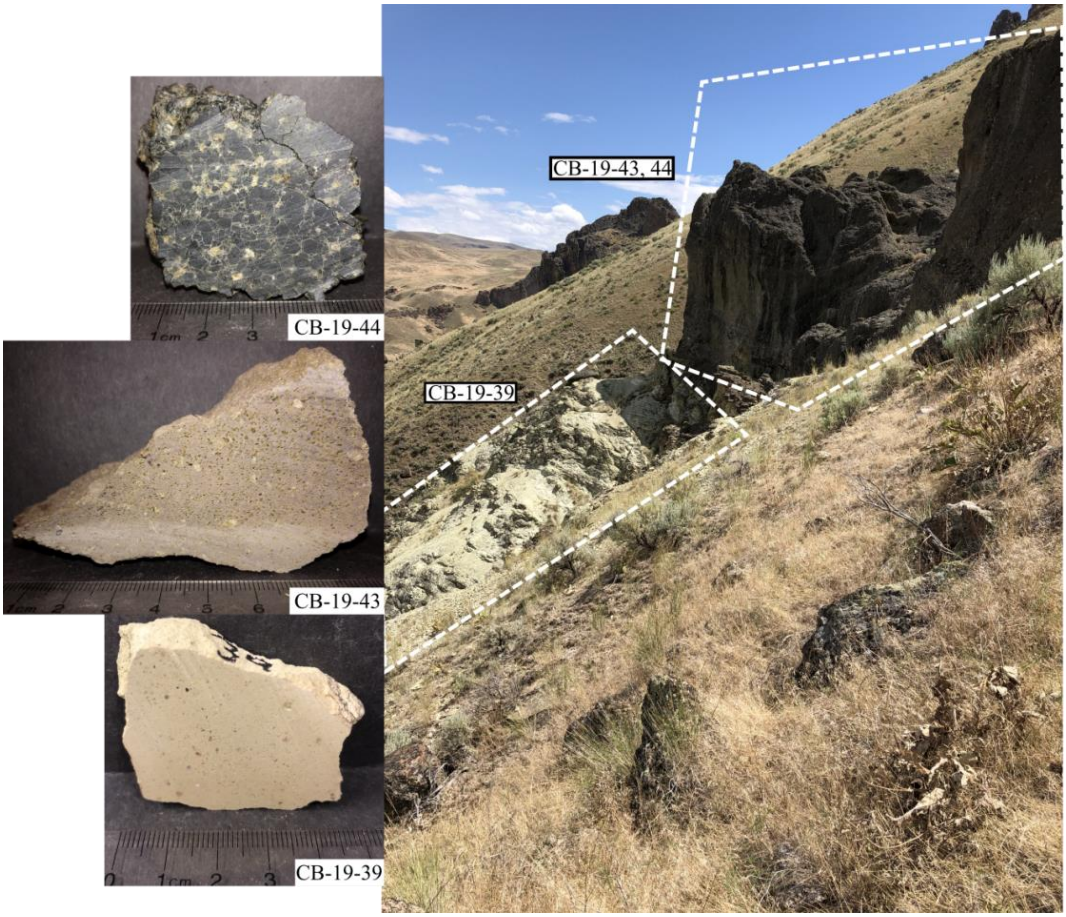

Figure 24. Field photo of Road Cut Middle section. Cross section of each sample is shown on the left, in order of stratigraphic, CB-19-39 collected from the base, and CB-19-44 collected from the top of the section. Photo looking south.

4.1.8 Road Cut – South

The final stratigraphic section to be described is the Road Cut South section (Figure 6). This is the southernmost section in the study area. The total exposed thickness of this section is approximately 80 m, although the thickness sampled is around 43 m as the top portion was too steep to hike. In this section, six samples were collected (Figure 25).

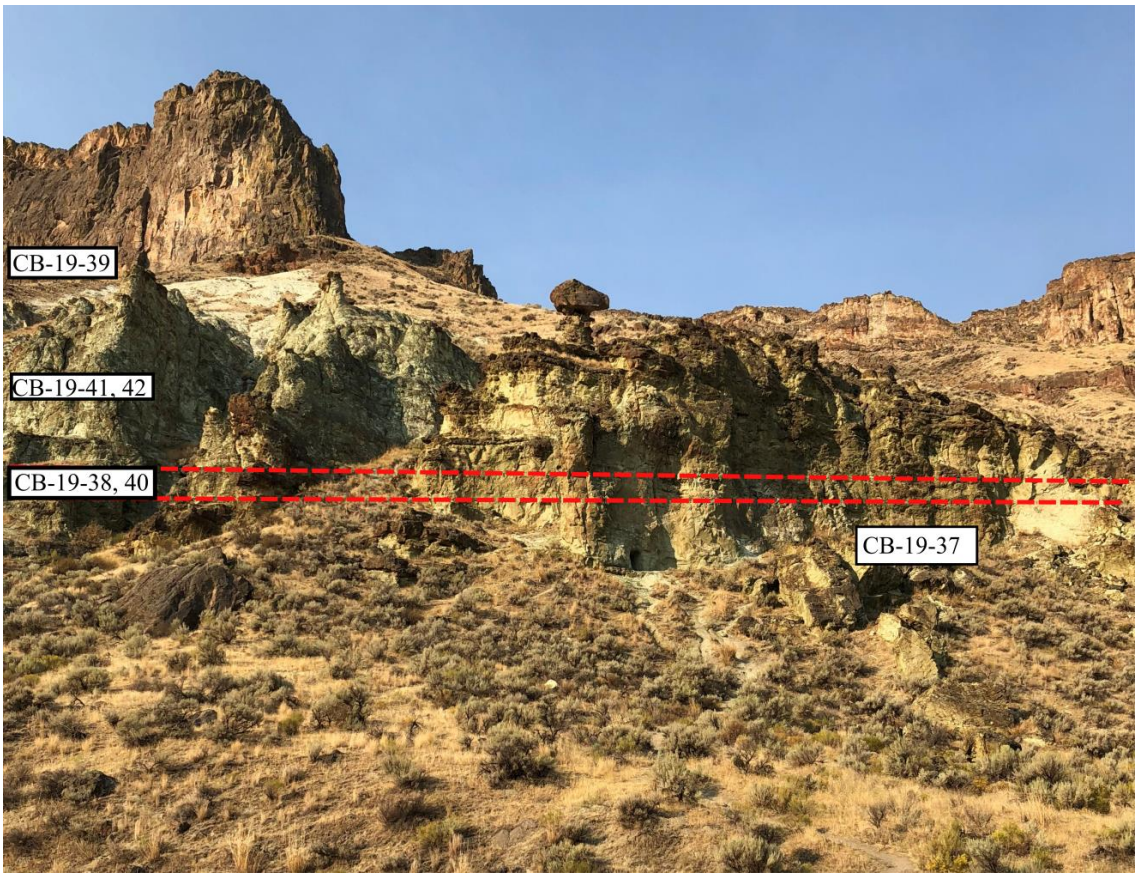

Figure 25. Road Cut South field photo, showing relative sample locations. Photo looking west.

The base is sample CB-19-37, the non-welded pumice rich lapilli tuff described in the Lithology of Units above. This is approximately 10 m thick. Above this is CB-19-38, which is a 0.25 m thick ash layer, having ash-sized phenocrysts. The next layer is a 0.3 m thick layer of CB-19-40. This poorly sorted layer had pumices from 1 mm to 1 cm and

phenocrysts less than 1 mm. CB-19-41 is approximately 10 m thick and has 5% lithic fragments and phenocrysts, both 5 mm and less in size. Pumices are not abundant. Sample CB-19-42 is similar as it is the same thickness and mainly phenocrysts present. The size of these phenocrysts are all ash sized. At the top of the sampled section is CB-19-39, which is also found in the other two road cut sections. In this section the thickness was approximately 12 m.

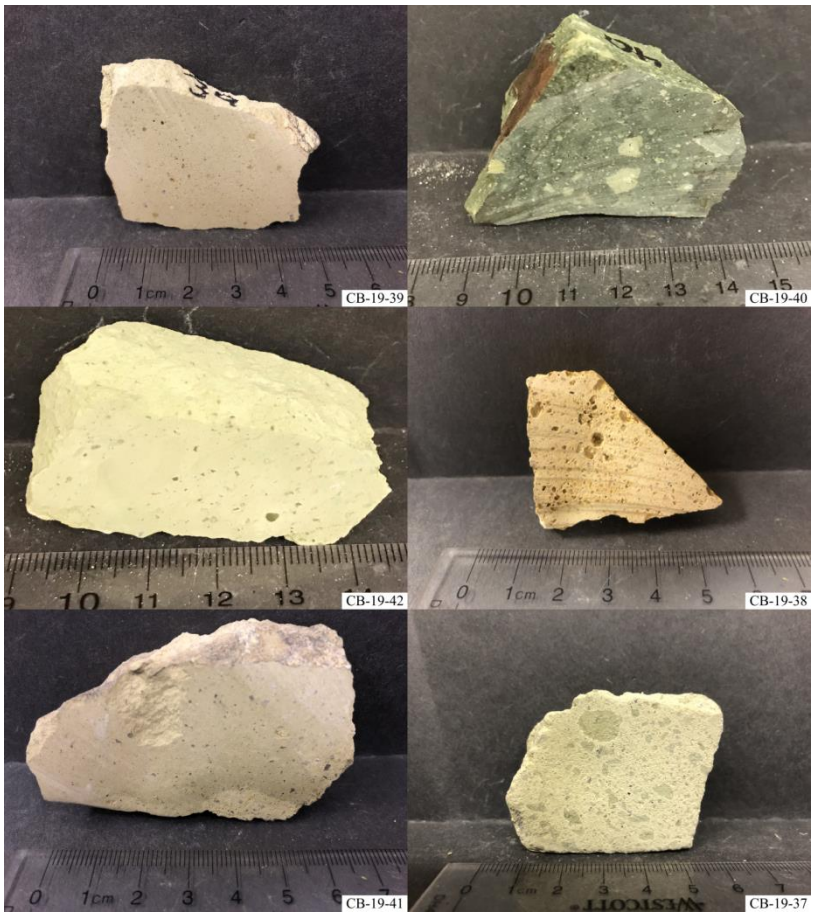

Figure 26. Cut hand samples the Road Cut South Sawtooth stratigraphic section. CB-19-39 was collected at the top of the section and CB-19-37 was collected from the bottom.

4.2 Lithology of Units

4.2.1 Facies of Pyroclastic Deposits

The majority of the stratigraphic sections were non-welded tuff sections below very prominent rhyolite lavas. Other samples types included rhyolitic and mafic lavas. Based on the findings from the stratigraphic sections, five main reoccurring pyroclastic facies were identified. These included fine ash deposits, surge deposits, lapilli tuffs, partially welded ignimbrites, and finally welded ignimbrites, described in more detail below.

Fine Ash Deposit

This fine ash unit is very pumice, lithic, and crystal poor. Glass shards in this sample maintain their Y-shape are seen in Figure 27B but developed axiolitic structure upon devitrification. Intact, although devitrified shards indicate that the grain size of this samples and lack of larger components is not due to reworking. It is a primary pyroclastic deposit that is well sorted and coarse bedding. No laminations or grading were observed. This suggests that the deposit could be the result from settling of ash after elutriation of fines during surge and ignimbrite eruptions.

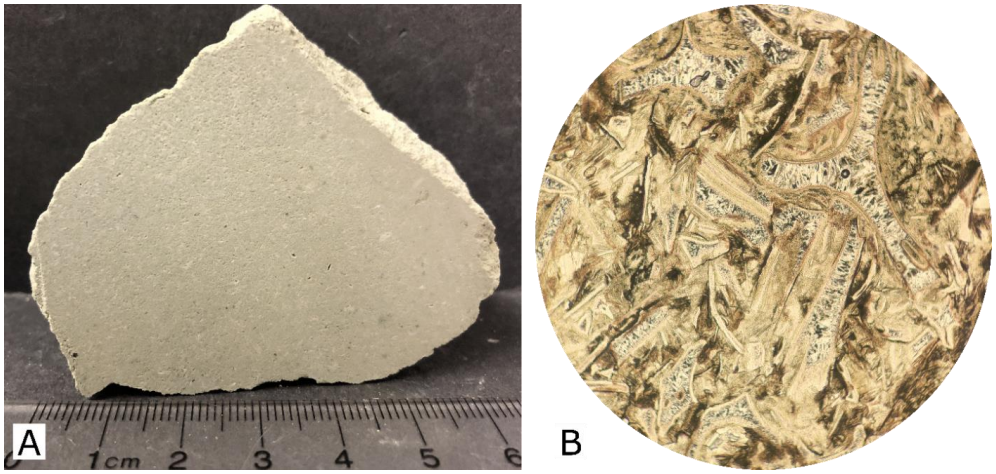

Figure 27. Top fine ash deposit. A) Photo of sawed piece of hand sample CB-19-82. B) Glass shards exhibiting Y-shape in PPL, 100x mag, diameter 0.2 mm.

Lapilli Tuff

Sample CB-19-37 is exemplary for a non-welded pumice rich lapilli tuff and it was collected from the base of the southern road column (Figure 28A). In thin section, ash-sized glass shards retain the characteristic Y-shape (Figure 28B). Pumice abundance is 15%, and size range from ash to medium-grained lapilli. The largest pumice fragment is 1cm. Pumices do not show evidence of flattening or elongation. No lithic fragments were observed. The phenocryst assemblage is primarily feldspars, no quartz or pyroxenes were observed. This outcrop displays massive bedding with no laminations and is poorly sorted. Thus I interpret the lapilli tuff facies to represent fine grained pumice rich ignimbrite deposition.

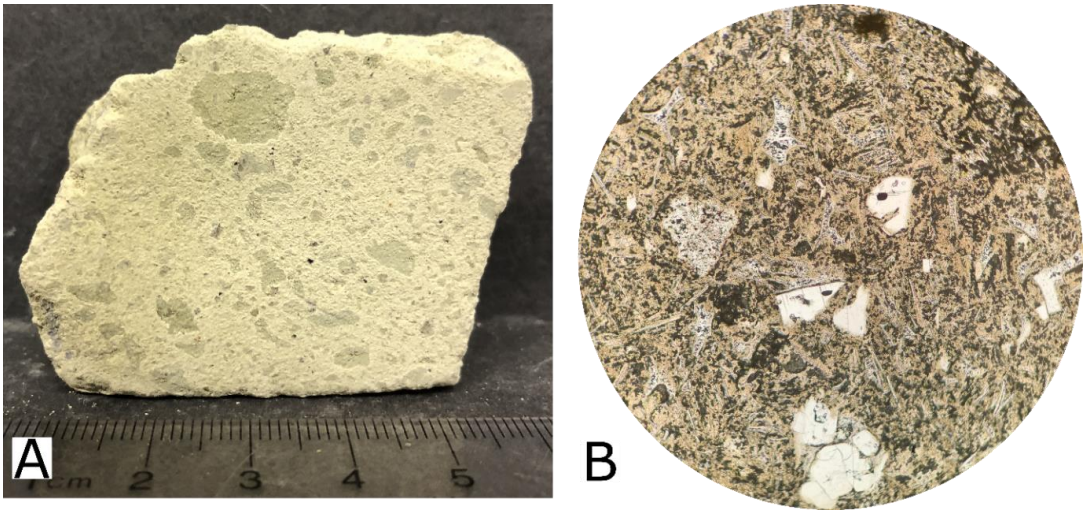

Figure 28. Pumice rich lapilli tuff. A) Cut slab of sample CB-19-37 showing abundance and size distribution of pumices. B) Picture of thin section of CB-19-37, showing Y-shaped glass shards. PPL, 25x mag, diameter 0.8 mm.

Two other lapilli tuffs were collected throughout the study area that are not associated with the unit described above. First is the non-welded coarse lapilli tuff that was observed in the Top Unwelded Ignimbrite unit found at the northern most section of the field area, the Grey Ash section (Figure 6). CB-19-51 is a pumice and lithic rich lapilli tuff (Figure 29A). Pumice abundance is approximately 15% and lithic abundance of 10%. The largest pumice in this sample is 1 cm. This is a poorly sorted outcrop that displays massive bedding, and no grading or laminations. The second is the coarse lapilli tuff found in surrounding a rhyolitic lava flow just before the entrance to the Sawtooth sections (Figure 6). This sample, CB-20-06 is very poorly sorted and is very pumice rich with abundances of greater than 20% (Figure 29B). Pumices in this sample ranged from 1 mm to 4.5 cm. Lithic fragments and phenocrysts were also abundant and ranged from ash to lapilli size. Like the other two samples, CB-20-06 is also interpreted to be an ignimbrite as well.

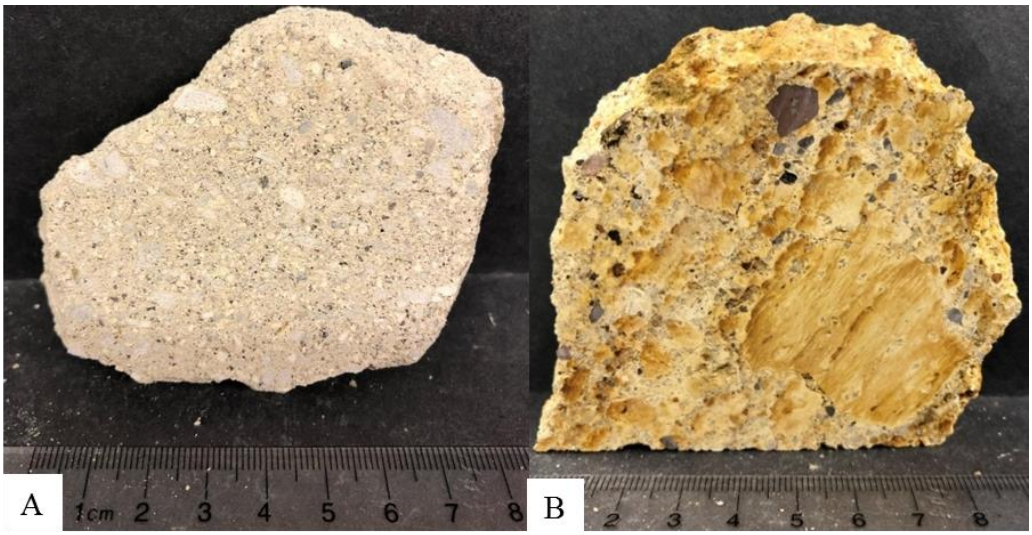

Figure 29. A) Lapilli tuff, CB-19-51 from the Top Unwelded Ignimbrite unit. B) Pumice rich CB-20-06.

Pumice and Lithic Rich Ignimbrite

Sample CB-19-48 comes from an ignimbrite that was collected in the northern road column. Glass shards maintain their Y and C shape (Figure 30B). Pumice abundance is approximately 10% ranges in size 1cm to less than 1mm. There are two textures seen in the pumices of this sample. First there are some vesiculated "onion" shaped lapilli that do not show any flattening. This vesiculated texture can be seen in the inset of Figure 30. The other lapilli are pumices that are slightly flattened. The "onion" shaped lapilli may be formerly dense obsidian lithics that revesiculated after entrainment in hot pyroclastic flows. Similar textures have been observed in the Diner Creek Tuff (Martin Streck., personal communication, 2021). Lithic abundance is approximately 8%. The largest lithic is 0.5cm wide, and is well sorted. Poorly sorted primary pyroclastic texture along with massive bedding indicates that this is an ignimbrite.

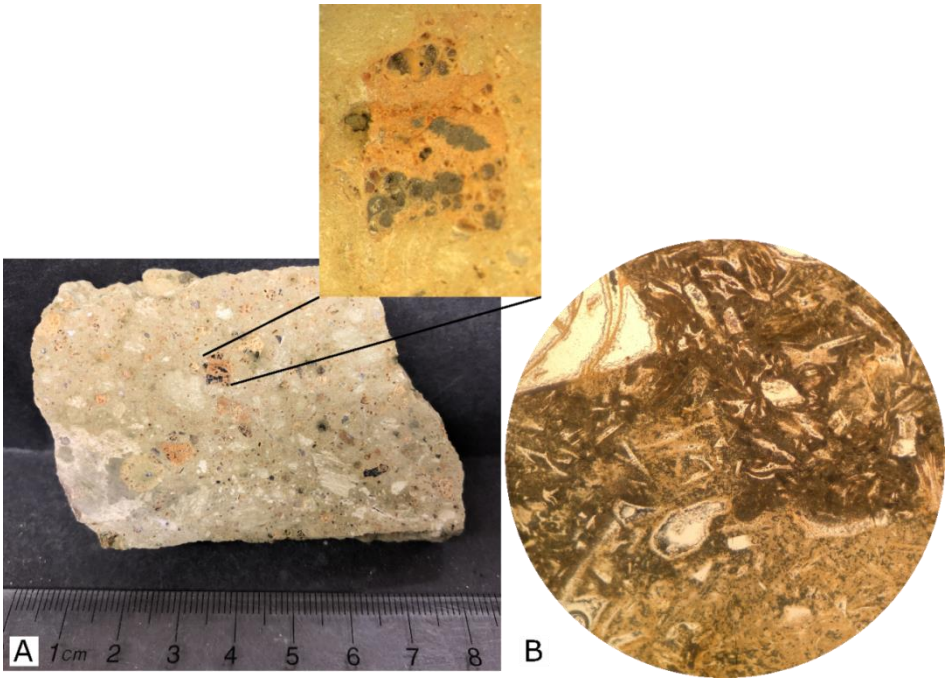

Figure 30. A) Cut slab of ignimbrite sample CB-19-48. Inset shows lapilli with vesiculated "onion" like texture and rhyolite inclusions. This pumice is 1.5cm. B) Thin section photo of samples CB-19-48, showing glass shards and small piece of pumice in top left. PPL, 10x mag, 0.2 mm diameter.

Surge Deposits

Characteristic surge deposits are finely laminated in outcrop (Figure 17) and layering can also be seen in rock slabs such as in Figure 31A. Hypothetically, bedding could also be due to sedimentary reworking of pyroclastic material but evidence against this is revealed under the microscope. An exemplary thin section of the surge deposits, sample CB-19-86b indicates the ash-sized glass shards maintain the characteristic Y-shape and shards are not sorted or broken (Figure 31B). This is a strong argument against an epiclastic deposit. In this thin section, the number of straight shards is relatively abundant. These deposits contain about 10% pumices, with sizes ranging from medium grained ash to medium grained lapilli. The largest pumice is 15 mm. Lithic abundance is less than 1% and are no larger than 2mm. These deposits are poorly sorted and have multiple normally graded layers, consistent with my interpretation of surge deposits.

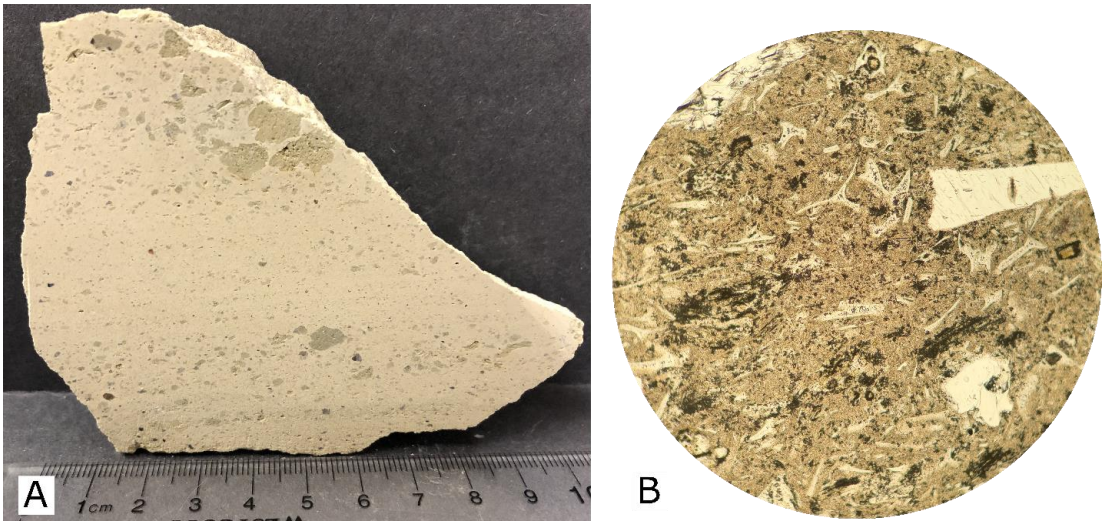

Figure 31. Hand sample and thin section view of surge deposit. A) Sawed section of sample. B) Photo of deposit in thin section, 100x magnification, 0.2 mm diameter. Glass shards, pumices, and crystals can be seen, in PPL.

Welded Ignimbrite

A welded ignimbrite, sample CB-19-67, crops out in the McIntyre column area. This ignimbrite includes lapilli to bomb-sized solid glass fragments (Figure 32A). The largest glass fragment in this sample is greater than 8cm long. Pumices are flattened and elongated in this sample, as seen in Figure 32B. This poorly sorted ignimbrite was approximately 1.5 m thick with no grading. The main phenocryst assemblage in this sample consists of feldspars and pyroxenes.

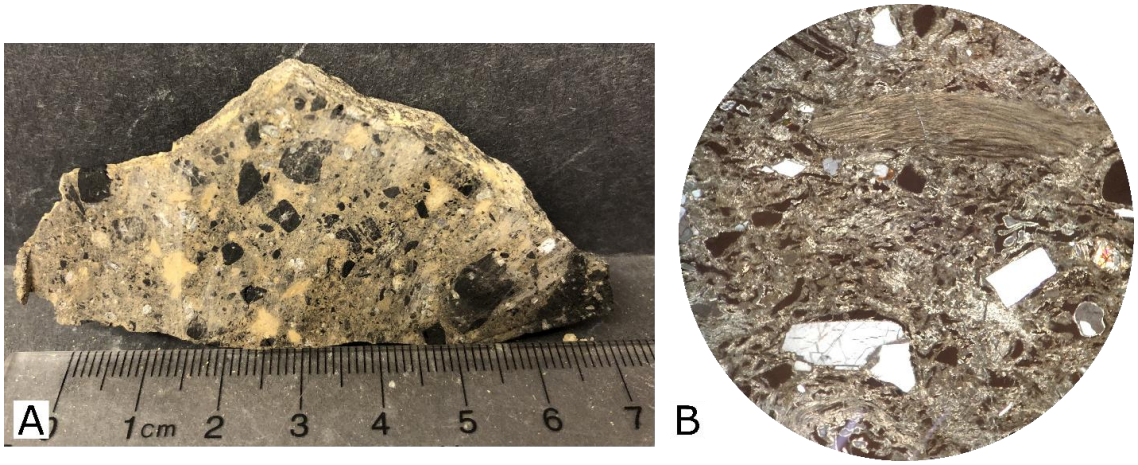

Figure 32. A) Cut slab showing ignimbrite samples CB-19-67. B) Thin section picture of CB-19-67. White phenocrysts are feldspars, black is glass pieces, and to the right is a flattened pumice. XPL, 10x mag, 0.2 mm diameter.

Partially Welded Ignimbrite

A second ignimbrite, sample CB-19-69, was collected in the McIntyre section below the welded ignimbrite represented by sample CB-19-67. This is a partially welded tuff with ash sized glass shards that are not as compressed as the sample above unit (Figure 33). These shards maintain Y-shape. Fiamme, flattened pumices, are found within this sample. Pumices are ash-sized and can only be seen clearly with the microscope. Lithic fragments in this sample are ash to fine grained lapilli, with abundance around 5%. These lithics are not as obviously rhyolite glass as in the welded ignimbrite above (sample CB-19-67), but do appear to be glassy. In the field, this sample exhibited massive bedding and no laminations or grading was observed.

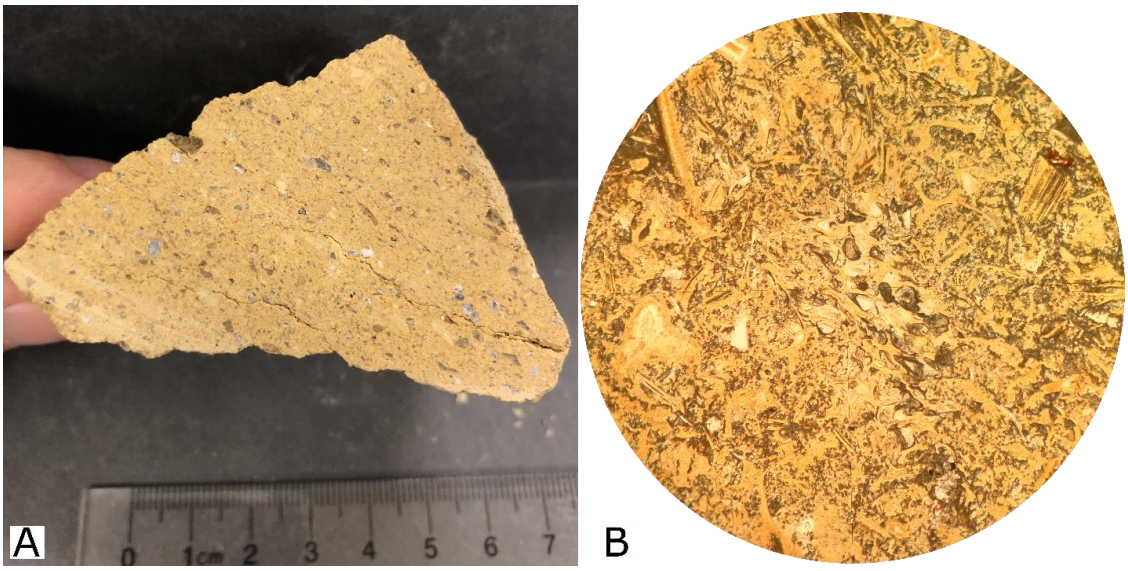

Figure 33. Sample CB-19-69, partially welded tuff. A) Hand sample showing fresh surface. B) Thin section image of CB-19-69, PPL, 100x mag, 0.2 mm diameter.

4.2.2 Rhyolitic Lavas

Rhyolite lavas crop out on top of sections at high and sometimes highest elevations, and seemingly top the stratigraphy. Other lavas outcrops occur at lower elevations, seemingly underlying the majority of the stratigraphic columns. A total of seven rhyolitic lava outcrops were collected in the study area. Previous mapping identified all rhyolite lavas as rhyolite of McIntyre Ridge. However, subtle textural differences among rhyolite lavas are evident in the field and become more apparent in thin sections and by considering mineralogical and geochemical data. All lavas displayed porphyritic texture with feldspar phenocrysts that are between 2-5mm, (Figure 34), however the abundance and feldspar texture vary. This difference is observed in contrasting Figure 34 and Figure 35.

Petrographic thin section analysis of two of these lavas showed similar features. Both samples were crystal poor, approximately 5%, with the most abundant phenocrysts being feldspar and pyroxene. Feldspars were slightly rounded but do not appear to be fully resorbed (Figure 34 C and D). Sample CB-19-44 contained yellow minerals which appear to be altered fayalite. Both included some melt inclusions, though not in high abundance. This low abundance of phenocrysts in the vitrophyre is characteristic of Old McIntyre Rhyolite.

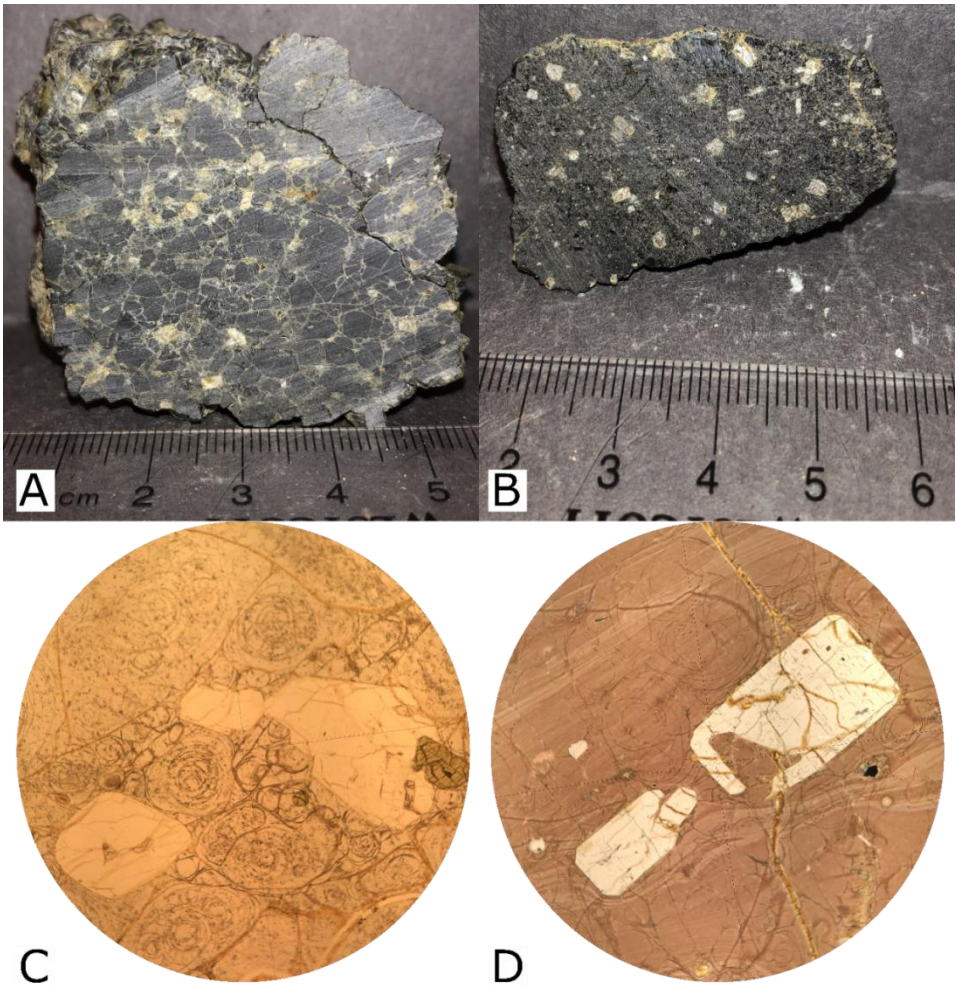

Figure 34. A) Cut slab exposing the fresh surface of rhyolite lava sample CB-19-44. B) Fresh surface of rhyolite sample CB-19-65. C) Rounded feldspars in sample CB-19-44, PPL 5x mag, 0.4 mm diameter. D) Rounded and slightly resorbed feldspars in sample CB-19-65, PPL 5x mag, 0.4 mm diameter.

Young McIntyre Rhyolite vitrophyre is characterized by a much greater abundance of phenocrysts than the Old McIntyre Rhyolite. Phenocryst abundance in this unit is approximately 20%, as seen in Figure 35. This sample was a piece of float found at the base of the Road Cut North section.

Figure 35. Hand sample of Young McIntyre Rhyolite. Clear difference in phenocryst abundance than samples CB-19-44 and CB-19-65 Old McIntyre.

The remaining rhyolitic lavas appear to be different from the McIntyre samples, texturally and petrographically. These lavas contain fewer phenocrysts, with a size less than 5mm, and a glassy groundmass. Most feldspar phenocrysts of these samples show a high degree of resorption in form of a spongy texture (Figure 36 D-F). Abundance of crystals among these samples was significantly lower than McIntyre lavas, approximately 3-5%.

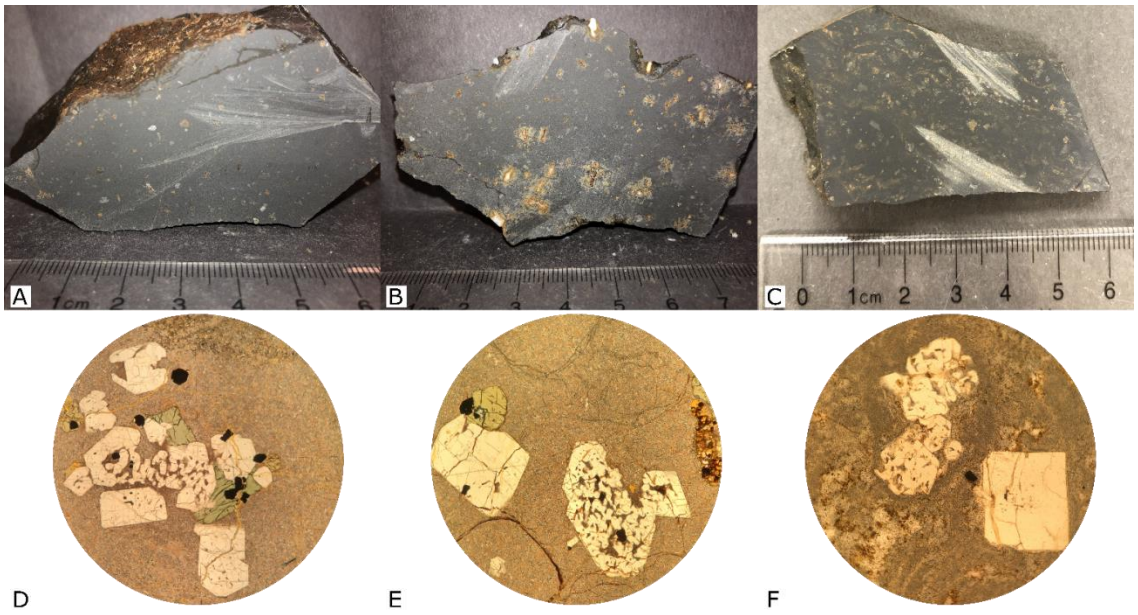

Figure 36. Rhyolitic lavas of the non-McIntyre variety. A) Hand sample of CB-19-32. B) Hand sample of CB-19-34. C) Hand sample of CB-19-87. D) Thin section photo of CB-19-32. E) Thin section photo of CB-19-34. F) Thin section photo of CB-19-87. All thin sections at 50x magnification and 0.4 mm diameter.

4.2.3 Basalt to Andesite Lavas

Basaltic to andesitic lavas were also found in the study area under- and overlying the rhyolite lavas. Basaltic lavas crop out exclusively as dikes, while andesitic lavas crop out as dikes and as columnar jointed flows. The basalt dikes, samples, CB-19-71 and CB-19-88, both have fine grained aphanitic texture (Figure 37). Sample CB-19-71 was collected from the eastern side of the study area, from a 1 m wide and 15 m long dike (Figure 38 A). The second basaltic sample, CB-19-88 was collected from a larger dike just east of the Sawtooth sections (Figure 38B). This dike was 10 m thick and 40 m long.

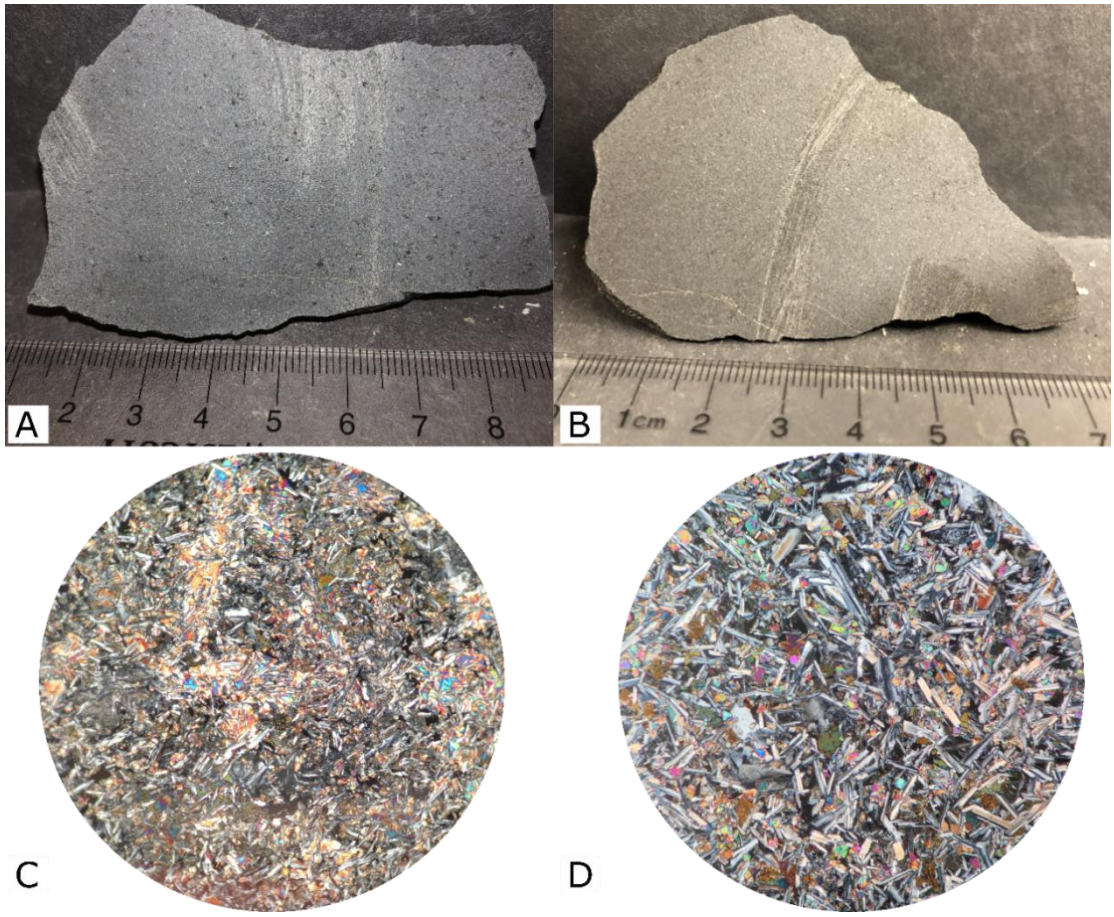

Figure 37. Basaltic sample slabs and thin section pictures. A) CB-19-71 hand sample slab. B) CB-19-88 hand sample slab. C) CB-19-71 thin section picture, XPL 100x mag. D) CB-19-88 thin section picture, XPL 100x mag. Both thin sections have a 0.2 mm diameter.

Figure 38. Mafic dikes and columns in the study area. A) Ridge exposure of CB-19-71 basaltic dike in the eastern section of the study area. Photo looking to the southeast. The dike is 1 m wide, 15 m long and trends roughly N-S. B) Cliff exposure of CB-19-88 basaltic dike. Field assistant is 1.75m tall for scale. Photo looking to the southeast. Dike intrudes sample CB-20-06, is 10 m thick and 40 m long, and trends roughly N-S.

Andesitic samples ranged in composition from basaltic trachyandesite to trachy-andesite and were present in the field as dikes, lava flows, and sometimes columnar jointed. The aphanitic lava flow CB-19-63b was found stratigraphically below the McIntyre stratigraphic section. Another sample of this composition was CB-18-06, a 20 m long dike found in the center of the study area. Finally, sample CB-19-79 was collected from a columnar jointed outcrop in the western most extent of the study area (Figure 39). The columns were approximately 5 m tall at the thickest point and 30 to 40 m long. Texturally, this sample was aphanitic as well.

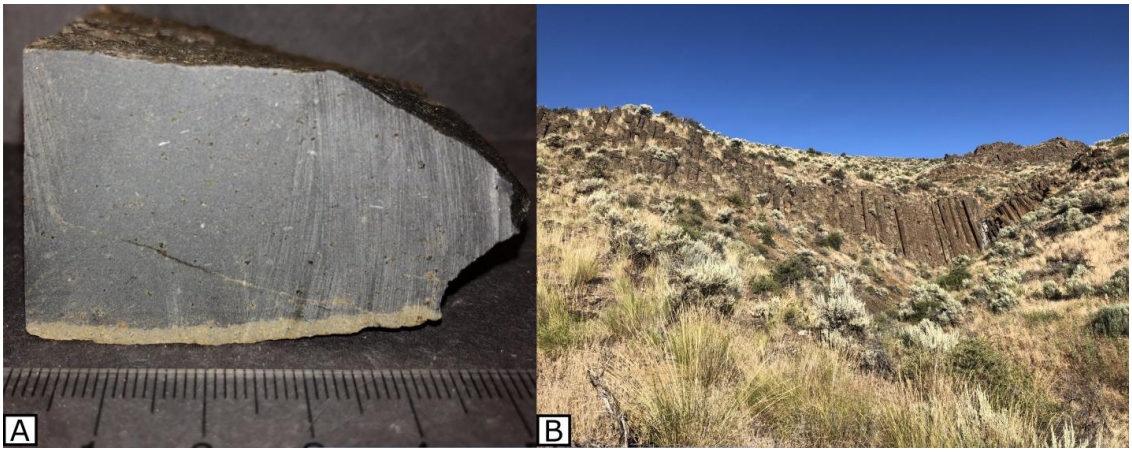

Figure 39. A) Hand sample of CB-19-63b aphanitic basaltic trachyandesite. B) Columnar jointed basaltic trachyandesite, CB-19-79 found stratigraphically below the western stratigraphic column. Columns were 5 m tall, spanning 30 to 40 m along a N-S trend. Photo looking west.

4.3 Geochemistry

Samples collected during field work were analyzed for bulk rock composition included rhyolitic tuffs and lavas, intermediate dikes, and mafic dikes and flows. Figure 40 shows analyzed samples plotted into a total alkali-silica diagram. The majority of samples were rhyolites, with some basalt to basaltic trachyandesite samples as well. Full XRF and ICP-MS data is found in the appendix.

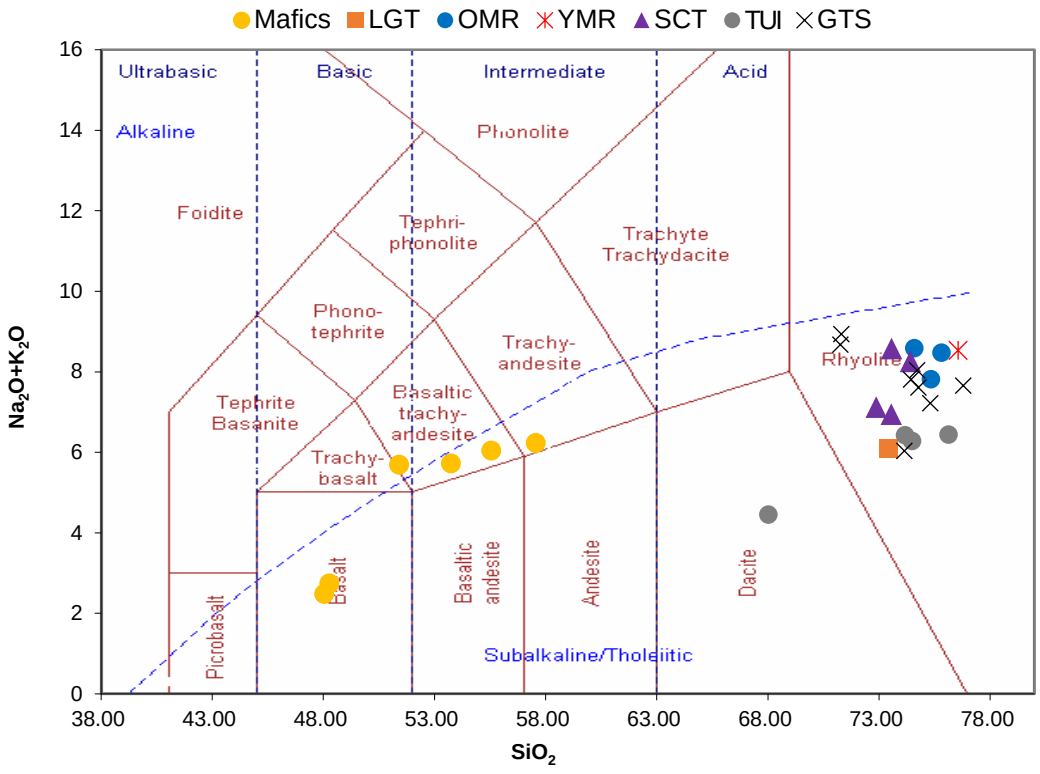

Figure 40. Bulk composition of samples collected and analyzed in this study. LGT - tuff of Leslie Gulch, OMR - Old McIntyre Rhyolite, YMR – Young McIntyre Rhyolite, SCT - tuff of Succor Creek, TUI – top upper ignimbrite, GTS – green tuff samples.

4.3.1 McIntyre Ridge Rhyolites

Four samples of McIntyre Ridge rhyolite lava were collected. In hand sample, only the amount of phenocrysts subtly distinguishes between Young McIntyre Rhyolite (YMR) and Old McIntyre Rhyolite (OMR) vitrophyre. Previous work by Emily Hess (2014) concluded that the northern most McIntyre sample was part of the Old McIntyre unit. Samples from Hess and Streck were included in this analysis to determine whether the samples found in this study were Young or Old McIntyre. No distinguishable difference in SiO_2 content for the two units is apparent. The SiO_2 range for YMR is 76-77% and for OMR is 74-77%. However, these units can be readily distinguished by FeO* and TiO_2 contents as well as trace elemental and mineral compositions (see below). YMR has a considerably lower concentrations of both FeO* and TiO_2 than OMR (Figure 41). The FeO* content for Young McIntyre is 0.71 – 1.66% and the TiO_2 content is 0.15-0.16%, while Old McIntyre FeO* content is 1.89-3.17% and TiO_2 is 0.23-032%. In both cases, OMR has almost double the concentration present in YMR samples.

Trace element concentrations also distinguish between Young and Old units. The most obvious distinguishing element is Ba. YMR samples have Ba concentrations in the 251-268 ppm range, while OMR samples have much higher Ba concentrations, 1152-1645 ppm (Figure 42). Zr also has very distinct concentrations distribution between the two, with YMR 295-320 ppm and OMR 631-743 ppm (Figure 42). There is no clear difference in Sr concentrations, as YMR ranges from 22-25 ppm and OMR overlaps this with a wider range of 16-36 ppm. In general, element contents of YMR tend to be slightly lower than observed in OMR, especially in Ba, Zr, Hf, and Ti (Figure 43). Likewise,

YMR rare earth elements (REE) are lower than OMR and shows a greater Eu depletion than OMR (Figure 44).

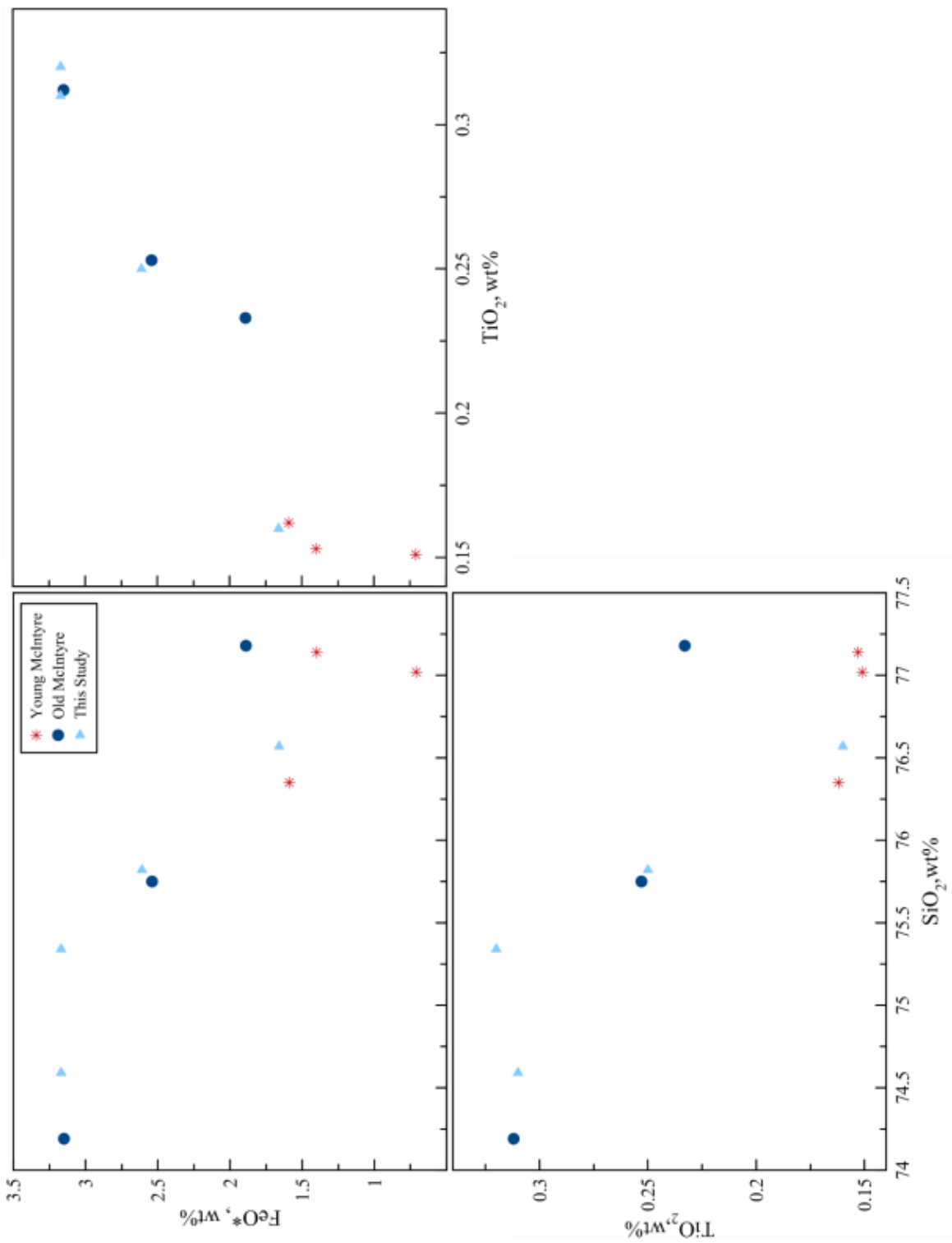

Figure 41. FeO* and TiO_2 concentrations plotted against SiO_2 wt%. Old McIntyre samples have greater concentrations of both FeO* and TiO_2 while the SiO_2 concentrations of the two units overlap. Red stars and blue dots are Young and Old McIntyre data from Hess (2014) and Streck (unpublished). Light blue triangles are data from this study.

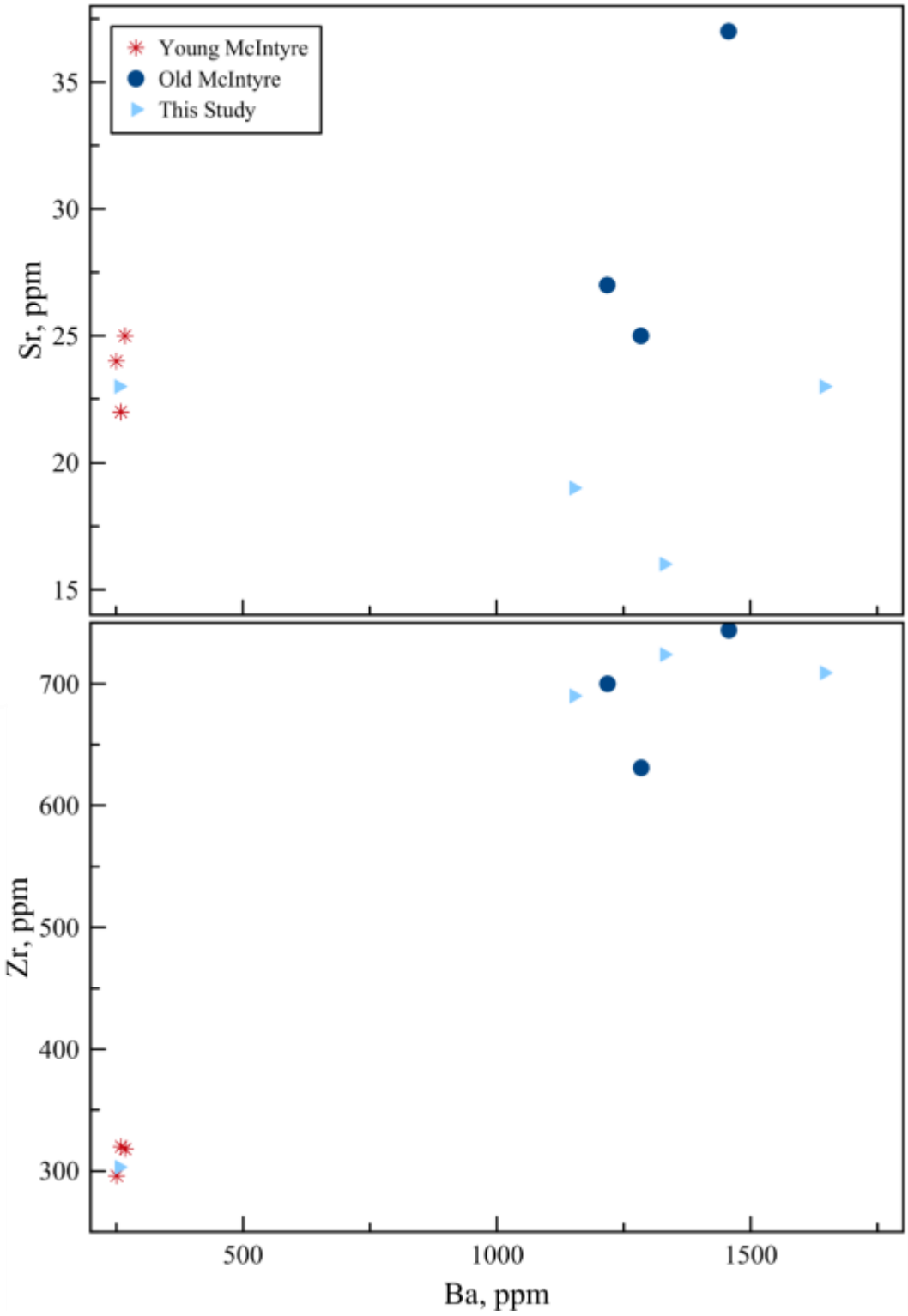

Figure 42. Trace element concentrations of Ba, Sr, and Zr of Young and Old McIntyre rhyolites. Red stars and blue dots are Young and Old McIntyre data from other studies respectively. Light blue triangles are data from this study.

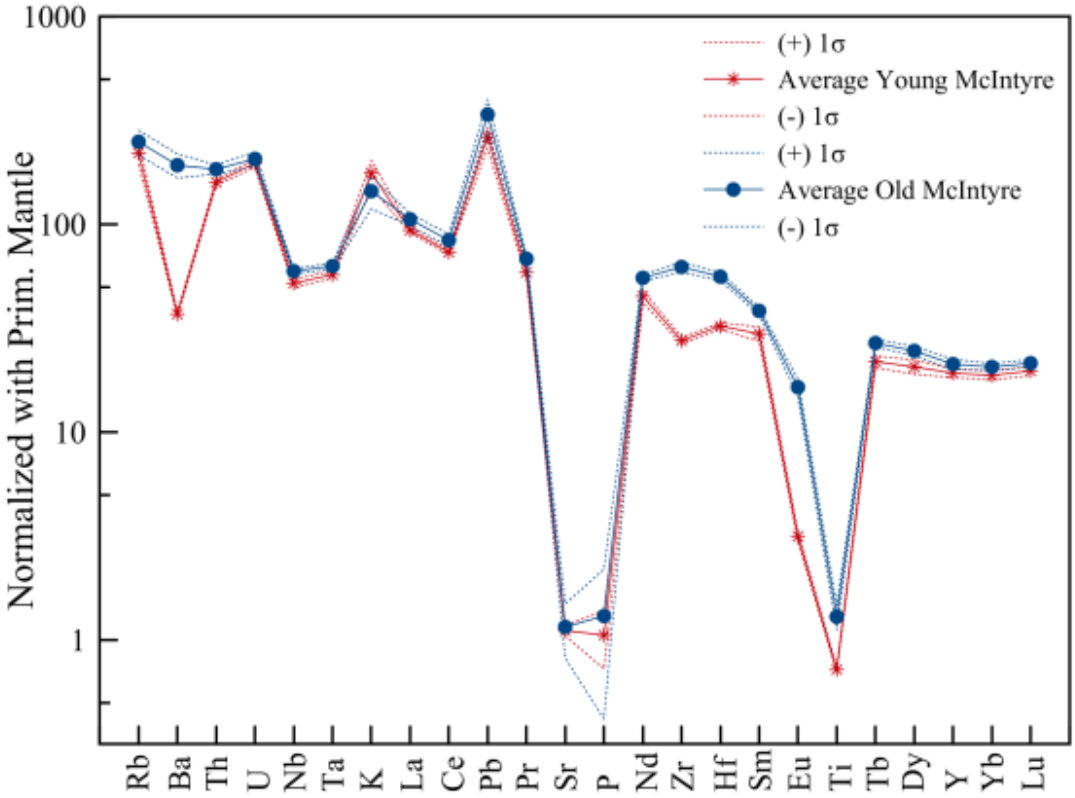

Figure 43. Trace element spider diagram comparison for Young and Old McIntyre rhyolites, normalized to primitive mantle values of Sun and McDonough, 1989.

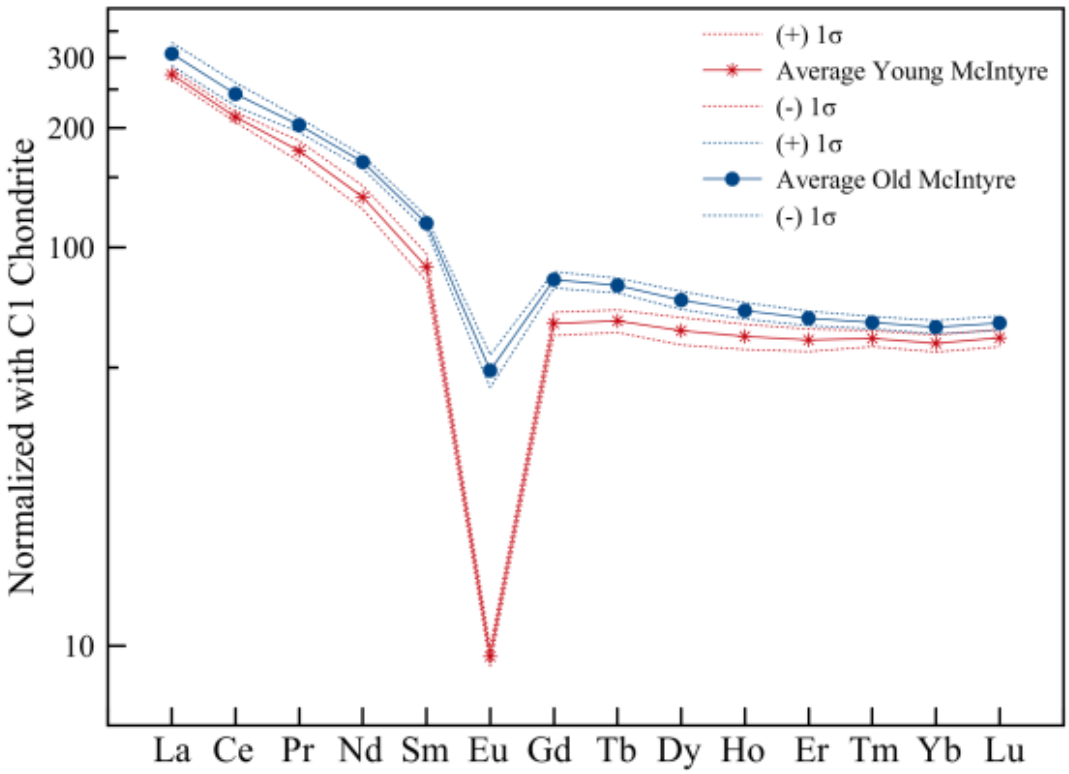

Figure 44. Rare earth element diagram of averaged data of Young and Old McIntyre rhyolites, normalized to chondrite of McDonough and Sun, 1995.

4.3.2 Rhyolite of Succor Creek

Four other rhyolite lavas were collected with outcrops all located at lower elevations than most McIntyre Rhyolite (Young and Old) outcrops. Major and trace element compositional data are used to help determine what units these rhyolite samples belong to. When plotted against tuff of Succor Creek (SCT) and LGT data from previous work by Streck and others (personal communication), it is apparent that these rhyolite samples have close compositional affinity to the samples of the tuff of Succor Creek. Hence, these rhyolites occurring as lavas and dikes are called rhyolite of Succor Creek.

The elements that distinguish between the tuff of Leslie Gulch and the tuff of Succor Creek are SiO2, FeO*, and Ba. The tuff of Leslie Gulch has a slightly higher SiO_2 concentration of 73 -78 wt% while SCT is lower, 72-74 wt%. FeO* content also distinguishes between these units. SCT samples have slightly higher concentrations of FeO*, 3-5 wt% than LGT samples with FeO* of, 1.9-3.8 wt%. SCT samples have considerably higher Ba concentrations than LGT samples (Figure 45). The range in Ba content for SCT is 1662 – 2110 ppm, while the tuff of Leslie Gulch range is 753 to 1563 ppm. Within the tuff of Leslie Gulch samples, it appears to be some variation, showing a lower and higher Ba group. Though both of these groups have Ba contents well below those of the SCT samples. Average trace element compositions of the tuff of Leslie Gulch are generally comparable to tuff of Succor Creek, except for higher Rb and Pb and lower Ba, Sr, Sm, and Ti (Figure 46). The tuff of Leslie Gulch is also more depleted in Eu than SCT, shown in Figure 47. The unknown rhyolite flows show comparable concentrations to SCT, as they exhibit lower SiO_2, and higher FeO* and Ba concentrations, plotting along SCT samples, Figure 45.

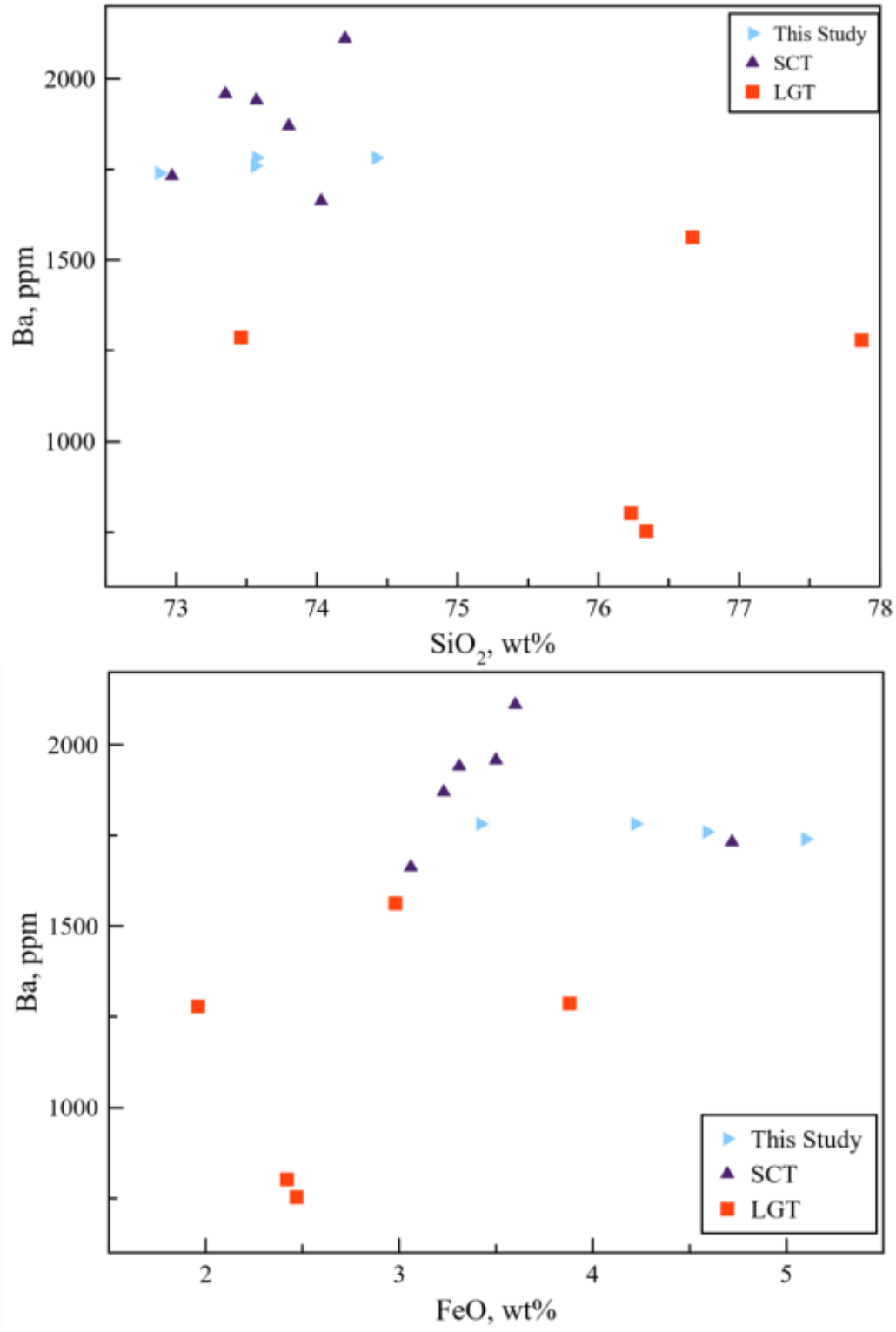

Figure 45. Ba vs SiO_2 and Ba vs FeO* concentrations. Purple triangles represent SCT samples from previous studies, orange squares represent LGT samples, and blue triangles are rhyolite lavas from this study.

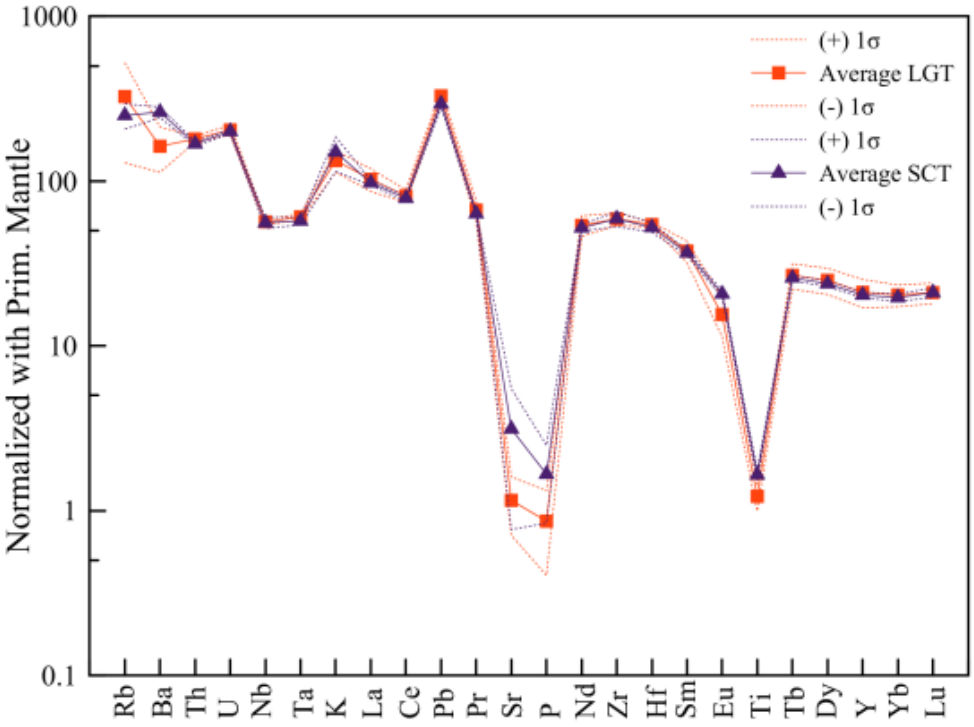

Figure 46. Trace element diagram for tuff of Leslie Gulch and tuff of Spring Creek averaged data. Normalized to primitive mantle values from Sun and McDonough, 1989.

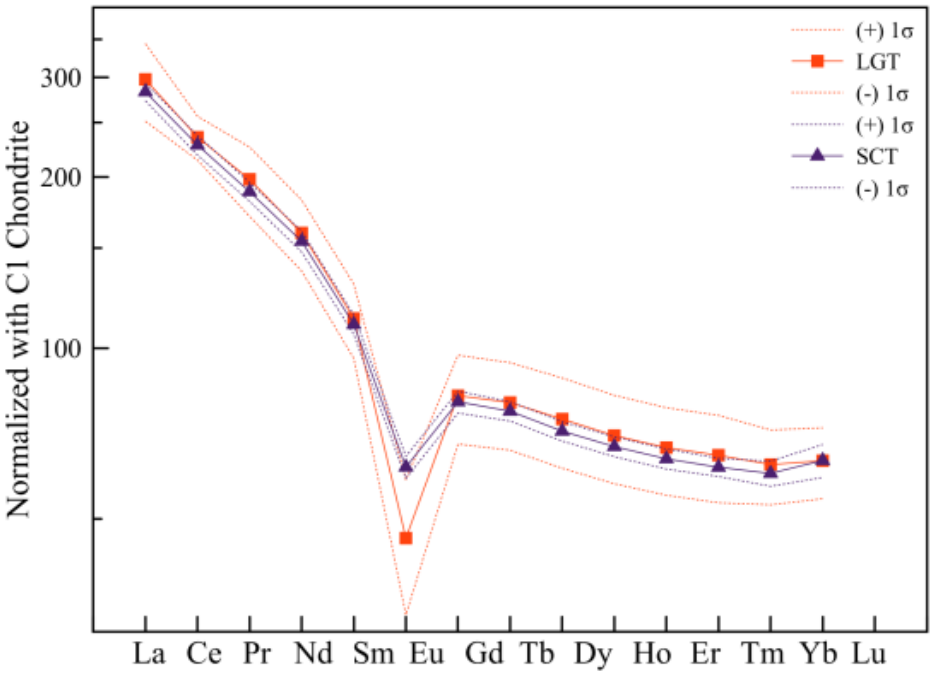

Figure 47. Tuff of Leslie Gulch and tuff of Succor Creek rare earth element diagram, normalized to chondrite values from McDonough and Sun, 1995.

4.3.3 Pyroclastic Samples

These include the surge deposits, lapilli tuffs, welded tuffs, and fine ash layers described in the earlier description of units. Except for welded tuff sample CB-19-67, all have high loss on ignition (LOI) values. Because of this, these samples have not been included for the compositional affinity evaluations of rhyolites. High LOI can be associated with element mobility alter the composition of the sample, particularly sodium and potassium.

Plotting the data for these green tuff samples along with LGT and SCT data, it appears that some of these samples plot within the constraints of LGT and SCT (Figure 48). Five of the samples have high Ba concentrations, and the other five have low Ba concentrations (Figure 48). There are also similarities with the SiO_2 wt% with the low Ba having higher SiO_2, and inversely low SiO_2 samples have high Ba concentrations. Figure 49 and Figure 50 show that the Green Tuff samples plot closely follow similar trends to the SCT, but have lower concentrations, especially in the REE diagram (Figure 50). In summary, based on bulk composition data alone, the green tuff samples could be associated with either rhyolite unit. For this reason, it is stratigraphic constraints along with age dates that is given preference in assigning which eruptive event green tuff samples belong to (see Discussion).

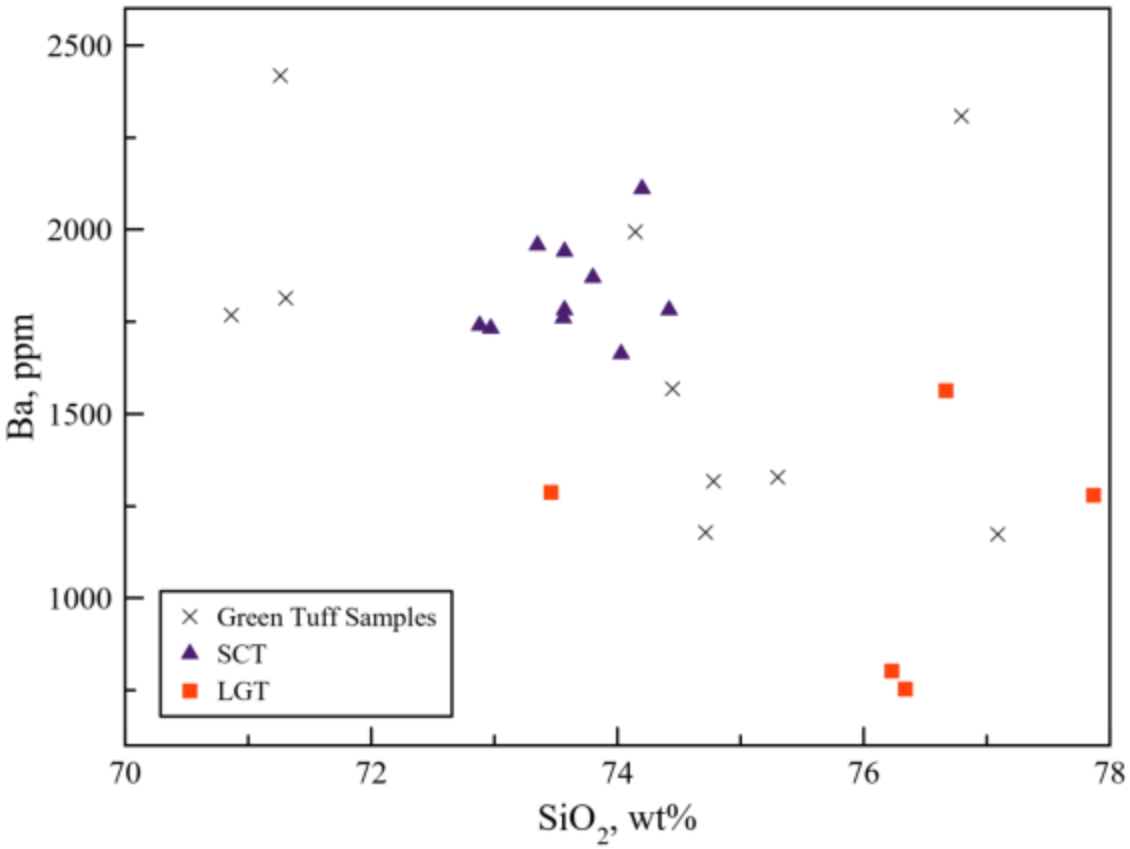

Figure 48. Green tuff samples plotted along with SCT and LGT samples.

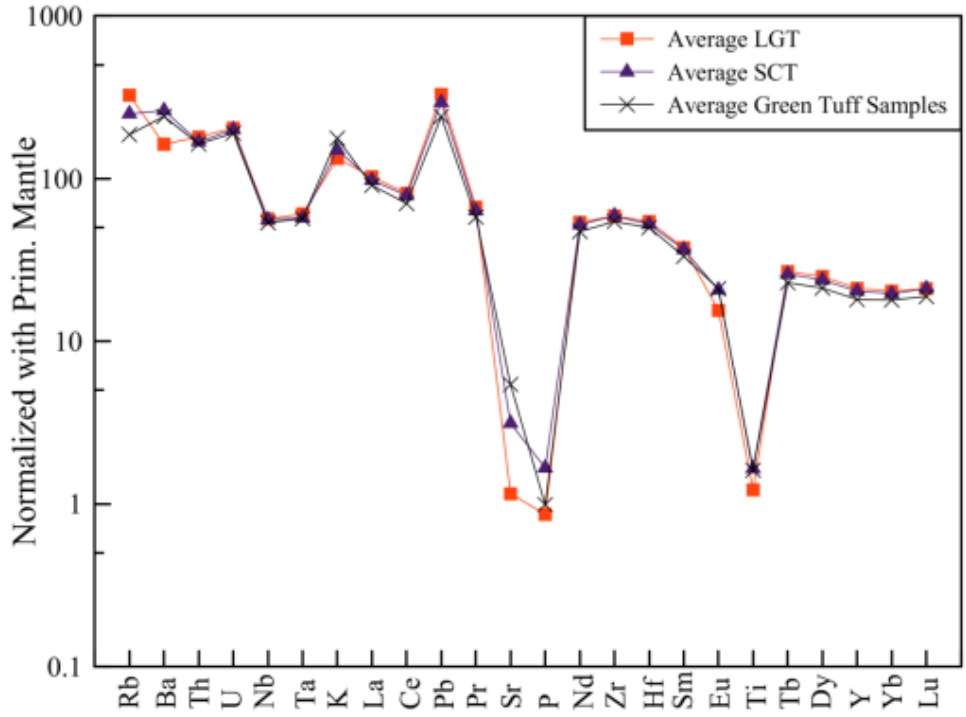

Figure 49. Trace element diagram of SCT and LGT data with Green Tuff sample data added. Normalized to primitive mantle from Sun and McDonough, 1989.

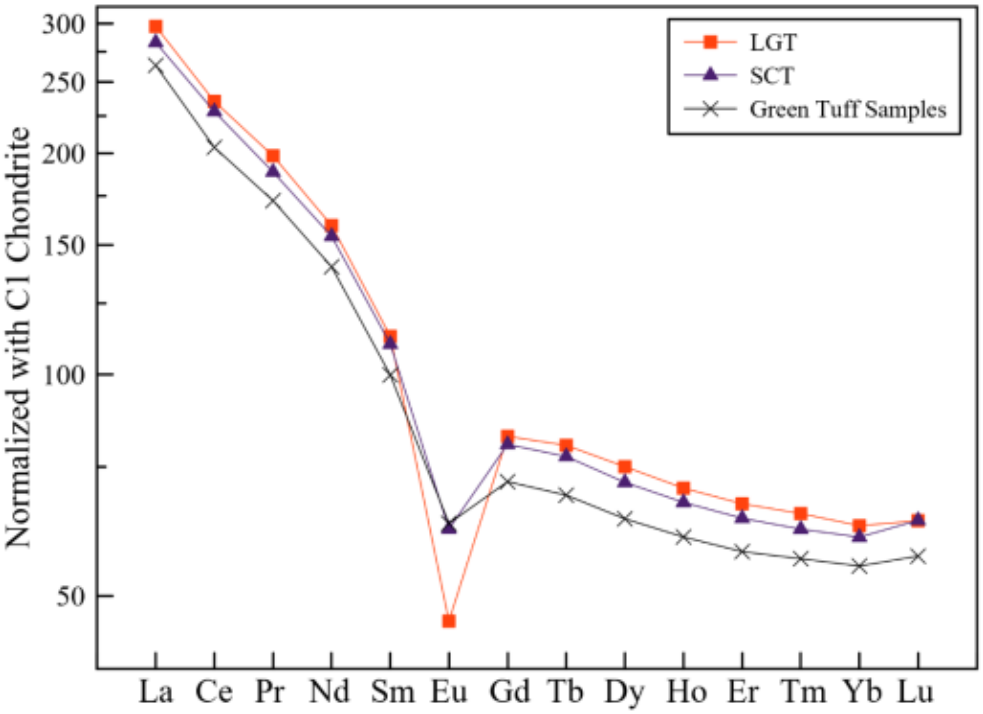

Figure 50. Rare earth element diagram of SCT and LGT data with Green Tuff samples added. Normalized to McDonough and Sun, 1995.

4.3.4 Top Unwelded Ignimbrite of "Grey Tuff" Section

Three samples of the top unwelded ignimbrite (TUI) were analyzed, including the fine grained, medium grained, and lithic rich samples of the section. To determine if this was an individual unit, or if part of one of the other samples or its own separate unit, they were plotted together using elements that were already determined to be distinctive between the rhyolite units. Figure 51 shows Ba concentrations plotted against FeO^{*} and Zr. Ba concentrations of the top unwelded ignimbrite range from 214 to 488 ppm. FeO* concentration range from 2.74 to 5.61 wt%. Zr concentration range from 232 to 326 ppm. Though the range of FeO* overlaps with tuff of Leslie Gulch, Old McIntyre Rhyolite, and tuff of Succor Creek, the lower Ba concentration distinguishes this top ignimbrite unit from the others. Similar range in Ba and Zr concentrations as observed in the top unwelded ignimbrite are found among samples of the Young McIntyre Rhyolite. Rare earth elements are considerably lower for the top unwelded ignimbrite unit compared to all others, except for the Eu depletion where Young McIntyre has a greater depletion than the TUI (Figure 52).

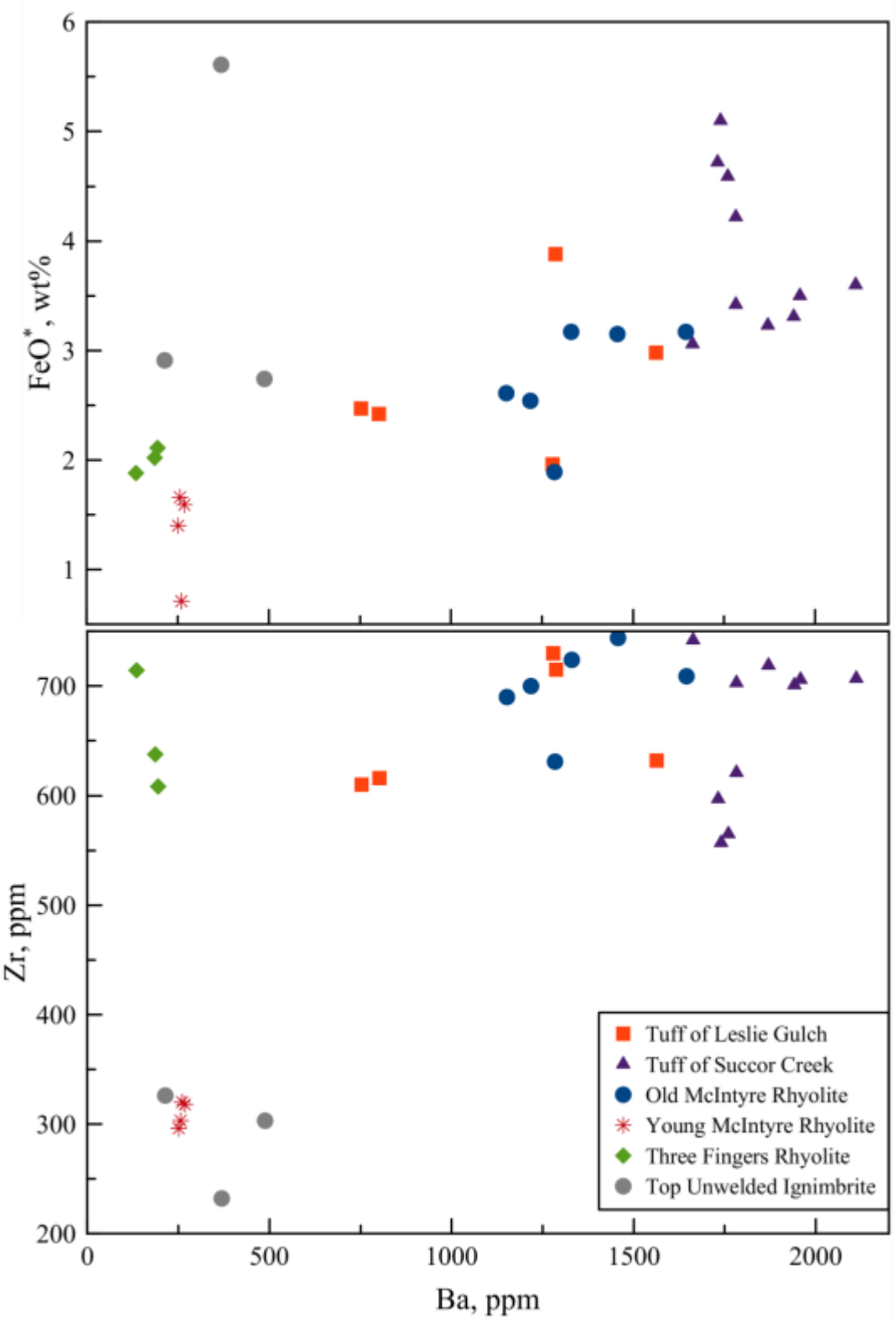

Figure 51. Ba vs FeO* and Zr plots showing distinction between units.

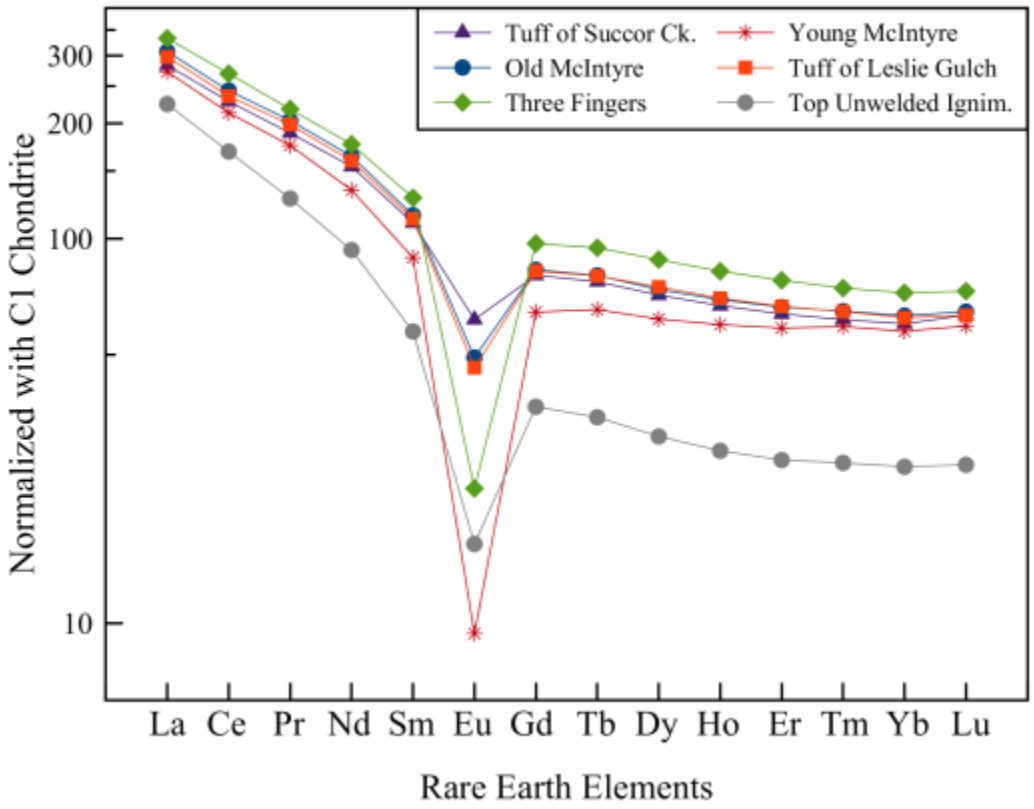

Figure 52. Rare earth element diagram of averaged data for all units, normalized to chondrite of McDonough and Sun, 1995.

With the above, it is conceivable that these tuffs either represent an early explosive phase of Young McIntyre rhyolite or are sourced from an eruptive center elsewhere in the Mahogany Mountain – Three Fingers rhyolite field or beyond.

4.3.5 Mafic Samples

Compositions of the six mafic samples range from basalt to basaltic trachyandesite. The two basalt samples, CB-19-71 and CB-19-88 were collected from dikes (Figure 37), one near to the Sawtooth section and the other on the eastern side of the Succor Creek road. These two samples are Picture Gorge Basalt-like, plot adjacent to Picture Gorge Basalt data from Cahoon et al. (2020), and these samples exhibit the characteristically low Th concentration described by Cahoon et al. (2020) (Figure 53).

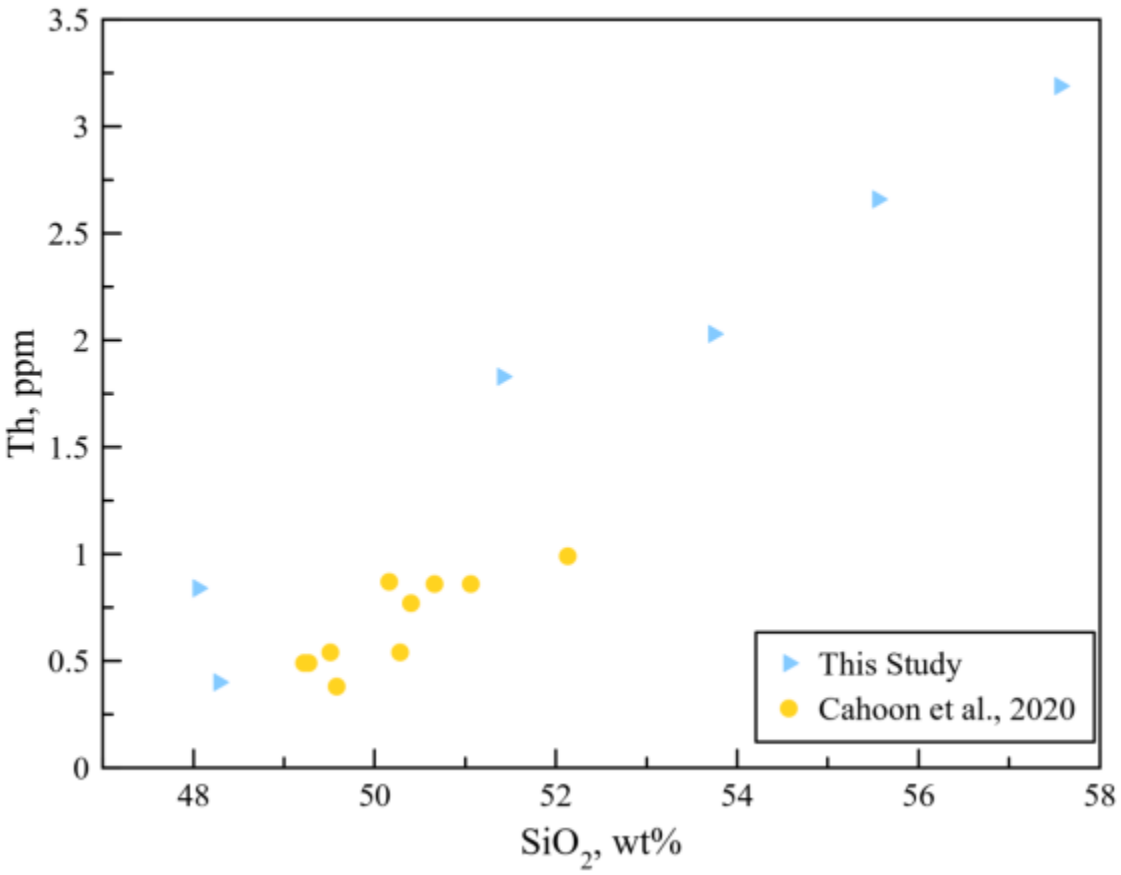

Figure 53. Mafic samples from this study plotted with data from Cahoon et al., 2020. Samples CB-19-71 & CB-19-88 collected from dikes in this study plot along previously determined PGB samples (yellow circles). The remaining four mafic samples from this study (blue triangles) have Th values greater than 1.5ppm.

Comparing the compositions of basalt dike samples CB-19-71 & CB-19-88 with Columbia River Basalt Group data from Wolff et al., (2008) provides further evidence for these samples being Picture Gorge Basalt-like (Figure 54). Of the Columbia River Basalt Group shown in this figure, the Picture Gorge Basalt (PGB) has characteristically lower concentrations of most trace elements. Sample CB-19-71 plots most similar to the PGB trace elements, and sample CB-19-88 follows the general PGB trend but has lower concentrations of most trace elements.

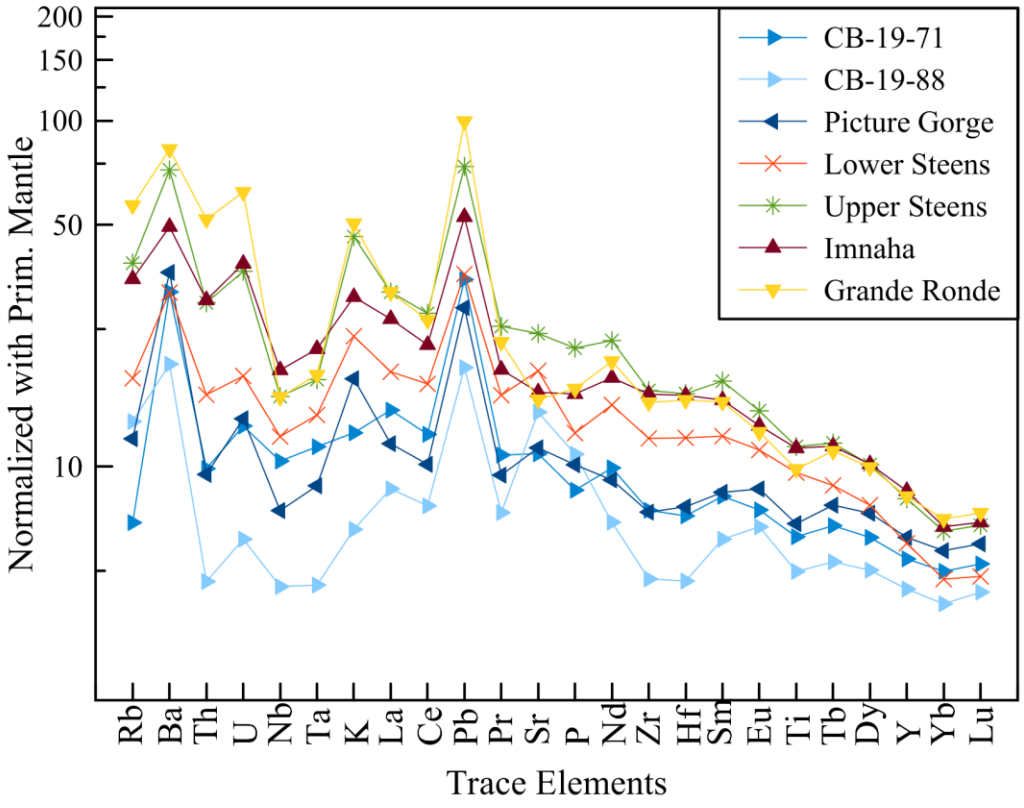

Figure 54. Average spider diagram of trace elements of Columbia River Basalt group data. Picture Gorge, Lower Steens, Upper Steens, Imnaha, and Grande Ronde data from Wolff et al., 2008. Samples CB-19-71 and CB-19-88 data from this study. Normalized to primitive mantle from Sun and McDonough, 1989.

4.4 Age Data

Three new $^{40}Ar/^{39}Ar$ ages have been determined for select samples of the study area. These include a pumice rich lapilli tuff sample from the basal exposure of the green tuff at Road Cut North section, a rhyolite lava capping the green tuff at the Road Cut South sections and that we correlate with the "Old" McIntyre Rhyolite (OMR), and a rhyolite lava sample capping the welded ignimbrite at McIntyre section and that we also correlate with the "Old" McIntyre Rhyolite (OMR). A sample of a tuff of Succor Creek lava was also sent to be dated, but the results have not yet been returned, though based on previous studies it is estimated this sample should be approximately 15.75 Ma.

Table 1. Plateau and Normal Isochron $^{40}Ar/^{39}Ar$ dates for tuff of Leslie Gulch, Young McIntyre, and Old McIntyre samples. "Mat. Dated" refers to "Material Dated", and "San" refers to sanidine.

			Plateau					Normal Isochron		
Sample ID	Unit	Mat. Dated	Age (Ma)	±2σ	Steps Plateau (n)	^{39}Ar (%)	MSWD	Age (Ma)	±2σ	Isochron MSWD
CB-18-02	TLG	San	15.98	0.05	21	74	4.3	15.99	0.05	3.84
CB-19-44	OMR	San	15.95	0.03	30	100	19.81	15.96	0.05	22.06
CB-19-65	OMR	San	16.02	0.02	30	100	4.55	16.02	0.03	4.87

4.5 Mineral Compositions

4.5.1 Pyroxenes

Pyroxene elemental data for eleven samples was measured using the SEM and the Electron Microprobe. Data previously acquired by the electron microprobe by Marcy (2013) and Streck (unpublished) were added in the evaluation to investigate the compositional spread of rhyolites observed in the study area and just adjacent to it. All samples plot as augite, and no sample has more than one type of pyroxene. Sample MS-13-24b, Young McIntyre, has compositional range of Wo_{41-43}, En_{13-20}, Fs_{37-44}, and is the only sample with an En concentration greater than 10%. The other samples were all En poor, with very low concentrations. Tuff of Leslie Gulch have compositional range of Wo_{42-43}, En_{0-1}, $Fs_{55-56.}$ Old McIntyre compositions range from Wo_{41-44}, $En_{0.14-0.8}$, and Fs_{55-58}. Tuff of Succor Creek samples have pyroxene compositions of Wo_{41-45}, En_{0-8}, and Fs_{49-55}. Finally, Three Fingers Rhyolites have ranges of Wo_{43-45}, En_{0-1}, and Fs_{54-55}. The averages of these samples are plotted on a ternary diagram in Figure 55. While pyroxene compositions are strongly overlapping in terms of pyx components, except for the Young McIntyre sample, minor elemental composition are more distinct among units (Figure 56).

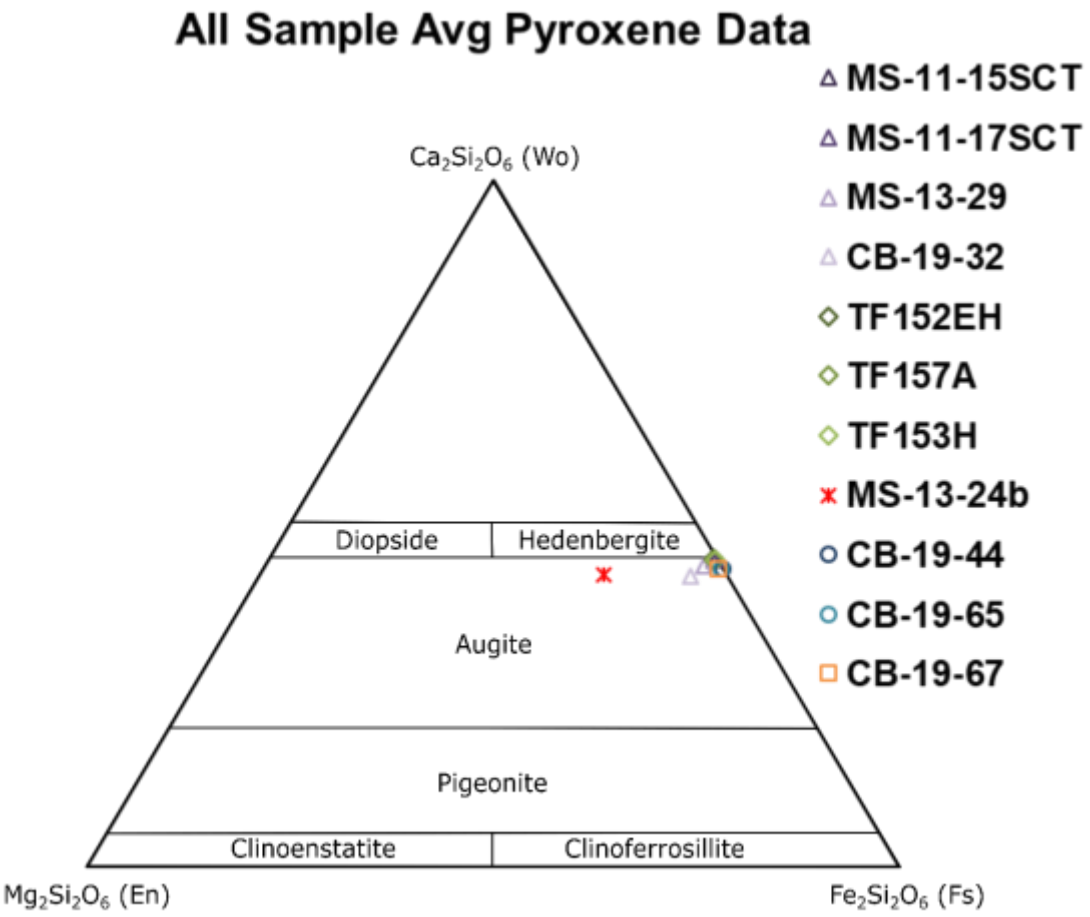

Figure 55. Pyroxene ternary diagram of average pyroxene compositions for each sample. Purple triangle symbolizes tuff/rhyolite of Succor Creek samples (MS-11-15SCT, MS-11-17SCT, MS-13-29, and CB-19-32). Green diamond symbolizes Three Fingers Rhyolites samples (TF152EH, TF157A, and TF153). Red star symbolizes Young McIntyre Rhyolite sample MS-13-24b. Blue circles symbolize Old McIntyre Rhyolite samples (CB-19-44 and CB-19-65). Orange square symbolizes tuff of Leslie Gulch sample CB-19-67.

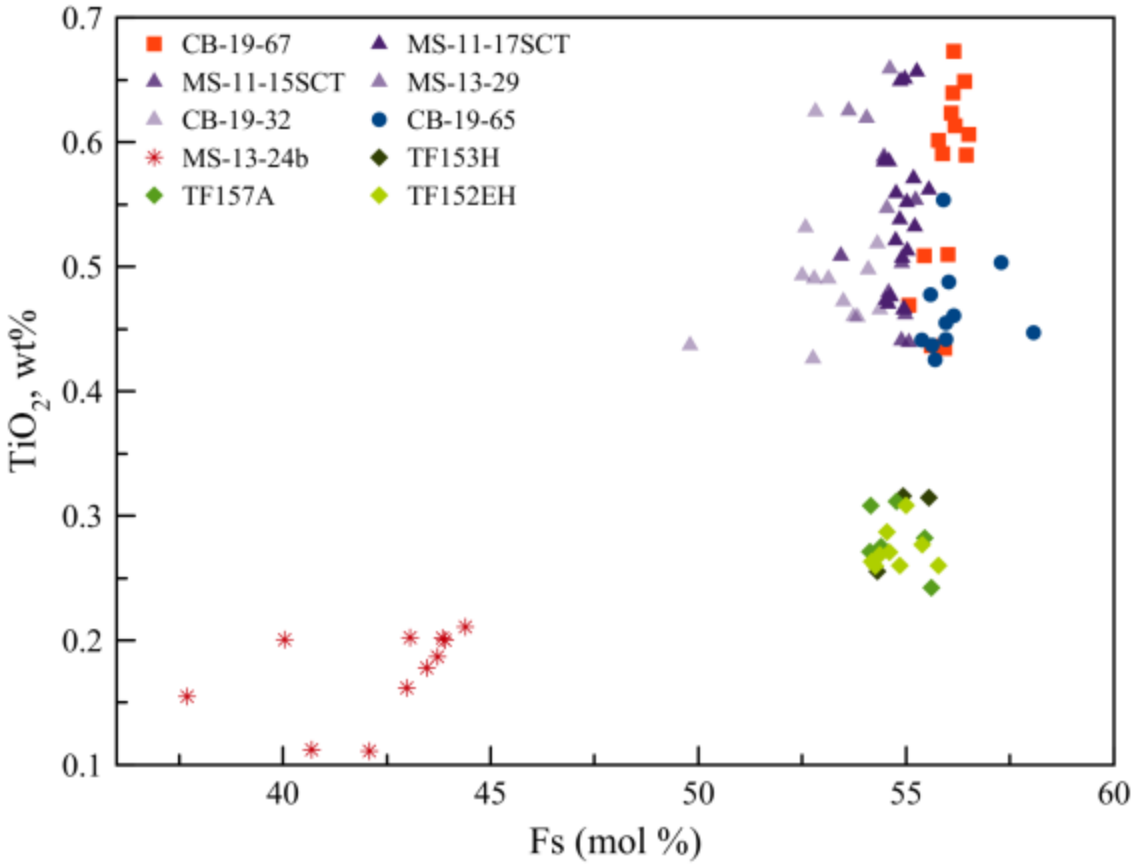

Figure 56. TiO2 vs Fs electron microprobe pyroxene data. Purple triangle symbolizes tuff/rhyolite of Succor Creek samples (MS-11-15SCT, MS-11-17SCT, MS-13-29, and CB-19-32). Green diamond symbolizes Three Fingers Rhyolites samples (TF152EH, TF157A, and TF153). Red star symbolizes Young McIntyre Rhyolite sample MS-13-24b. Blue circles symbolize Old McIntyre Rhyolite sample CB-19-65. Orange squares symbolize tuff of Leslie Gulch sample CB-19-67.

4.5.2 Feldspar Data

Feldspar compositional data for six samples from this study was combined with feldspar data from additional work completed in the area. This includes data from tuff of Leslie Gulch, tuff of Succor Creek, Old and Young McIntyre, Three Fingers rhyolite, and green tuff samples. The average feldspar compositions of these samples are found in Figure 57. Of the nineteen samples analyzed, nine samples have only sanidine, six samples have only anorthoclase, three samples have both anorthoclase and sanidine feldspars, and one sample has anorthoclase and oligoclase.

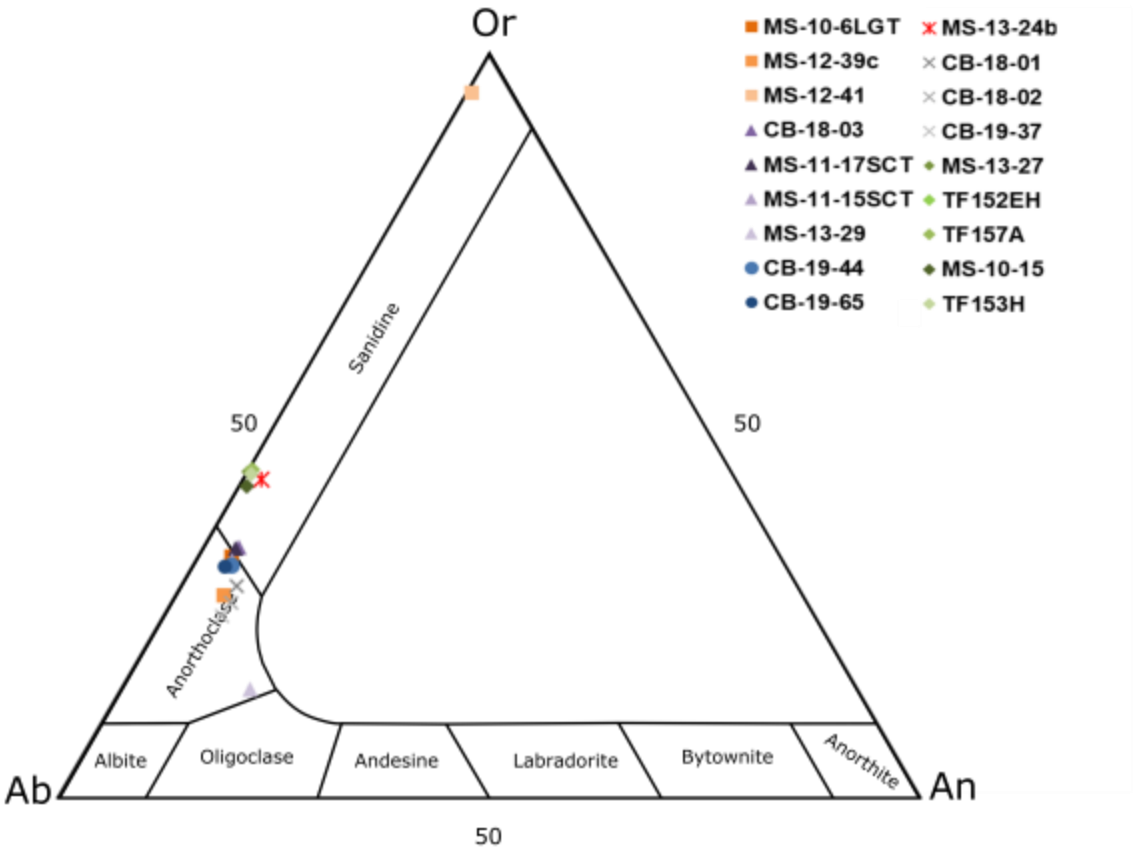

Figure 57. Average feldspar compositions of samples. Purple triangle symbolizes tuff/rhyolite of Succor Creek samples (MS-11-15SCT, MS-11-17SCT, MS-13-29, and CB-19-32). Green diamond symbolizes Three Fingers Rhyolites samples (MS-13-27, MS-10-15, TF152EH, TF157A, and TF153). Red star symbolizes Young McIntyre Rhyolite sample MS-13-24b. Blue circles symbolize Old McIntyre Rhyolite samples (CB-19-44 and CB-19-65). Orange square symbolizes tuff of Leslie Gulch samples (MS-10-6LGT, MS-12-39c, MS-12-41). Grey x symbolizes green tuff samples (CB-18-01, CB-18-02, and CB-19-37).

5. Discussion

5.1 Interpreting Ages of Units along the eastern margin of Mahogany Mountain – Three Fingers Rhyolite Field

5.1.1 Age Constraints of 'Green Tuff' Samples

Samples included in the geochemical grouping "green tuff samples" were collected from all stratigraphic sections other than the Grey Ash section. Due to the high LOI values, we choose to examine age dates and stratigraphic relationships to determine which eruptive unit they are a part of. Sample CB-18-02, a non-welded pumice rich lapilli tuff, was collected from the base of the Road Cut south stratigraphic section. The $^{40}Ar/^{39}Ar$ age of this sample is 15.98 ± 0.05 Ma. This age best correlates with previous ages obtained for the tuff of Leslie Gulch (Martin Streck, personal communication). Streck and others have dated two samples of the tuff of Leslie Gulch collected from Leslie Gulch and produced ages of 15.88 ± 0.03 and 15.86 ± 0.05 Ma, respectively.

5.1.2 Comparing ages of Old McIntyre Rhyolite and tuff of Leslie Gulch

For this study, two samples of Old McIntyre Rhyolite were dated. One from the top of the McIntyre Section and the other from the top of the middle Road Cut section. $^{40}Ar/^{39}Ar$ ages of these were 16.02 ± 0.02 Ma and 15.95 ± 0.03 Ma, respectively (Table 2). The age of the overlying Old McIntyre in the Road Cut section is indistinguishable from the age of the tuff of Leslie Gulch also collected in this section, 15.98 ± 0.05 Ma (Figure 56). This overlap in ages and similar compositions suggests that magma that

produced the Old McIntyre Rhyolite and the one that generated the composite tuff of Leslie Gulch are part of the same magma body.

Figure 58. Stratigraphic relationships in the Road Cut sections.

5.1.3 Distinguishing Old and Young McIntyre Rhyolites

The two new ages dates and geochemical data produced by this study help to further distinguish between an Old and Young McIntyre rhyolite. Previous work by Benson and Mahood (2016) and Ferns (1993) suggested the McIntyre Ridge rhyolite was a single unit. Hess (2014) dated two samples of McIntyre Ridge rhyolite, Old McIntyre which dated to 15.94 ± 0.16 and Young McIntyre which dated to 15.76 ± 0.02. The date for this Old McIntyre unit correlates with the two age dates from this study and are within error of one another. A clear age difference of approximately 200 - 250 k.y. is present between the eruptions of the Old McIntyre Rhyolite and the Young McIntyre Rhyolite.

5.1.4 Rhyolite of Succor Creek

At the time of this writing, a sample of the rhyolite of Succor Creek is in progress for $^{40}Ar/^{39}Ar$ dating, though has not yet been completed. It is presumed to return an age date of approximately 15.75 Ma. This estimate is based on the tuff of Succor Creek

sample dated by Marcy (2013), which produced an $^{40}Ar/^{39}Ar$ age date of 15.74 ± 0.09. These rhyolites are compositionally very similar to the tuff of Succor Creek, although also similar to both the composite tuff of Leslie Gulch and Old McIntyre. If this date holds true for the rhyolite of Succor Creek sample, this suggests the rhyolite of Succor Creek and the tuff of Succor Creek represent the same magma body yet record an effusive as well as an explosive eruptive episode. Also, both represent a unit younger than the composite tuff of Leslie Gulch/ Old McIntyre rhyolite. I will also draw from stratigraphic evidence to further shed light on this observation (see below).

Table 2. $^{40}Ar/^{39}Ar$ age dates of samples in the Three Fingers - Mahogany Mountain volcanic field, in order from oldest to youngest. Data from: [1]This study, [2]Streck and others (personal communication), [3]Hess (2014), [4]Marcy (2013), [5]Benson and Mahood (2016).

Unit	Sample ID	Age (Ma)	Error (±2σ)
Old McIntyre Rhyolite[1]	CB-19-65	16.02	0.02
Old McIntyre Rhyolite[5]	TB-112	16.01	0.27
Tuff of Leslie Gulch[1]	CB-18-02	15.98	0.05
Tuff of 'Spring Creek'[5]	TB-304A	15.97	0.37
Old McIntyre Rhyolite[1]	CB-19-44	15.95	0.03
Tuff of Leslie Gulch[5]	TB-109	15.94	0.05
Old McIntyre Rhyolite[3]	EJ-12-12	15.94	0.16
Tuff of 'Spring Creek'[5]	TB-161	15.93	0.04
Tuff of Leslie Gulch[2]	MS-10-06	15.88	0.03
Tuff of Leslie Gulch[2]	MS-12-39b	15.86	0.05
Three Fingers Rhyolite[5]	TB-196	15.82	0.06
Young McIntyre Rhyolite[3]	EJ-12-14	15.76	0.02
Three Fingers Rhyolite[4]	TF88A	15.74	0.08
Tuff of Succor Creek[2]	MS-11-15SCT	15.74	0.09

5.2 Stratigraphic Relationships within the Three Fingers Caldera

5.2.1 Stratigraphic constraints on eruptive sequence

Obtained radiometric ages from samples throughout the study area overlap with analytical error. The ages are also inconsistent and do not show a clear age trend. Younger ages are found in lower stratigraphic units and vice versa and thus conflict with stratigraphic principles. Despite that the new radiometric ages are highly precise with 2 sigma errors mostly on the order of 20,000 to 90,000 years (Table 2). This clearly indicates the resolutions of these ages are insufficient to resolve the eruptive chronology, and thus we rely on the careful evaluation of stratigraphy outlined above to draw our conclusions. Figure 59 shows a basic schematic stratigraphic column outlining the likely eruptive stratigraphy of the study area.

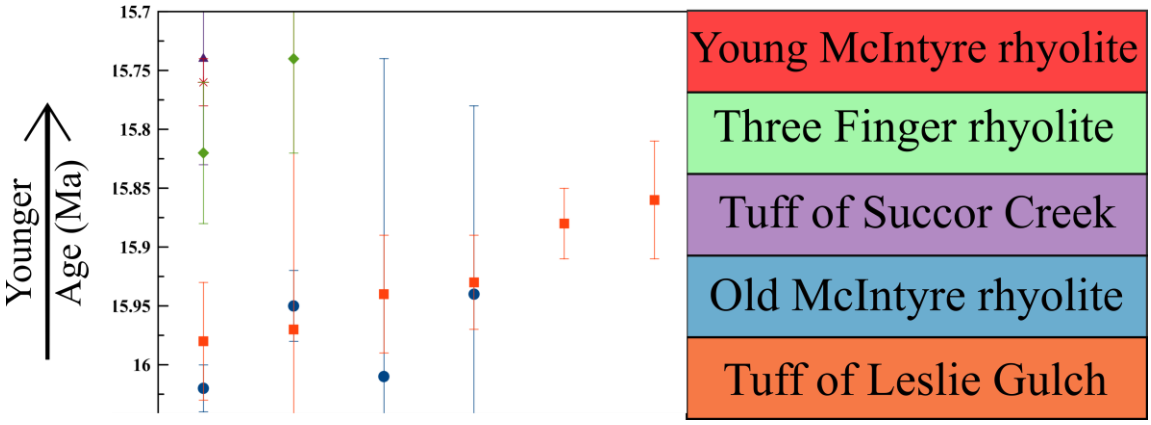

Figure 59. Schematic stratigraphic column of the units within the study area.

Throughout the study area, specifically in the Road Cut sections, Western Section, and McIntyre Section, Old McIntyre overlies the composite tuff of Leslie Gulch indicating that composite tuff of Leslie Gulch erupted before Old McIntyre, despite that $^{40}Ar/^{39}Ar$ ages of Old McIntyre are generally older than the LGT. Furthermore, Old McIntyre rhyolite underlies Young McIntyre rhyolite in the Road Cut section (Figure 58) indicating that it erupted before. Though the ages and compositions of the tuff of Leslie Gulch and Old McIntyre are similar, it is also the emplacement styles which help to differentiate them. Old McIntyre is an effusive rhyolite lava while the tuff of Leslie Gulch was generated during pyroclastic eruptions. Furthermore, the earlier eruptions of the tuff of Leslie Gulch must have been influenced by the interaction with water, as evidenced by the deposition style of surges deposits and pervasive clinoptilolite as the secondary alteration mineral (Benson and Mahood, 2016) and thus had lower emplacement temperatures. The later tuff of Leslie Gulch deposits had higher temperature emplacement, as the interaction with water subsided.

Furthermore, rhyolite of Succor Creek is younger than tuff of Leslie Gulch based on the intrusive relationships. No field stratigraphic relationships have been found to place Succor Creek rhyolite, Young McIntyre rhyolite, and adjacent rhyolites to the west, Three Fingers rhyolite, in a chronological order and hence our eruptive sequence is inferred based on both chemical and mineralogical data for these lithologies. The rhyolite/ tuff of Succor Creek is closest in composition to overlying units, tuff of Leslie Gulch and Old McIntyre (Figure 49, Figure ***51***) while the Three Fingers and Young McIntyre rhyolites are considerably more differentiated (with lower Ba, lower Eu/Eu*

trace elements (Figure 51,Figure *52*)). Thus, of these three the rhyolite/ tuff of Succor Creek is likely the oldest, followed by Three Fingers, and the youngest unit is the Young McIntyre which may correlate with tuffs of the Grey Tuff section (aka Lonesome tuff, see section 5.3.2).

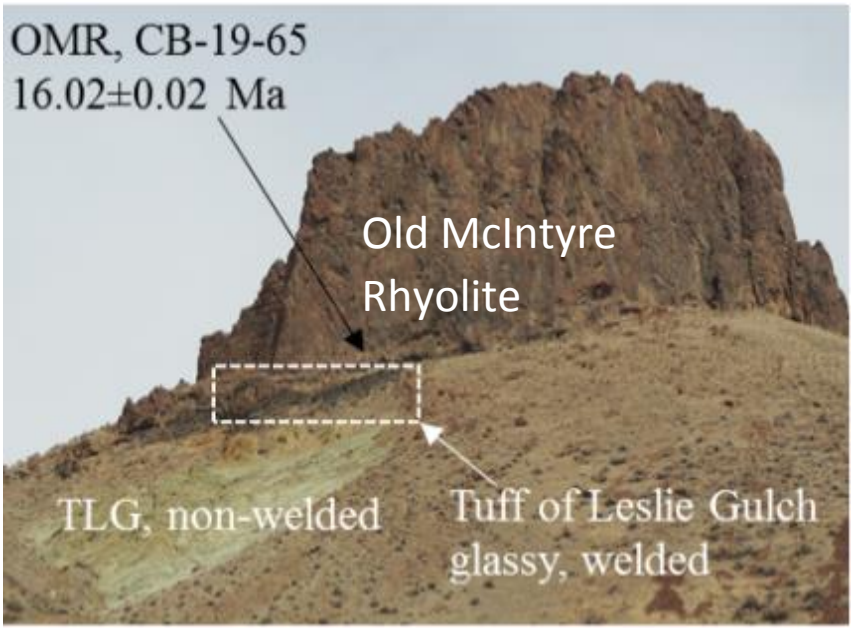

Figure 60. Field photo of McIntyre Stratigraphic section highlighting main units found in this section; tuff of Leslie Gulch and Old McIntyre rhyolite.

In short, the sequence of stratigraphy begins with the eruption of andesite lava that crop out below the tuff of Leslie Gulch at the McIntyre section. This was followed by the deposition of the tuff of Leslie Gulch deposits that occurred between 15.85 Ma and 16.0 Ma. The tuff of Leslie Gulch was followed by the eruption of the Old McIntyre rhyolite. The rhyolite of Succor Creek then intruded the tuff of Leslie Gulch in the middle of the study area. The Young McIntyre rhyolite erupted after the rhyolite of Succor Creek. The Sucker Creek formation was deposited above the tuff of Leslie Gulch, with an

unconformity between the units observed. At this point, it is likely that the dikes of Picture Gorge-like basalts intruded Rhyolite of Succor Creek and Sucker Creek Formation. Post deposition of the Sucker Creek formation, normal faulting continued.

Comparing the schematic stratigraphic section in Figure 59 to the schematic sections composed of Benson and Mahood (2016) and Vander Meulen (1989) findings (Section 2.3; Figure 3 and Figure ***4***), this study provides a more detailed and comprehensive eruptive story. This study differs from Benson and Mahood (2016) as it divides the McIntyre rhyolite into two separate units, rearranges the tuff of Leslie Gulch and Old McIntyre, and introduces the tuff of Succor Creek. This study also differs from Vander Meulen (1989) similarly to the difference with Benson and Mahood (2016) and eliminates the name of the tuff of Spring Creek, and detailing more of the pre and post caldera units.

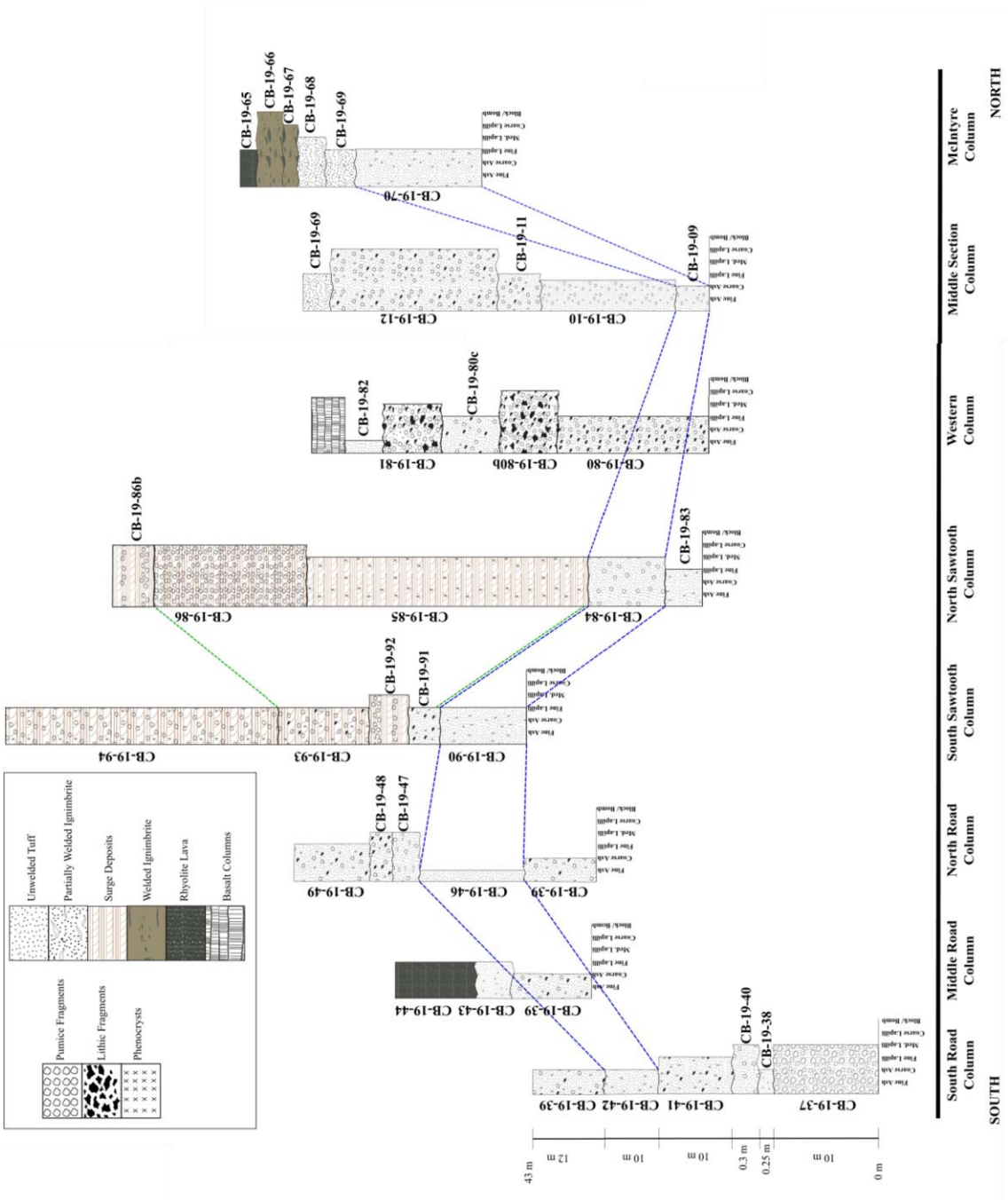

Figure 61. Stratigraphy of the eight main stratigraphic sections in the study area from south to north. Blue dotted lines join the correlative fine ash 'datum'. Green dashed line between correlative surge deposits.

5.2.2 Faulting and Intrusive Relationships

Rhyolite of Succor Creek is stratigraphically lower than and seemingly overlain by the older units. To explain how this younger unit is mapped below older units, we suggest that the rhyolite of Succor Creek in the middle of the study area could be the result of intrusive relationships and represent a crypto dome. Additionally, complex horst and graben extensional faulting is observed to postdate emplacement and offsets the rhyolite. If this is a crypto dome, it would have be emplaced horizontal to sub horizontal and any tilt is interpreted to reflect post emplacement deformation of the unit. We document evidence for complex crypto dome-like intrusion and normal faulting (Figure 63, Figure 64). Three outcrops of these rhyolites are found at the northern edge of the road columns, exposures continue for almost 1 km north (Figure 62). The dikes slightly to the north of the base of the road columns underlie and cut through the tuff of Leslie Gulch. Two other dikes have well exposed contacts with the tuff of Leslie Gulch (Figure 62). The northernmost exposure of these rhyolite magma dikes is overlain by mostly tuffaceous sediments of the younger Sucker Creek formation that unconformably overlies the section of dike and tuff of Leslie Gulch as seen in Figure 63 and in Figure 64 as the white and light brown tilted layers to the left of the dike. The Sucker Creek formation is composed of sedimentary and volcanic units of middle to late Miocene in age (Kittleman et al., 1965).

Figure 62. Rhyolite of Succor Creek dikes (labeled as intrusive contacts) cutting through and underlying composite tuff of Leslie Gulch. The tuff of Leslie Gulch is bright green in this image, the intrusive contacts are labeled and form ridges dark tan-brown in color that disrupt the outcrops of Leslie Gulch. Image from Google Earth.

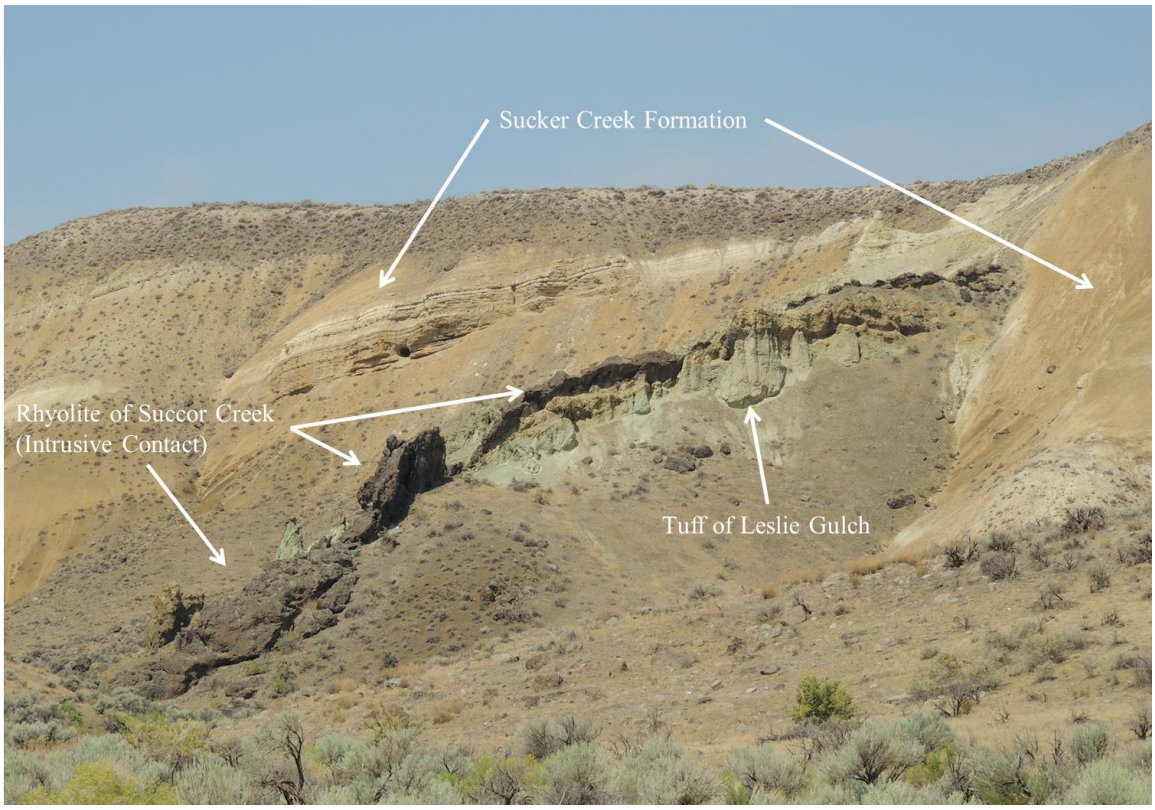

Figure 63. Rhyolite of Succor Creek cutting through composite of Leslie Gulch country rock.

The Sucker Creek formation is also exposed at lower elevation than the prominent ridge with Old McIntyre rhyolite overlying LGT at the McIntyre section (Figure 64) and because of this, prior work suggested that the Sucker Creek formation is older than the ridge capping OMR (Lawrence, 1988). Contrary to that, we propose that the Sucker Creek formation (on the hanging wall) is down dropped by normal faulting and placed in a fault contact with older stratigraphic units of tuff of Succor Creek and tuff of Leslie Gulch on the footwall. This juxtaposition of younger lithologies against older lithologies combined with earlier inflation of older stratigraphy from a rhyolitic intrusion has resulted in the complex stratigraphic and structural relationships observed in this area (Figure 63)., Normal faulting offset the strata of Sucker Creek formation and possibly

rhyolite of Succor Creek as is also suggested by the ~15 degree tilt of the presumed formerly horizontal layers of the Sucker Creek formation (Figure 64). This faulting may have been first active sometime after the eruption of the Old McIntyre Rhyolite and before the emplacement of the younger Sucker Creek formation but continued to be active afterwards to fault the Sucker Creek formation itself as also seen in Figure 63. Evidence for early initiation comes from other N-S normal faults that affected the Mahogany Mountain – Three Fingers rhyolite field in general and which the fault(s) discussed here are part of. In Leslie Gulch there are nearly vertical, north trending rhyolite dikes (e.g. Fig 18. in Ferns et al., 2017) that were emplaced most likely along such north trending faults. These dikes can be compositionally correlated with Three Fingers rhyolite that yielded ages of 15.82 to 15.74 Ma (Table 2). The rhyolite dikes at Succor Creek, however, may even predate the dikes in Leslie Gulch as erosion clearly removed material as is observed by the unconformity between overlying Sucker Creek formation and section of tuff of Leslie Gulch with rhyolite dike (Figure 64). Initiation of faulting by intrusive activity is a possibility, but doubtful if dikes fed the rhyolite of Succor Creek.

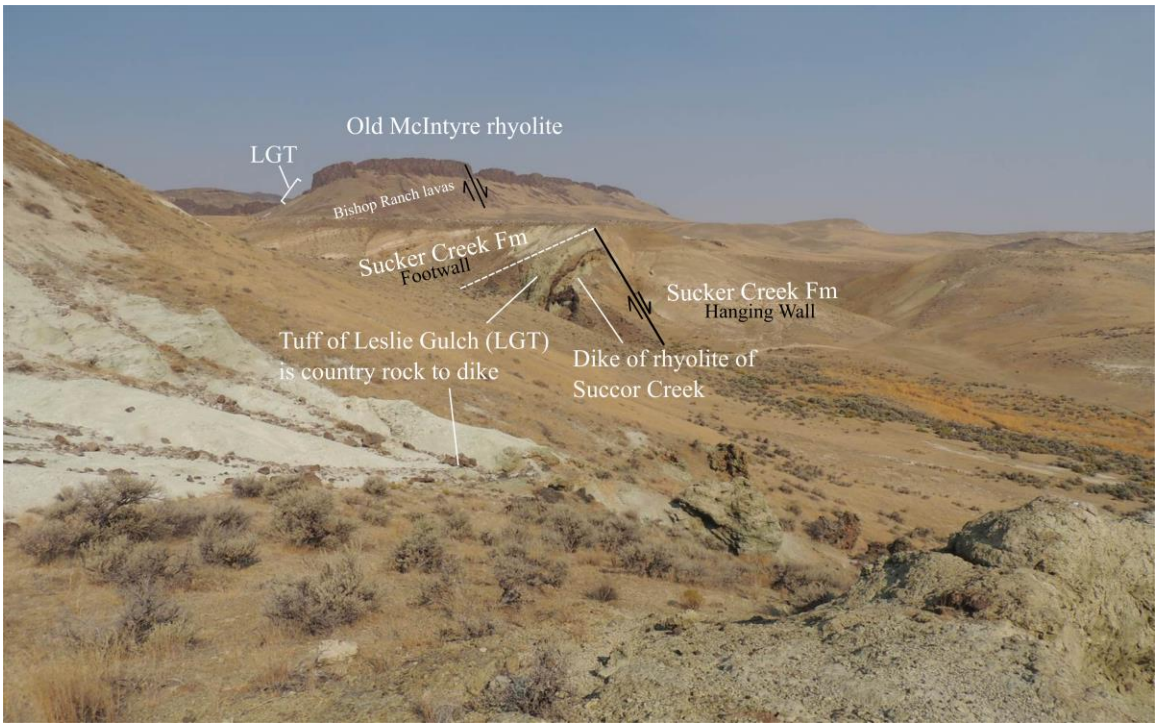

Figure 64. Photo looking northward at fault interpreted east of the McIntyre section. LGT is the tuff of Leslie Gulch. In the foreground a fault is shown in black displacing the tuff of Sucker Creek formation downward on the east, and back-tilting the Sucker Creek formation ~15° on the footwall (to the west) in what is likely a broader horst and graben system of extensional faults in the region. This fault exposure projects to the cliff fault exposure in the background of the photo, which has a similar degree of back-tilt on the footwall – shown by the tilted annotation for the Bishop Ranch lavas.

5.3 Newly named units of the Mahogany Mountain - Three Fingers rhyolite field

5.3.1 Composite tuff of Leslie Gulch

The composite tuff of Leslie Gulch includes the ignimbrites, surge deposits, and other pyroclastic deposits, and fall deposits found throughout the entire study area. While the stratigraphy is variable, we generally see a lower and upper pyroclastic flow section, mostly non-welded. Separating the two is a fine grained section. A densely welded ignimbrite is found in the north of the study area directly underlying the Old McIntyre Rhyolite. The composite tuff of Leslie Gulch began erupting at 16.0 Ma and finished erupting at approximately 15.86 (Streck and others, personal communication; Marcy, 2013).

5.3.2 Tuff of Succor Creek

After careful mapping and consistent application of a stratigraphic datum we find that units that were previously mapped as intra caldera tuff of Spring Creek by Vander Meulen (1989) along Succor Creek are actually part of the composite tuff of Leslie Gulch as based on stratigraphic and age dates presented here. Marcy (2014) and Ferns et al. (2017) previously recognized a second series of younger ignimbrites which are exposed along the eastern margin of the study area which they called the tuff of Spring Creek. These ignimbrites are now renamed here by this study to the tuff of Succor Creek to avoid confusion with the naming in previous studies (e.g. Benson and Mahood, 2016).

5.3.3 Lonesome Tuff

This study also proposes a name for the 'Top Unwelded Ignimbrite' unit, found at the Grey Ash section of the study area (Section 4.1 Stratigraphy; Figure 6). We name this unit the Lonesome Tuff, which is named after Lonesome Road north of the sampled outcrop (Figure 6). This unit is found is a few localities within the northeastern part of the study area and is presumed to be found north of the study area.

The source of the Lonesome Tuff (LT) is unknown. Geochemically, this unit is distinct from the Old McIntyre Rhyolite, tuff of Leslie Gulch, and the tuff of Succor Creek (Section 4.3.4; Figure 51). Compositional similarities with the Young McIntyre Rhyolite suggest that the Lonesome Tuff could potentially be an explosive phase of the YMR, based on the pyroclastic facies observed (Section 4.1 Stratigraphy; Figure 8; Section 4.3.4; Figure 51). Comparing geochemical data of this study with those of Hess (2014), both units have comparable concentrations of some trace and rare earth elements, such as Ba, Sr, Zr, Eu, Rb, and Nb (Figure 65). Trace element concentrations for the YMR samples are in general slightly more enriched than the Lonesome Tuff samples (Figure 65). This enrichment is also observed in the rare earth element diagram though both units have similar Eu depletion, except for Lonesome Tuff sample CB-19-54 (Figure 65). Major element data of these samples is not comparable, which could be attributed to alteration exhibited in the Lonesome Tuff ignimbrite. Future research into the Lonesome Tuff could provide an age date and petrographic analyses to determine if this is an explosive phase of the Young McIntyre Rhyolite.

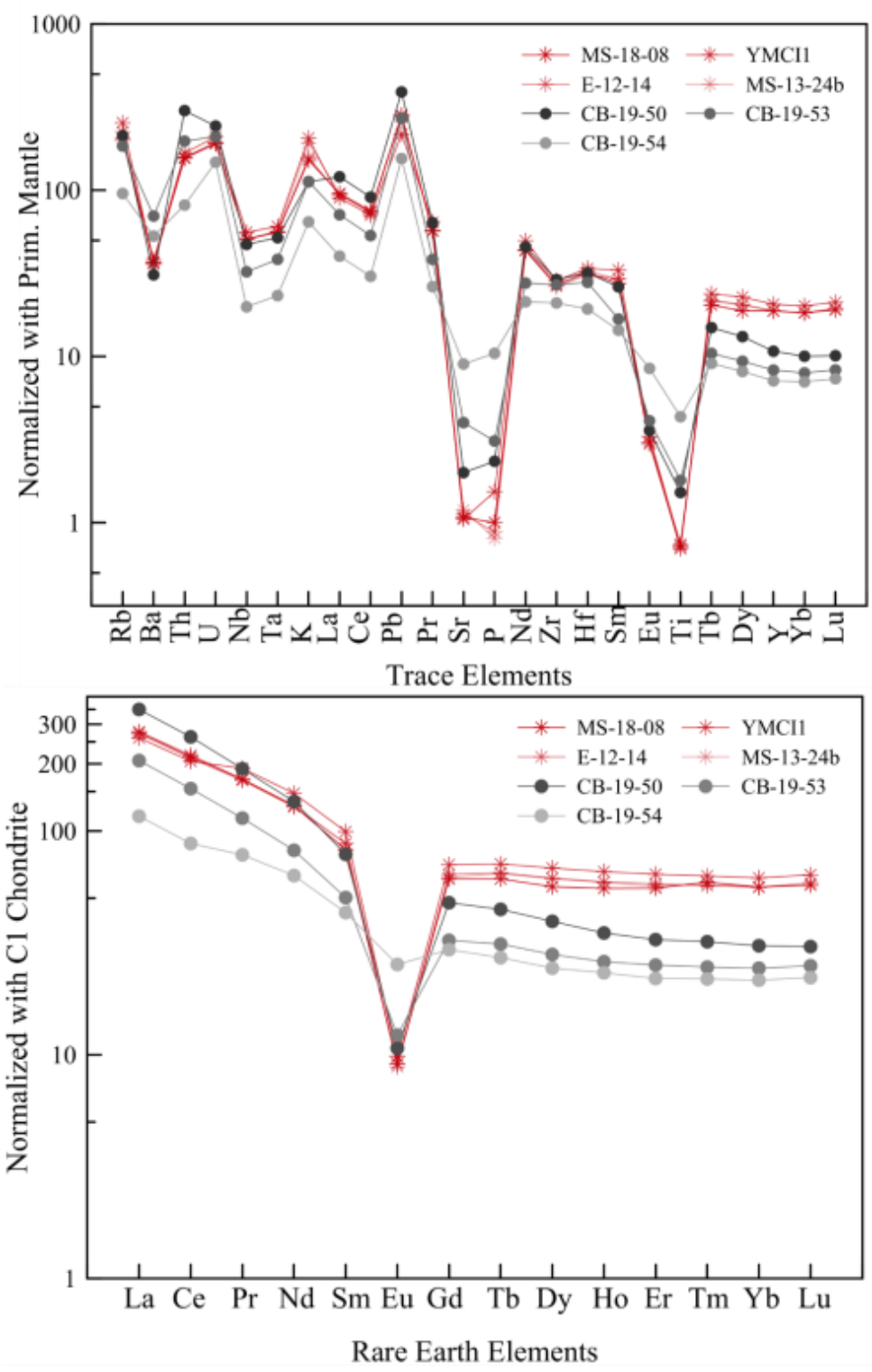

Figure 65. Trace Element and Rare Earth Element diagrams of Young McIntyre Rhyolite (red) from Hess (2014) and Lonesome Tuff (grey) samples from this study.

6. Conclusion

Over 250,000 years between 16.0 to 15.75 Ma, explosive and effusive silicic volcanism was rampant throughout the Mahogany Mountain – Three Fingers Rhyolite Field. This study focuses on the northwestern margin of this rhyolite field along Succor Creek where explosive and effusive rhyolites are intercalated and are key to answering outstanding questions about provenance and caldera sources. Detailed stratigraphic data of nine sections, precise $^{40}Ar/^{39}Ar$ age dates, and mineralogical and compositional data reveal new insights into the eruptive chronology, compositional and mineralogical identity of rhyolite units, and petrologic relationships of tuffs and lavas. More specifically key findings are the following:

1) Thick (ranging from 30 to 80 m) non-welded tuff sections that crop out below prominent cliff forming rhyolite lavas are lithologically diverse but all preserve primary pyroclastic deposition consisting of ignimbrites, fallout and surge deposits. Grain sizes are mostly small lapilli to ash sized with no to 5% phenocrysts and variable amounts of lithic fragments. These tuffs are records of a multicyclical explosive episode that likely lasted less than ~20,000 years, from the ages of these samples. We correlate these tuffs with the early phase of the tuff of Leslie Gulch.

2) Prominent rhyolite cliffs that were previously mapped as rhyolite of McIntyre Ridge consist in fact of two rhyolite units; the names for these were adopted from Hess (2014) and are Old and Young McIntyre rhyolite. Old McIntyre erupted immediately after the tuff of Leslie Gulch at ~15.9 Ma and crops out along the northern side with one small outcrop sandwiched between units on the south side of the study area. It has

compositional characteristics that make it nearly indistinguishable to the tuff of Leslie Gulch. Young McIntyre rhyolite erupted at 15.76 Ma and crops out from the south part of the study area all the way to the southern mapped extent of McIntyre Ridge rhyolite. Its distinguishable characteristics include higher phenocrysts content, low Ba, smaller Eu/Eu*, lower Zr, Nb, and less Fe rich pyroxene than Old McIntyre.

3) A third rhyolite lava named here rhyolite of Succor Creek is exposed at lower elevation in the middle part along McIntyre Ridge. Rhyolite of Succor Creek also occurs as dikes cutting tuff of Leslie Gulch as thin ignimbrite units on the eastern side of the study area. A previous age date of 15.74 Ma indicates eruption after Old McIntyre rhyolite and great chemical affinity to Old McIntyre/ tuff of Leslie Gulch suggests it preceded Young McIntyre rhyolite.

4) Stratigraphically youngest rhyolite deposits are thin tuffs names here Lonesome Tuff and that crop out in the northcentral section of the study area. Compositionally they are closest to Young McIntyre rhyolite yet pyroclastic material deposited may also have a source from elsewhere in the Mahogany Mountain – Three Fingers area or beyond.

5) Basaltic andesitic underlie and basalt lavas overlie or cut rhyolites as dikes.

6) Fossiliferous tuffaceous sediments and thin tuffs of the Sucker Creek Formation overlie all and are preserved in down dropped grabens with early normal faulting likely predating deposition of sediments.

Based on these key findings, we favor the one caldera model proposed by Benson and Mahood (2016) but maintain that the tuff of Leslie Gulch erupted from the

Mahogany Mountain caldera of Rytuba (1991) and Vander Meulen (1989) and we do not favor the lager Roster Comb Caldera model. Whether eruption of the tuff of Succor Creek was associated with caldera formation is unsure but given its small distribution it is more likely that it was not. As for the Three Fingers Caldera, this may be the eruptive location of the younger units found throughout the study area.

7. References

Barry, T.L., Kelley, S.P., Reidel, S.P., Camp, V.E., Self, S., Jarboe, N.A., Duncan, R.A., and Renne., P.R., 2013. Eruption chronology of the Columbia River Basalt Group, *in* Reidel, S.P., Camp, V.E., Ross, M.E., Wolff, J.A., Martin, B.,S., Tolan, T.L., and Wells, R.E., eds., The Columbia River Flood Basalt Province: Geological Society of America Special Paper 497, p.45-66, doi:10.1130/2013.2497(02)

Benson, T. R., Mahood, G. A., 2016, Geology of the Mid-Miocene Rooster Comb Caldera and Lake Owyhee Volcanic Field, eastern Oregon: Silicic volcanism associated with Grand Ronde flood basalt: Journal of Volcanology and Geothermal Research, v. 309, p. 96-117. doi:10.1016

Cahoon, E.B., Streck, M.J., Koppers, A.A.P., Miggins, D.P., 2020, Reshuffling the Columbia River Basalt chronology; Picture Gorge Basalt, the earliest- and longest-erupting formation: Geology, v. 48, p. 348-352. doi:10.1130/G47122.1

Camp, V.E., Ross, M.E., Hanson, W.E., 2003, Genesis of flood basalts and Basin and Range volcanic rocks from Steens Mountain to the Malheur River Gorge, Oregon: GSA Bulletin, v. 115, no 1, p. 105-128

Camp, V.E., Reidel, S.P., Ross, M.E., Brown, R.J., Self, S., 2017, Field-trip Guide to the Vents, Dikes, Stratigraphy, and Structure of the Columbia River Basalt Group, Eastern Oregon and Southeastern Washington: U.S. Geological Survey Scientific Investigations Report 2017-5022-N, doi:10.3133/sir20175022N

Coble, M.A., and Mahood, G.A., 2012, Initial impingement of the Yellowstone plume located by widespread silicic volcanism contemporaneous with Columbia River flood basalts: Geology, doi:10.1130/G32692.1

Cummings, M.L., Evans, J.G., Ferns, M.L., Lees, K.R., 2000, Stratigraphic and structural evolution of the Middle Miocene synvolcanic Oregon-Idaho Graben: GSA Bulletin, v. 112, p. 668-682, doi:10.1130/0016-7606(2000)112<668:SASEOT>2.0.CO;2

Downing, K.F., and Park L.E., 1998, Geochemistry and Early Diagenesis of Mammal-Bearing Concretions from the Sucker Creek Formation (Miocene) of Southeastern Oregon: PALAIOS, v. 13, p. 14-27, doi:131.252.96.10

Ferns, M.L., Cummings, M.L., Evans, J.G., 1993, Geologic map of the Mahogany Mountain 30 x 60 Minute Quadrangle, Malheur County, Oregon, and Owyhee County, Idaho: Oregon Department of Geology and Minerals Industries

Ferns, M.L., 1997, Field trip guide to the eastern margin of the Oregon-Idaho graben and the middle Miocene calderas of the Lake Owyhee volcanic field: Oregon Geology, v. 59, p. 9-20

Ferns, M.L., and McClaughry, J.D., 2013, Stratigraphy and volcanic evolution of the middle Miocene to Pliocene La Grande-Owyhee eruptive axis in eastern Oregon, *in* Reidel, S.P., Camp, V.E., Ross, M.E., Wolff, J.A., Martin, B.,S., Tolan, T.L., and Wells, R.E., eds., The Columbia River Flood Basalt Province: Geological Society of America Special Paper 497, p.401-427, doi:10.1130/2013.2497(16)

Ferns, M.L., Streck, M.J., McClaughry, J.D., 2017, Field-trip guide to Columbia River flood basalts, associated rhyolites, and diverse post-plume volcanism in eastern Oregon: U.S. Geological Survey Scientific Investigations Report 2017-5022-O, 71 p., https://doi.org/10.3133/sir201750220

Ford, M.T., Grunder, A.L., Duncan, R.A., 2013, Bimodal volcanism of the High Lava Plains and Northwestern Basin and Range of Oregon: Distribution and tectonic implications of age-progressive rhyolites, v. 0, p. 1-22, doi:10.1002/ggge.20175

Henry, C. D., Castor, S.B., Starkel, W.A., Ellis, B.S., Wolff, J.A., Laravie, J.A., McIntosh, W.C., Heizler, M.T., 2017, Geology and evolution of the McDermitt caldera, northern Nevada and southeastern Oregon, western USA. *Geosphere*; 13 (4): 1006-1112

Hess, E.N., 2014, Strontium, Lead, and Oxygen Isotopic Signatures of Mid-Miocene Silicic Volcanism in Eastern Oregon: Dissertations and Theses, Portland State University, Paper 2079, doi:10.157/etd.2077

Hooper, P.R., Binger, G.B., Lees, K.R., 2002; Ages of the Steens and Columbia River flood basalts and their relationship to extension-related calc-alkaline volcanism in eastern Oregon: GSA Bulletin, v. 114; no. 1; p. 43-50

Jackson, R.A., 2021, New Perspectives on Prolific and Voluminous Rhyolite Volcanism of the Mahogany Mountain – Three Fingers Rhyolite Field, Eastern Oregon: Dissertations and Theses, Portland State University

Jordan, B.T., Grunder, A.L., Duncan, R.A., and Deino, A.L., 2004, Geochronology of age-progressive volcanism of the Oregon High Lava Plains: Implications for the plume interpretation of Yellowstone: Journal of Geophysical Research: Solid Earth, v. 109, p. 1-19, doi:10.1029/2003JB002776.

Johnson, D.M., Hooper, P.R., Conrey, R.M., 1999, XRF Analysis of Rocks and Minerals for Major and Trace Elements on a Single Low Dilution Li-tetraborate Fused Bead: Advances in X-ray Analysis, v. 41, p. 843-867

Lawrence, D.C., 1988, Geologic field trip guide to the northern Succor Creek area, Malheur County, Oregon: Oregon Geology, v. 50, p. 14-23

Kittleman, L.R., Green, A.R., Hagood, A.R., Johnson, A.M., McMurrary, J.M., Russell, R.G., Weeden, D.A., 1965, Cenozoic Stratigraphy of the Owyhee Region, Southeastern Oregon: Museum of Natural History, v. 1, p. 3-14

Marcy, P.I., 2013, Revisiting Volcanology and Composition of Rhyolites and Associated REE Rich Mafic Clasts of the Three Fingers Caldera, SE Oregon. *Dissertations and Theses.* Paper 1543. https://pdxscholar.library.pdx.edu/open_access_etds/1543 doi:10.15760/etd.1542

McDonough, W.F., and Sun, S.-s., 1995, The composition of the Earth: Chemical Geology, v. 120, p. 223-253, doi:10.1016/0009-2541(94)00140-4

Reidel, S.P., Camp, V.E., Tolan, T.L., and Martin, B.S., 2013, The Columbia River flood basalt province: Stratigraphy, areal extent, volume, and physical volcanology, *in* Reidel, S.P., Camp, V.E., Ross, M.E., Wolff, J.A., Martin, B.S., Tolan, T.L., and Wells, R.E., eds., The Columbia River Flood Basalt Province: Geological Society of America Special Paper 407, p. 1-43, doi:10.1130/2013.2497(01)

Rytuba, J.J., Vander Meulen, D.B., Barlock, V.E., Ferns, M.L., 1991, Hot spring gold deposits in the Lake Owyhee Volcanic Field, Eastern Oregon. In: Buffa, R.H., Coyner, A.R., Great Basin Symposium: The Geology and Ore Deposits of the Great Basin: Field Trip Guidebook Compendium. Geological Society of Nevada, Reno, NV, p. 633-712

Rytuba, J.J., 1994, Evolution of volcanic and tectonis features in caldera settings and their importance in localization of ore deposits: Economic Geology, v. 89, p. 1687-1696, doi:10.2113/gsecongeo.89.8.1687

Sun, S.-s., and McDonough, W.F., 1989, Chemical and isotopic systematics of oceanic basalts: implications for mantle composition and processes: Geological Society Special Publications, v. 42, p. 313-345

Vander Meulen, and D.B., 1989, Intracaldera Tuffs and Central-Vent Intrusions of the Mahogany Mountain Caldera, Eastern Oregon: USGS Open-File Report 89-77, USGS Menlo Park, California

Webb, B.M., Streck, M.J., McIntosh, W.C., and Ferns, M.L., 2018, The Littlefield Rhyolite and associated mafic lavas: Bimodal volcanism of the Columbia River magmatic province, with constraints on age and storage sites of Grande Ronde Basalt magmas: Geosphere, v. 15, no. 1, https://doi.org/10.1130/GEOS01695.1

Wolff, J. & Ramos, F. & Hart, G. & Patterson, J. & Brandon, A., 2008, Columbia River flood basalts from a centralized crustal magmatic system: Nature Geoscience. doi:1. 10.1038/ngeo124.

Young, B.C., 2020, Testing the Correlation of Trace Element Characteristics with the Petrology and Temperature of Eruption of mid-Miocene Rhyolites in Eastern Oregon: Dissertations and Theses. Portland State University, Paper 5520, doi:10.15760/etd.7394

Appendix A: $^{40}Ar/^{39}Ar$ Age Dates of Samples

EXP#20F11261 > CB-18-02 > Sanidine > SWENTON (18-58)
EASTERN OREGON > MAHOGANY MOUNTAIN
20-OSU-01 (1C30-20) > Total Fusion > Dan Miggins

Information on Analysis and Constants Used in Calculations

Project = **SWENTON (18-58)**
Sample = **CB-18-02**
Material = **Sanidine**
Location = **Mahogany Mountain**
Region = **Eastern Oregon**
Analyst = **Dan Miggins**
Irradiation = **20-OSU-01 (1C30-20)**
Position = **X: 0 | Y: 0 | Z/H: 39.41116 mm**
FCT-NM Age = **28.201 ± 0.023 Ma**
FCT-NM Reference = **Kuiper et al (2008)**
FCT-NM 40Ar/39Ar Ratio = **9.50440 ± 0.0154**
FCT-NM J-value = **0.00163351 ± 0.00000266**
Air Shot 40Ar/36Ar = **298.1840 ± 0.4175**
Air Shot MDF = **1.00031565 ± 0.00043712 (L**
Experiment Type = **Total Fusion**
Extraction Method = **Single Crystal Laser H**
Heating = **62 sec**
Isolation = **1.62 min**
Instrument = **ARGUS-VI-F**
Preferred Age = **Ideogram Age**
Age Classification = **Eruption Age**
IGSN = Undefined
Rock Class = Undefined
Lithology = Undefined
Lat-Lon = Undefined - Undefined
Age Equations = **Min et al. (2000)**
Negative Intensities = **Allowed**
Collector Calibrations = **36Ar**
Decay 40K = **5.463 ± 0.107 E-10 1/a**
Decay 39Ar = **2.940 ± 0.016 E-07 1/h**
Decay 37Ar = **8.230 ± 0.012 E-04 1/h**
Decay 36Cl = **2.257 ± 0.015 E-06 1/a**
Decay 40K(EC,β⁺) = **0.580 ± 0.014 E-10 1/a**
Decay 40K(β⁻) = **4.884 ± 0.099 E-10 1/a**
Atmospheric 40/36(a) = **298.56 ± 0.31**
Atmospheric 38/36(a) = **0.1885 ± 0.0003**
Production 39/37(ca) = **0.0006425 ± 0.00000**
Production 38/37(ca) = **0.0001800 ± 0.000017**
Production 36/37(ca) = **0.0002703 ± 0.00000**
Production 40/39(k) = **0.000607 ± 0.000059**
Production 38/39(k) = **0.012077 ± 0.000011**
Production 36/38(cl) = **262.80 ± 1.71**
Scaling Ratio K/Ca = **0.430**
Abundance Ratio 40K/K = **1.1700 ± 0.0100 E-0**
Atomic Weight K = **39.0983 ± 0.0001 g**

Results	0(a)/36(a) ±2σ	r)/39(k) ±2σ	Age ±2σ (Ma)	MSWI	39Ar(k (%,n)	K/Ca ±2σ
Age Plateau		5.36865 ± 0.00288 ± 0.05%	**15.98 ± 0.05 ± 0.33%**	4.30 0% 1.63 ####	73.78 21 2σ Confidence Limit Error Magnification	2.99 ± 0.41
			Full External Error ± 0.83 Analytical Error ± 0.01			
Total Fusion		5.34893 ± 0.00323 ± 0.06%	**15.92 ± 0.05 ± 0.33%**		30	3.45 ± 0.00
			Full External Error ± 0.83 Analytical Error ± 0.01			
Normal Isochron	**272.00 ± 22.8 ± 8.4%**	5.37250 ± 0.00453 ± 0.08%	**15.99 ± 0.05 ± 0.34%**	3.84 0% 1.65 ####	73.78 21 2σ Confidence Limit Error Magnification	
			Full External Error ± 0.83 Analytical Error ± 0.01			
Inverse Isochron	**274.04 ± 21.71 ± 7.9%**	5.37256 ± 0.00434 ± 0.08%	**15.99 ± 0.05 ± 0.33%**	3.61 0% 1.65 #### 3%	73.78 21 2σ Confidence Limit Error Magnification Spreading Factor	
			Full External Error ± 0.83 Analytical Error ± 0.01			

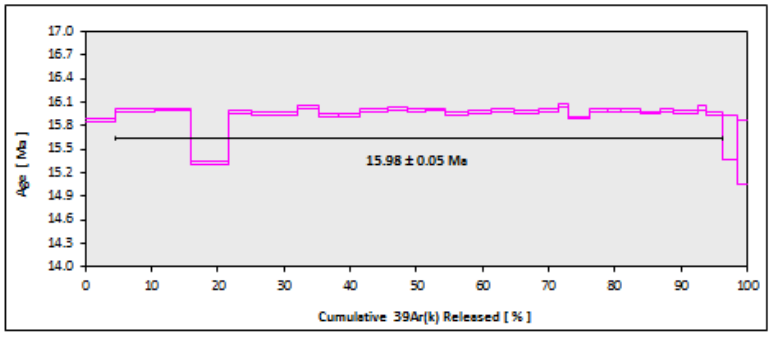

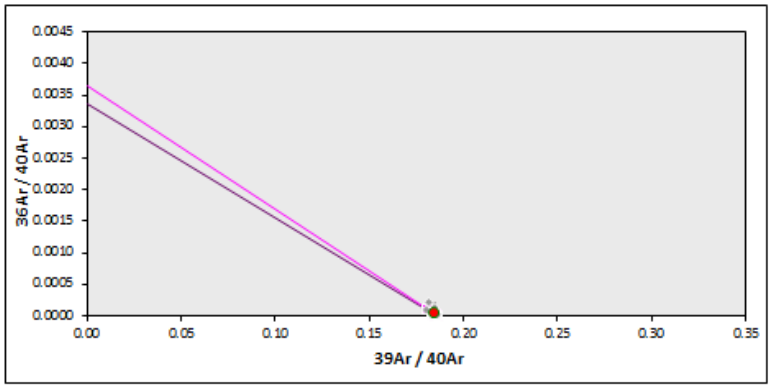

Figure 66. Total fusion $^{40}Ar/^{39}Ar$ age of sample CB-18-02, composite tuff of Leslie Gulch.

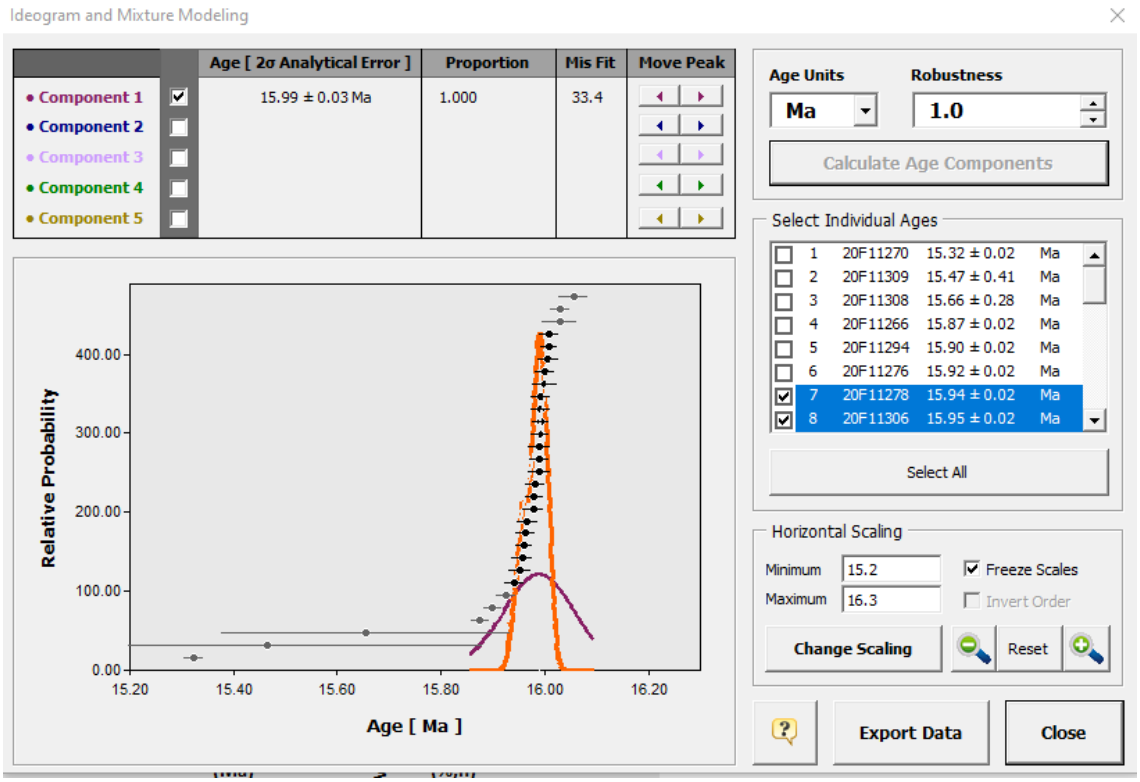

Figure 67. $^{40}Ar/^{39}Ar$ ideogram of sample CB-18-02, composite tuff of Leslie Gulch.

EXP#20F24712 > CB-19-44 > Sanidine > SWENTON (20-01)
EASTERN OREGON > RHYOLITE DOME
20-OSU-01 (1D10-20) > Total Fusion > Dan Miggins

Information on Analysis and Constants Used in Calculations

Project = **SWENTON (20-01)**
Sample = **CB-19-44**
Material = **Sanidine**
Location = **Rhyolite Dome**
Region = **Eastern Oregon**
Analyst = **Dan Miggins**
Irradiation = **20-OSU-01 (1D10-20)**
Position = **X: 0 | Y: 0 | Z/H: 10.09125 mm**
FCT-NM Age = **28.201 ± 0.023 Ma**
FCT-NM Reference = **Kuiper et al (2008)**
FCT-NM 40Ar/39Ar Ratio = **9.39239 ± 0.0067**
FCT-NM J-value = **0.00165299 ± 0.00000119**
Air Shot 40Ar/36Ar = **297.3260 ± 0.3390**
Air Shot MDF = **1.00103892 ± 0.00038788 (1**
Experiment Type = **Total Fusion**
Extraction Method = **Single Crystal Laser H**
Heating = **62 sec**
Isolation = **1.62 min**
Instrument = **ARGUS-VI-F**
Preferred Age = **Ideogram Age**
Age Classification = **Eruption Age**
IGSN = Undefined
Rock Class = Undefined
Lithology = Undefined
Lat-Lon = Undefined - Undefined
Age Equations = **Min et al. (2000)**
Negative Intensities = **Allowed**
Collector Calibrations = **36Ar**
Decay 40K = **5.463 ± 0.107 E-10 1/a**
Decay 39Ar = **2.940 ± 0.016 E-07 1/h**
Decay 37Ar = **8.230 ± 0.012 E-04 1/h**
Decay 36Cl = **2.257 ± 0.015 E-06 1/a**
Decay 40K(EC,β⁺) = **0.580 ± 0.014 E-10 1/a**
Decay 40K(β⁻) = **4.884 ± 0.099 E-10 1/a**
Atmospheric 40/36(a) = **298.56 ± 0.31**
Atmospheric 38/36(a) = **0.1885 ± 0.0003**
Production 39/37(ca) = **0.0006425 ± 0.00000**
Production 38/37(ca) = **0.0001800 ± 0.000017**
Production 36/37(ca) = **0.0002703 ± 0.00000**
Production 40/39(k) = **0.000607 ± 0.000059**
Production 38/39(k) = **0.012077 ± 0.000011**
Production 36/38(cl) = **262.80 ± 1.71**
Scaling Ratio K/Ca = **0.430**
Abundance Ratio 40K/K = **1.1700 ± 0.0100 E-0**
Atomic Weight K = **39.0983 ± 0.0001 g**

Results	0(a)/36(a) ±2σ	r)/39(k) ±2σ	Age ±2σ (Ma)	MSWI	39Ar(k (%,n)	K/Ca ±2σ
Age Plateau		5.29511 ± 0.00686 ± 0.13%	**15.95 ± 0.03 ± 0.19%**	19.81 0% 1.53 4.4511	100.00 30 2σ Confidence Limit Error Magnification	6.3 ±0.5
			Full External Error ±0.83 Analytical Error ±0.02			
Total Fusion		5.29569 ± 0.00179 ± 0.03%	**15.95 ± 0.02 ± 0.15%**		30	7.3 ±0.1
			Full External Error ±0.83 Analytical Error ±0.01			
Normal Isochron	**298.11 ± 4.97 ± 2%**	5.29621 ± 0.01508 ± 0.28%	**15.96 ± 0.05 ± 0.32%**	22.06 0% 1.53 4.697	100.00 30 2σ Confidence Limit Error Magnification	
			Full External Error ±0.83 Analytical Error ±0.05			
Inverse Isochron	**298.99 ± 4.88 ± 1.6%**	5.29405 ± 0.01480 ± 0.28%	**15.95 ± 0.05 ± 0.31%**	21.45 0% 1.53 4.631 27%	100.00 30 2σ Confidence Limit Error Magnification Spreading Factor	
			Full External Error ±0.83 Analytical Error ±0.04			

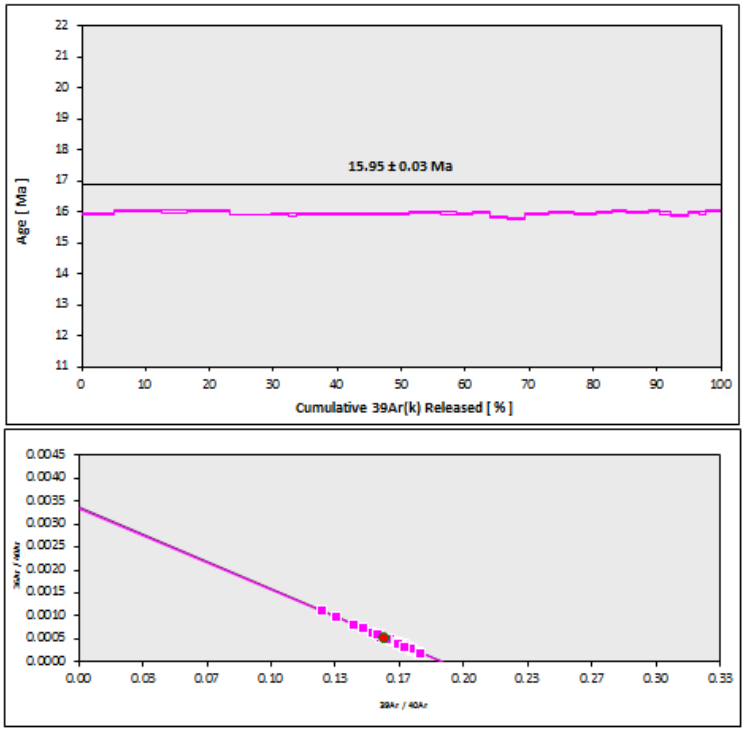

Figure 68. Total fusion $^{40}Ar/^{39}Ar$ age of sample CB-19-44, Old McIntyre Rhyolite.

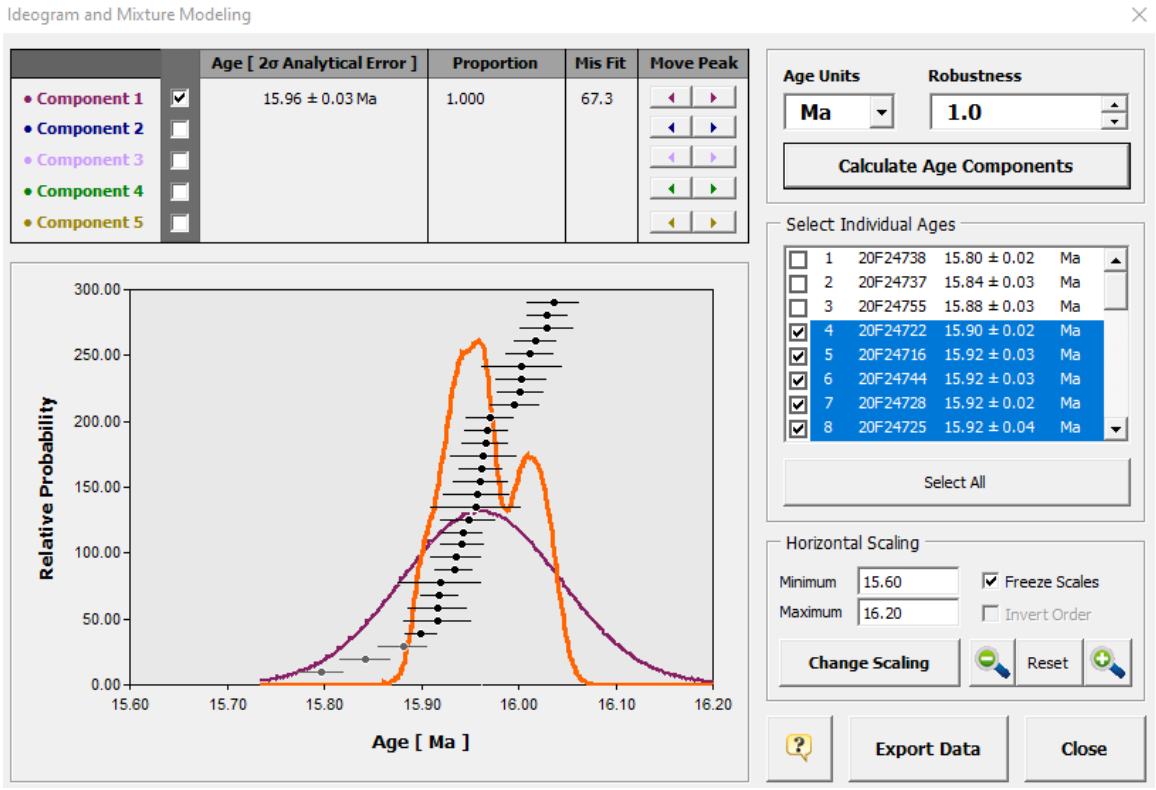

Figure 69. $^{40}Ar/^{39}Ar$ ideogram of sample CB-19-44, Old McIntyre Rhyolite.

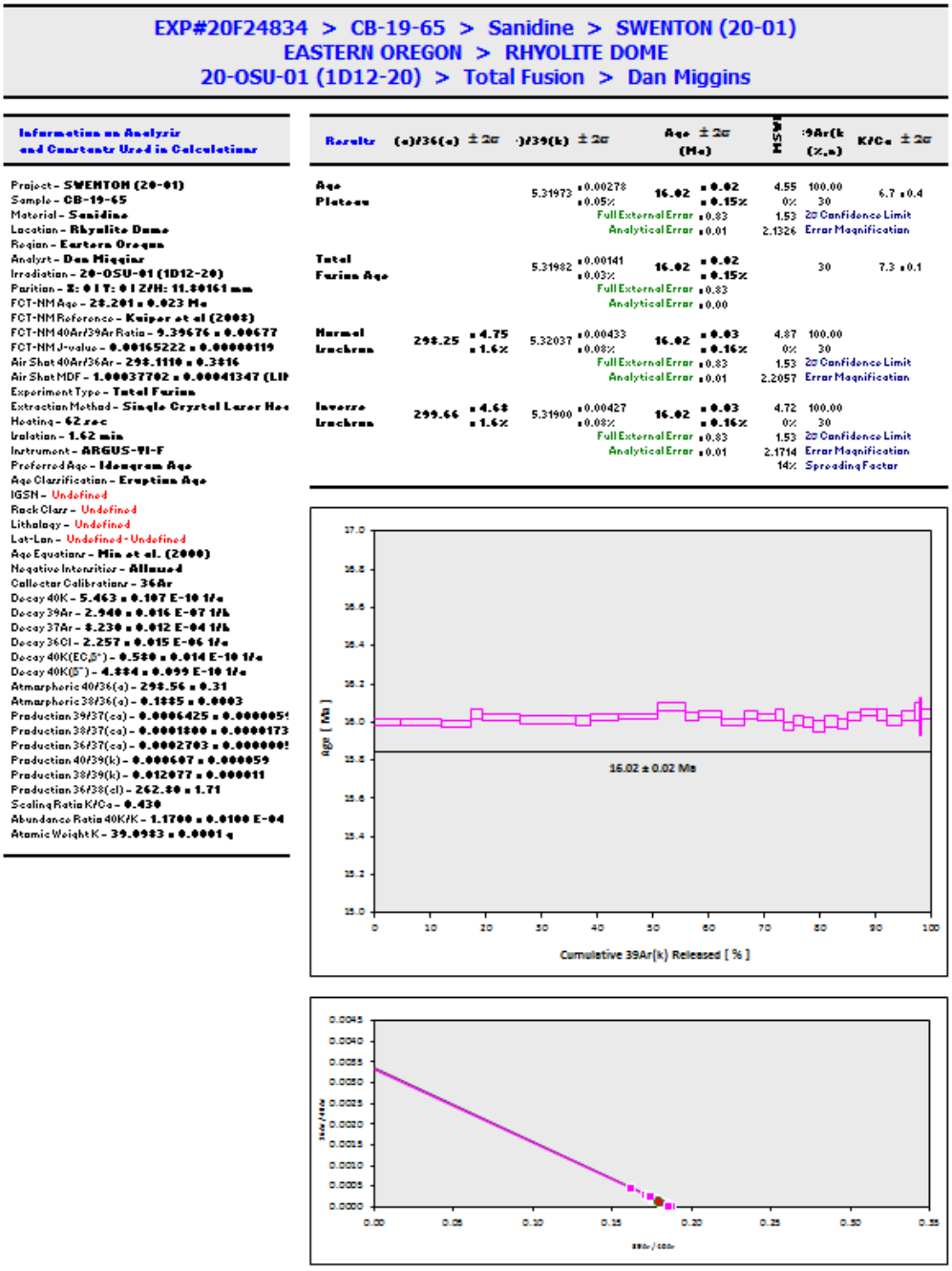

Figure 70. Total fusion $^{40}Ar/^{39}Ar$ age of sample CB-19-65, Old McIntyre Rhyolite.

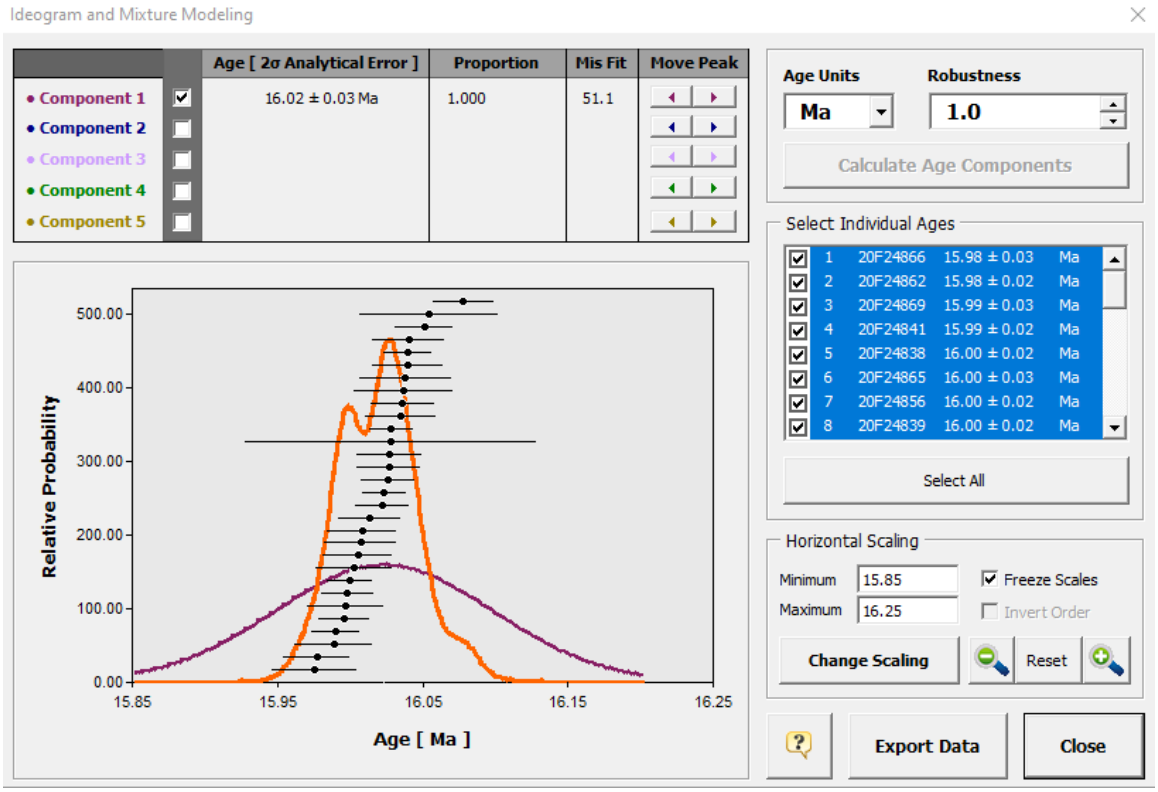

Figure 71. $^{40}Ar/^{39}Ar$ ideogram of sample CB-19-65, Old McIntyre Rhyolite.

Appendix B: Thin Section Scans

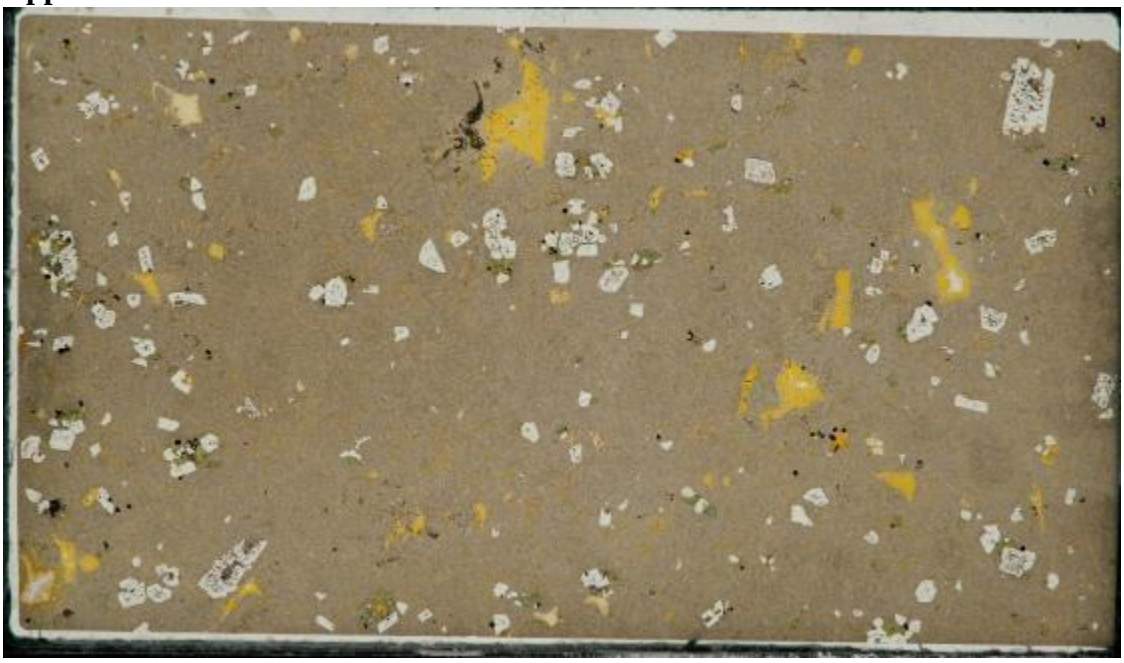

Figure 72. PPL thin section scan of sample CB-19-32.

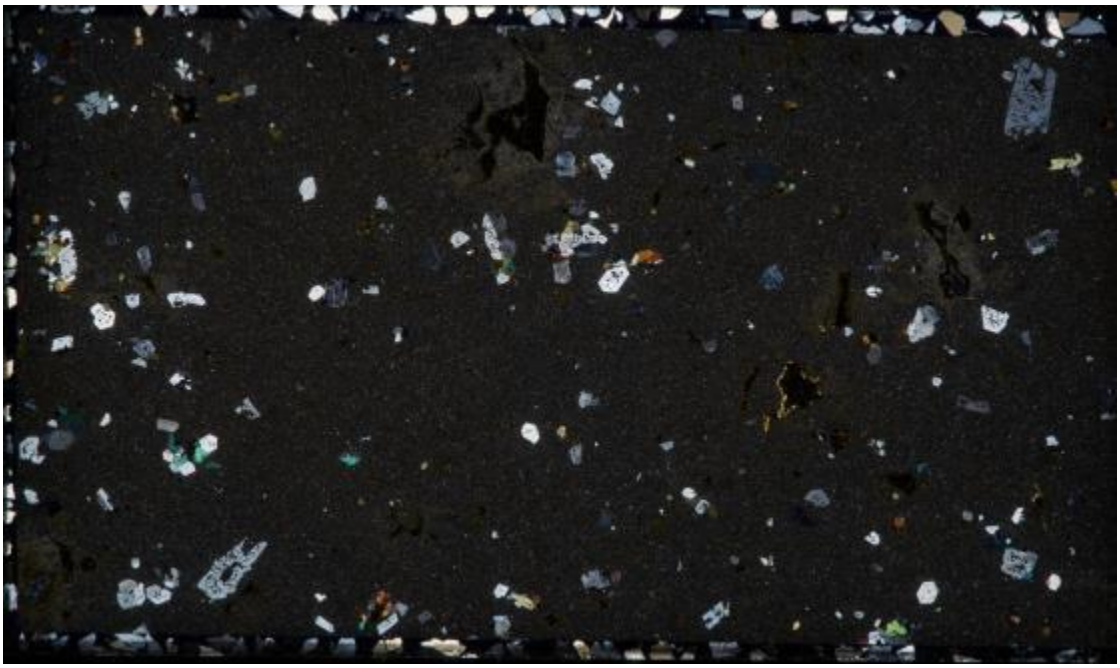

Figure 73. XPL thin section scan of sample CB-19-32.

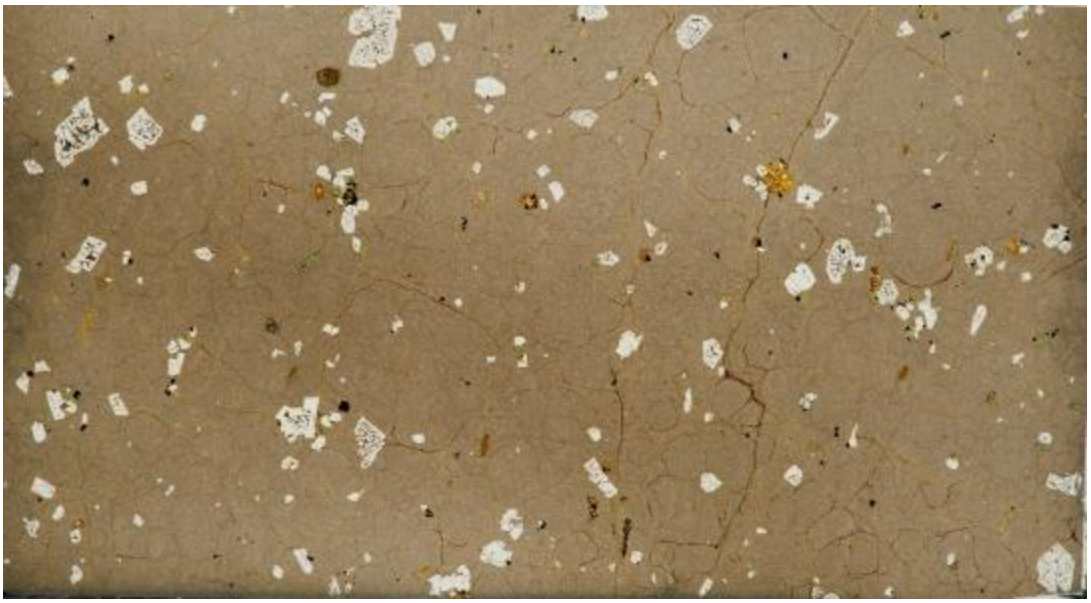

Figure 74. PPL thin section scan of sample CB-19-34.

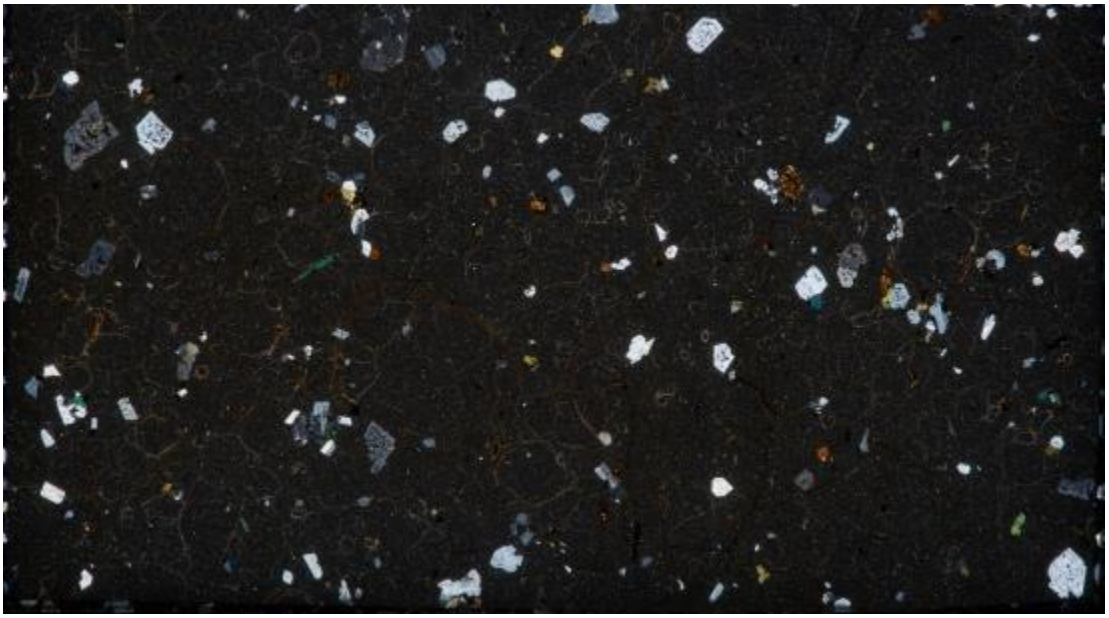

Figure 75. XPL thin section scan of sample CB-19-34.

Figure 76. PPL thin section scan of sample CB-19-37.

Figure 77. XPL thin section scan of sample CB-19-37.

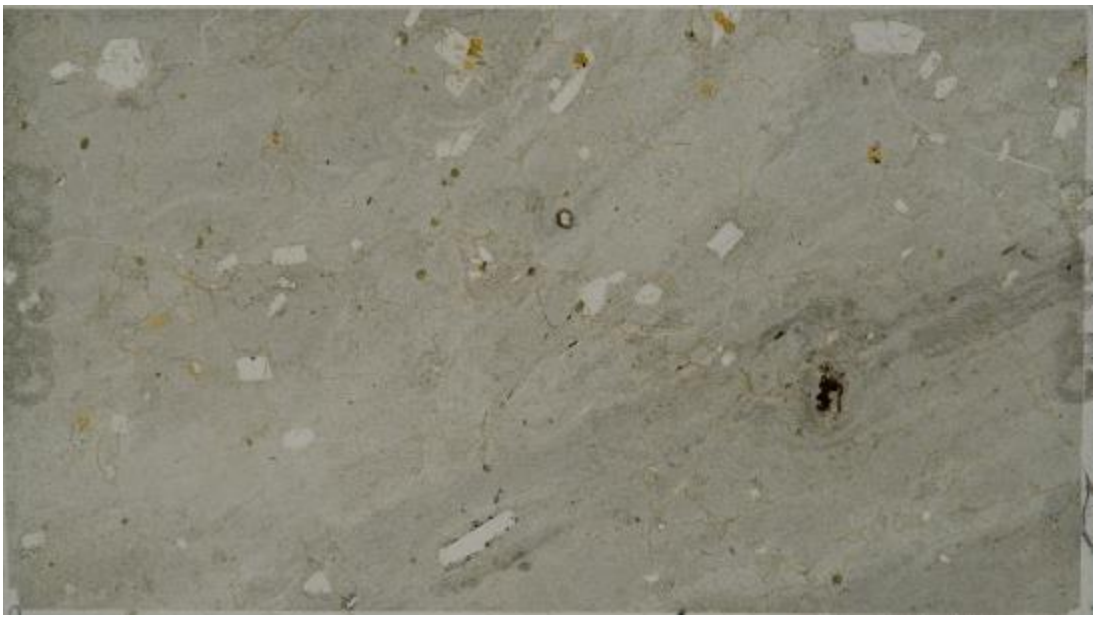

Figure 78. PPL thin section scan of sample CB-19-44.

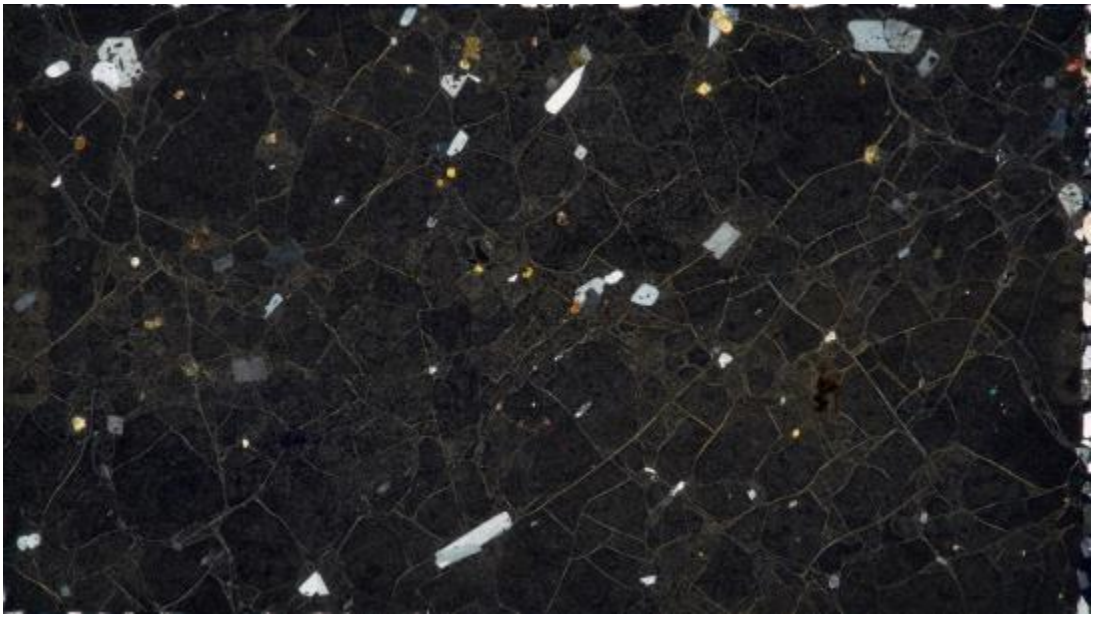

Figure 79. XPL thin section scan of sample CB-19-44.

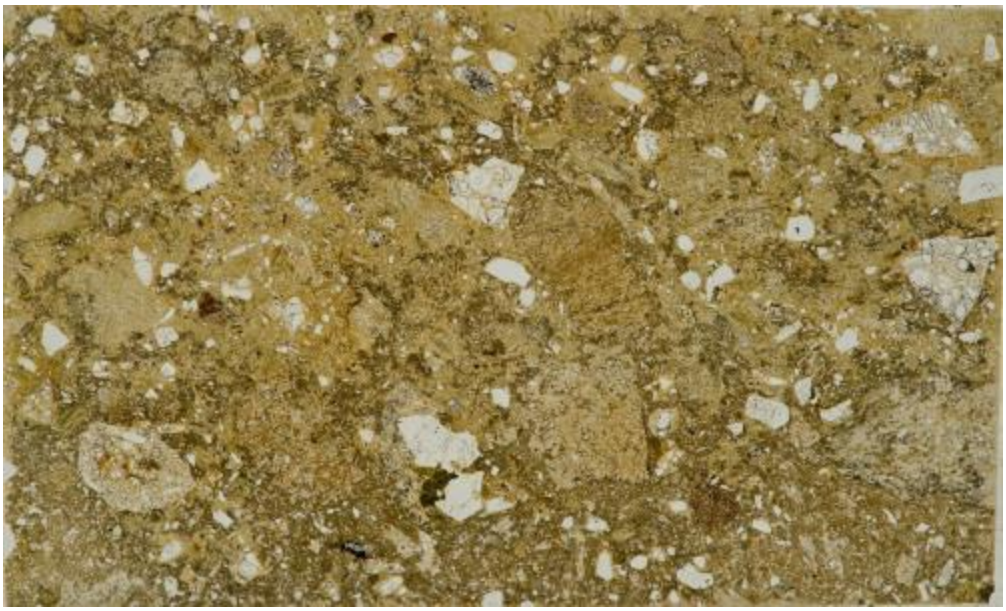

Figure 80. PPL thin section scan of sample CB-19-48.

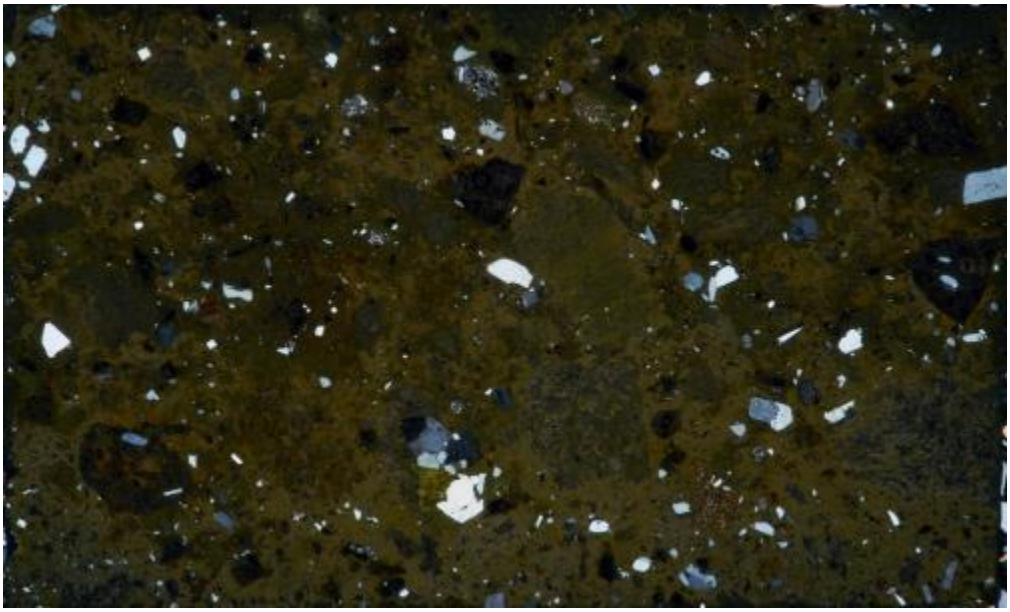

Figure 81. XPL thin section scan of sample CB-19-48.

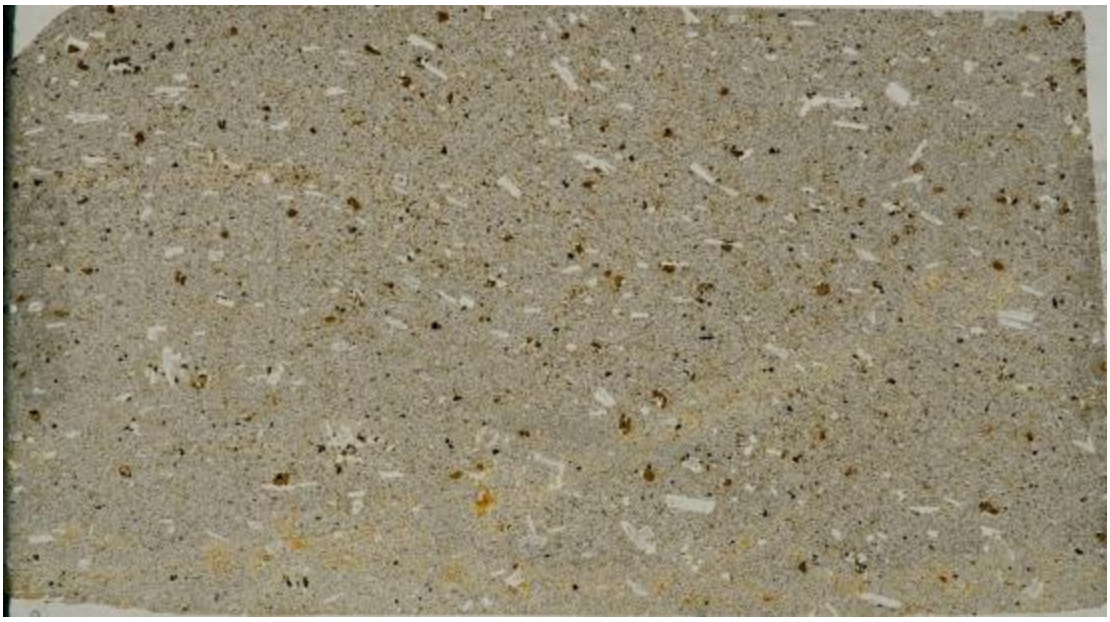

Figure 82. PPL thin section scan of sample CB-19-63b.

Figure 83. XPL thin section scan of sample CB-19-63b.

Figure 84. PPL thin section scan of sample CB-19-65.

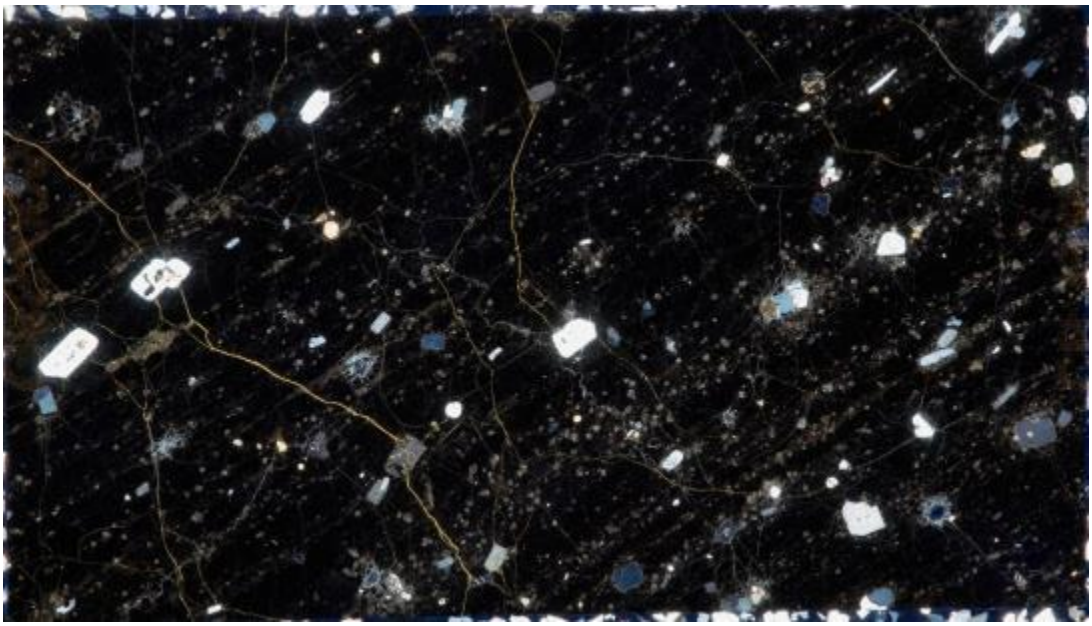

Figure 85. XPL thin section scan of sample CB-19-65.

Figure 86. PPL thin section scan of sample CB-19-66.

Figure 87. XPL thin section scan of sample CB-19-66.

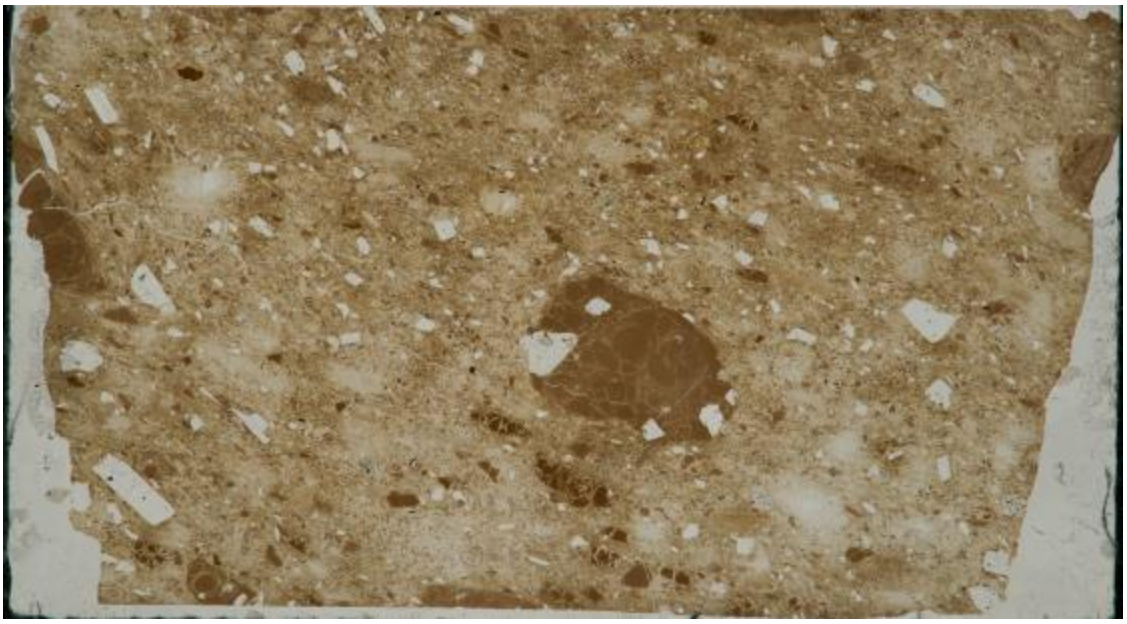

Figure 88. PPL thin section scan of sample CB-19-67.

Figure 89. XPL thin section scan of sample CB-19-67.

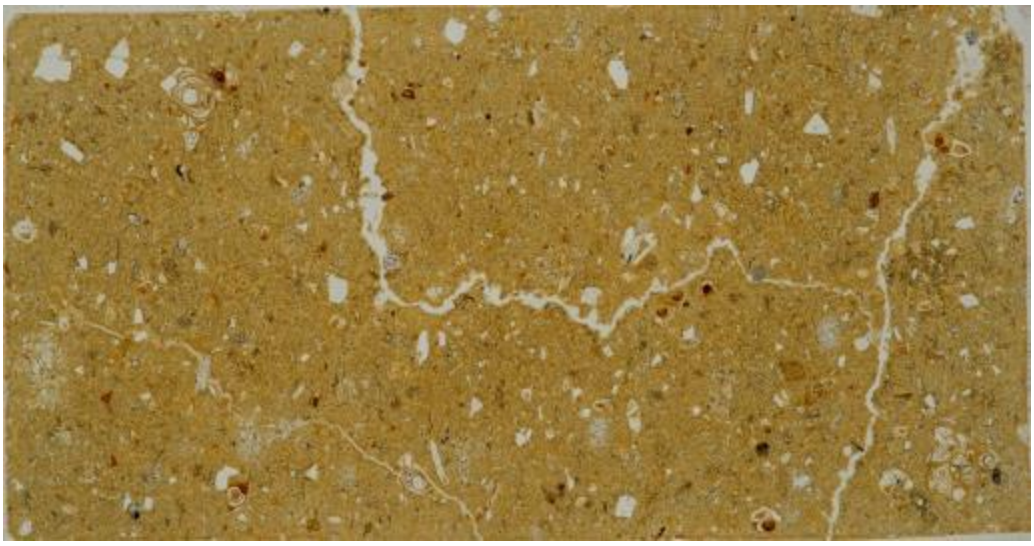

Figure 90. PPL thin section scan of sample CB-19-69.

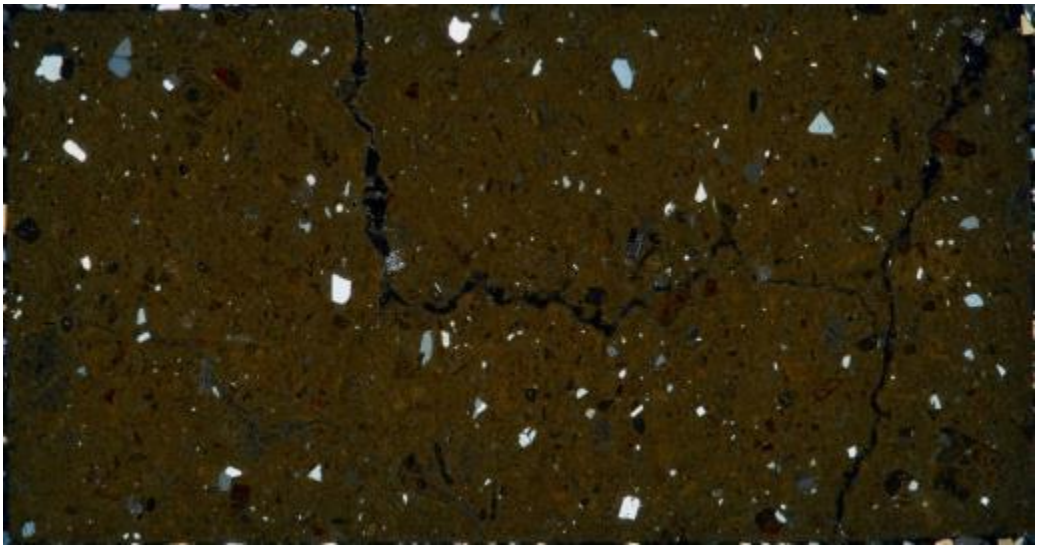

Figure 91. XPL thin section scan of sample CB-19-69.

Figure 92. PPL thin section scan of sample CB-19-71.

Figure 93. XPL thin section scan of sample CB-19-71.

Figure 94. PPL thin section scan of sample CB-19-82.

Figure 95. XPL thin section scan of sample CB-19-82.

Figure 96. PPL thin section scan of sample CB-19-86b.

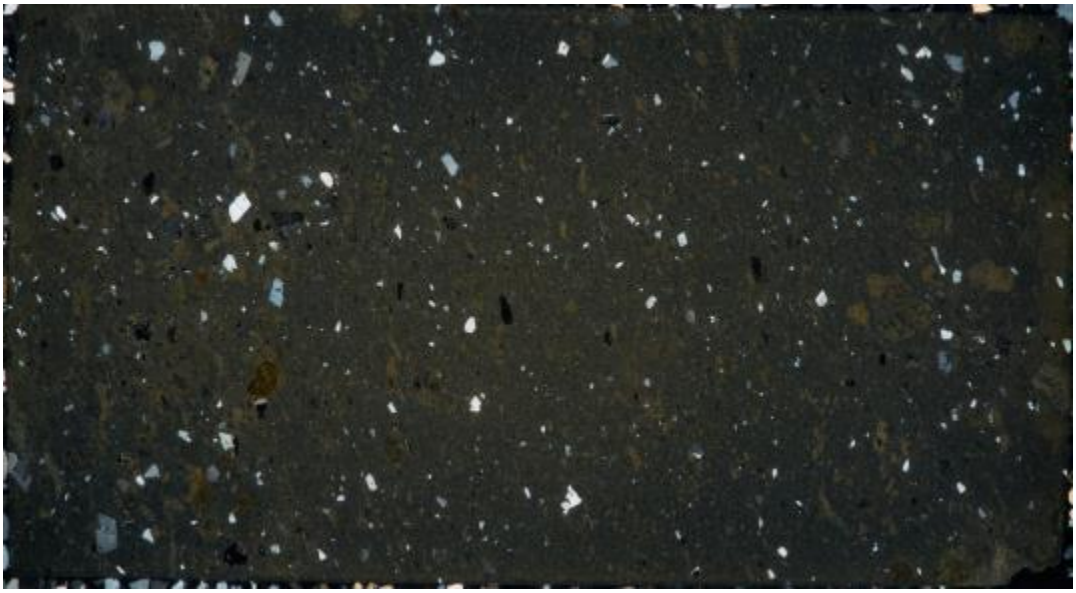

Figure 97. XPL thin section scan of sample CB-19-86b.

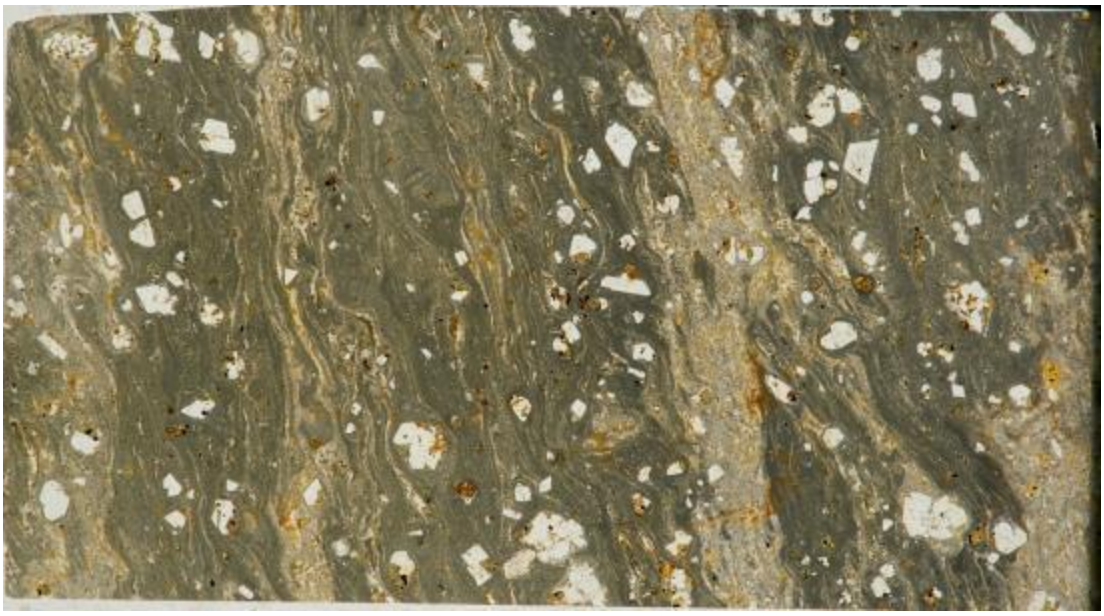

Figure 98. PPL thin section scan of sample CB-19-87.

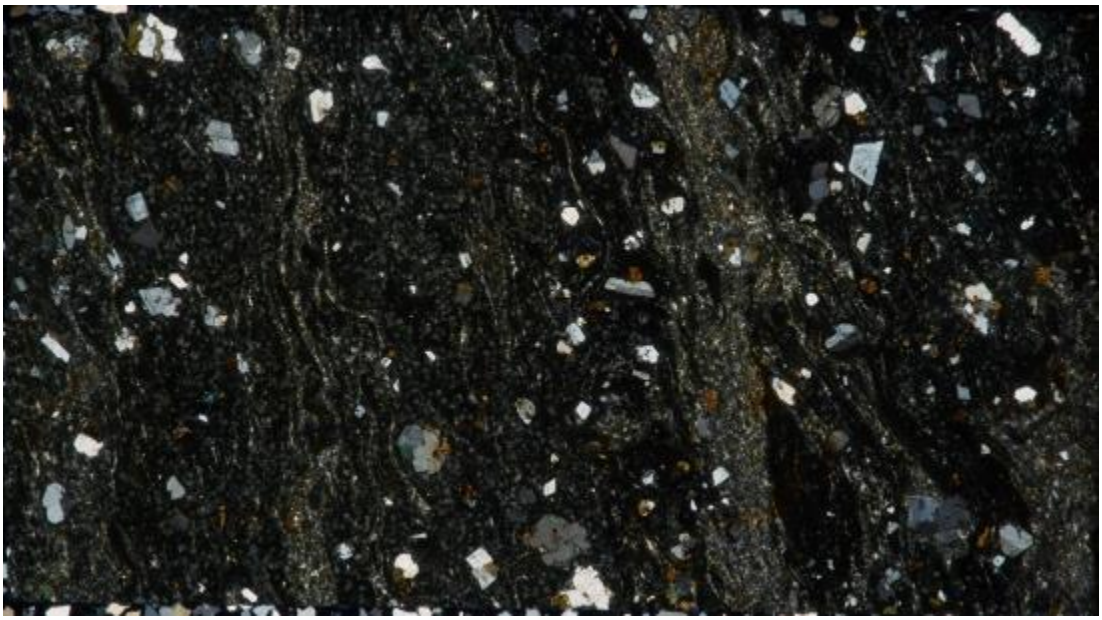

Figure 99. XPL thin section scan of sample CB-19-87.

Figure 100. PPL thin section scan of sample CB-19-88.

Figure 101. XPL thin section scan of sample CB-19-88.

Appendix C: Compositional Data of Bulk Samples

X-Ray Fluorescence (XRF) Data

Table 3. XRF major and trace element compositions for rhyolite and tuff of Succor Creek unit.

Sample ID	**CB-18-05**	**CB-19-32**	**CB-19-34**	**CB-19-87**	**MS-11-15SCT**
Coordinates	43.501, -117.138	43.498, -117.135	43.498, -117.135	43.495, -117.156	43.512, -117.123
Sample Type	Dike	Lava Flow	Lava Flow	Lava Flow	Welded glassy tuff
XRF, normalized wt%					
SiO_2	74.42	73.56	72.88	73.57	73.80
TiO_2	0.34	0.38	0.38	0.38	0.316
Al_2O_3	12.58	12.58	12.48	12.40	12.49
FeO	3.42	4.59	5.10	4.22	3.32
MnO	0.08	0.12	0.14	0.09	0.068
MgO	0.02	0.05	0.05	0.09	0.05
CaO	0.85	1.74	1.80	0.65	0.83
Na_2O	3.22	4.01	3.97	4.17	3.40
K_2O	5.04	2.94	3.15	4.40	5.79
P_2O_5	0.03	0.05	0.05	0.03	0.023
XRF, ppm					
Ni	2	2	1	1	0
Cr	1	4	4	2	3
Sc	2	6	6	3	1
V	3	2	4	3	5
Ba	1754	1713	1691	1757	1768
Rb	161	175	175	123	135
Sr	18	135	131	109	27
Zr	713	547	545	622	669
Y	96	87	84	86	93
Nb	44.6	34.5	35.3	39.3	41.6
Ga	24	23	23	25	24
Cu	4	4	3	3	6
Zn	169	154	156	161	165
Pb	23	19	19	21	23
La	64	61	61	66	62
Ce	133	127	127	136	139
Th	13	13	13	14	14
Nd	69	65	63	67	68
U	4	4	4	5	6

Table 4. Continued XRF major and trace element compositions for tuff of Succor Creek unit.

Sample ID	MS-10-12SCT	MS-10-8SCT	MS-10-13SCT	MS-11-17SCT	MS-13-29
Coordinates	43.512, -117.123	43.512, -117.124	43.514, -117.125	43.515, -117.125	43.496, -117.154
Sample Type	Welded glassy tuff	Welded glassy tuff	Welded glassy tuff	Welded glassy tuff	Rhyolite lava
XRF, normalized wt%					
SiO_2	73.57	74.03	73.35	74.20	72.97
TiO_2	0.356	0.320	0.359	0.364	0.380
Al_2O_3	12.62	12.42	12.67	12.80	12.42
FeO	3.31	3.06	3.50	3.60	4.72
MnO	0.087	0.067	0.083	0.086	0.117
MgO	0.15	0.03	0.13	0.08	0.08
CaO	1.06	0.80	1.00	0.98	1.49
Na_2O	3.47	3.48	3.64	4.50	3.57
K_2O	5.30	5.77	5.23	3.37	4.21
P_2O_5	0.080	0.019	0.034	0.023	0.034
XRF, ppm					
Ni	3	2	3	1	2
Cr	2	1	3	2	2
Sc	3	2	2	2	3
V	11	3	5	4	4
Ba	1845	1588	1880	1971	1709
Rb	146	140	140	215	184
Sr	50	22	25	24	109
Zr	660	704	681	658	582
Y	101	98	95	91	94
Nb	41.5	43.8	43.2	42.6	37.7
Ga	24	24	24	24	24
Cu	7	4	5	4	3
Zn	171	175	175	174	164
Pb	22	24	23	21	21
La	67	65	64	62	64
Ce	143	140	134	133	135
Th	14	14	14	13	15
Nd	73	73	69	70	66
U	4	4	4	5	5

Table 5. XRF major and trace element compositions for Mafic samples.

Sample ID	CB-19-63b	CB-19-71	CB-19-88	CB-19-77	CB-19-79	CB-18-06
Coordinates	43.510, -117.152	43.514, -117.139	43.497, -117.155	43.510, -117.123	43.509, -117.164	43.501, -117.138
Sample Type	Mafic	PG-like basalt	PG-like basalt	Mafic	Basalt Columns	Dike
XRF, normalized wt%						
SiO_2	53.74	48.05	48.28	55.55	51.41	57.56
TiO_2	1.48	1.36	1.08	1.31	1.86	1.19
Al_2O_3	16.56	15.86	17.95	16.58	15.51	16.68
FeO	10.80	10.74	10.28	9.86	13.11	8.58
MnO	0.19	0.18	0.19	0.14	0.24	0.27
MgO	3.62	10.45	8.16	3.09	3.99	3.07
CaO	7.28	10.70	11.09	6.94	7.49	5.98
Na_2O	4.02	2.10	2.54	4.03	3.94	3.93
K_2O	1.70	0.38	0.20	2.01	1.74	2.30
P_2O_5	0.61	0.19	0.24	0.48	0.70	0.44
XRF, ppm						
Ni	25	173	191	26	4	21
Cr	0	386	83	4	0	0
Sc	25	38	31	24	30	20
V	295	264	234	264	283	219
Ba	833	230	144	908	808	1011
Rb	24	6	10	20	27	22
Sr	565	229	293	473	478	454
Zr	128	82	53	140	177	160
Y	32	25	20	32	40	33
Nb	8.8	7.3	2.5	9.4	10.4	11.0
Ga	20	16	16	20	22	19
Cu	78	79	114	117	30	74
Zn	116	80	77	94	141	100
Pb	7	2	3	9	6	10
La	25	11	7	24	28	25
Ce	51	24	14	50	55	48
Th	2	0	0	2	2	3
Nd	30	14	9	27	33	25
U	1	1	1	1	1	3

Table 6. XRF major and trace element compositions for Unwelded Top Ignimbrite.

Sample ID	CB-19-50	CB-19-53	CB-19-54	CB-19-72
Coordinates	43.531, -117.144	43.530, -117.144	43.530, -117.144	43.513, -117.133
Sample Type	Lonesome Tuff	Lonesome Tuff	Lonesome Tuff	Lonesome Tuff
XRF, normalized wt%				
SiO_2	74.49	74.17	68.02	76.13
TiO_2	0.33	0.39	0.94	0.40
Al_2O_3	13.54	13.78	15.69	12.63
FeO	2.91	2.74	5.61	2.44
MnO	0.04	0.06	0.08	0.03
MgO	0.89	0.80	1.88	0.82
CaO	1.46	1.56	3.10	1.05
Na_2O	2.89	3.02	2.50	2.16
K_2O	3.39	3.40	1.94	4.27
P_2O_5	0.05	0.07	0.23	0.07
XRF, ppm				
Ni	3	5	12	1
Cr	7	9	23	4
Sc	5	6	13	4
V	18	28	76	9
Ba	211	482	365	979
Rb	135	119	63	166
Sr	51	92	205	75
Zr	319	300	229	491
Y	48	37	33	58
Nb	33.5	23.2	13.7	40.8
Ga	19	17	17	17
Cu	9	10	19	5
Zn	60	51	83	52
Pb	27	20	11	26
La	79	48	28	81
Ce	154	91	52	150
Th	25	15	7	32
Nd	58	36	29	58
U	5	4	3	9

Table 7. XRF major and trace element compositions for Old McIntyre.

Sample ID	**CB-19-44**	**CB-19-65**	**CB-20-04**	**OMCI1**	**EJ-12-11**	**EJ-12-12**
Coordinates	43.488, -117.136	43.513, -117.155	43.505, -117.166		43.518, -117.152	43.521, -117.152
Sample Type	Vitrophyre	Vitrophyre	Vitrophyre			
XRF, normalized wt%						
SiO_2	75.34	75.82	74.59	75.75	77.18	74.19
TiO_2	0.32	0.25	0.31	0.253	0.233	0.312
Al_2O_3	12.43	12.12	12.39	12.00	11.62	12.92
FeO	3.17	2.61	3.17	2.54	1.89	3.15
MnO	0.08	0.06	0.08	0.039	0.033	0.071
MgO	0.03	0.03	0.03	0.21	0.02	0.51
CaO	0.81	0.62	0.82	0.20	0.11	1.05
Na_2O	2.97	4.59	4.81	3.92	3.64	4.41
K_2O	4.84	3.88	3.77	5.02	5.24	3.38
P_2O_5	0.01	0.02	0.02	0.066	0.032	0.015
XRF, ppm						
Ni	2	2	2	4	3	3
Cr	2	2	1	4	2	2
Sc	1	1	2	1	1	1
V	4	3	4	6	3	1
Ba	1292	1123	1606	1188	1248	1439
Rb	199	160	153	138	143	161
Sr	16	17	21	25	22	34
Zr	717	686	719	641	605	727
Y	94	103	96	90	97	100
Nb	43.2	42.6	43.6	42.0	40.7	44.9
Ga	23	24	25	25	23	26
Cu	4	4	4	5	6	3
Zn	162	159	165	163	143	181
Pb	21	24	22	21	33	25
La	66	73	70	67	80	66
Ce	136	149	141	127	163	147
Th	15	15	13	17	16	15
Nd	69	74	72	66	78	75
U	5	5	4	4	4	4

Table 8. XRF major and trace element compositions for Young McIntyre.

Sample ID	**MS-18-08**	**YMCI1**	**EJ-12-14**	**MS-13-24b**
Coordinates	43.490, -117.134		43.471, -117.124	43.422, -117.134
Sample Type	Vitrophyre	devitrified	Vitrophyre	Vitrophyre
XRF, normalized wt%				
SiO_2	76.57	77.02	77.14	76.35
TiO_2	0.16	0.151	0.153	0.162
Al_2O_3	12.24	12.56	12.17	12.16
FeO	1.66	0.71	1.40	1.59
MnO	0.04	0.006	0.038	0.030
MgO	0.20	0.01	0.14	0.11
CaO	0.58	0.15	0.49	0.53
Na_2O	3.95	3.15	3.70	3.26
K_2O	4.58	6.20	4.74	5.80
P_2O_5	0.02	0.033	0.019	0.018
XRF, ppm				
Ni	2	0	3	4
Cr	2	4	2	2
Sc	2	2	1	2
V	4	2	4	6
Ba	256	255	247	262
Rb	136	158	140	126
Sr	24	20	20	23
Zr	318	314	297	311
Y	89	93	88	87
Nb	37.4	39.9	36.8	36.3
Ga	23	25	23	22
Cu	5	3	5	5
Zn	105	51	105	104
Pb	21	17	21	20
La	66	58	65	63
Ce	131	122	126	128
Th	13	15	14	14
Nd	57	64	57	56
U	5	4	5	4

Table 9. XRF major and trace element compositions for tuff of Leslie Gulch.

Sample ID	CB-19-67	MS-10-6LGT	MS-12-41	MS-17-15	MS-18-07
Coordinates	43.513, -117.155	43.550, -117.103	43.314, -117.219	43.299, -117.271	43.297, -117.263
Sample Type					
XRF, normalized wt%					
SiO_2	73.46	77.87	76.67	76.34	76.23
TiO_2	0.34	0.272	0.273	0.22	0.22
Al_2O_3	13.16	11.33	11.76	12.26	12.17
FeO	3.88	1.96	2.98	2.47	2.42
MnO	0.09	0.022	0.077	0.07	0.06
MgO	1.31	0.01	0.10	0.09	0.00
CaO	1.64	0.12	0.40	1.46	0.61
Na_2O	2.83	3.58	3.36	3.48	4.24
K_2O	3.27	4.79	4.36	3.59	4.03
P_2O_5	0.02	0.033	0.016	0.01	0.01
XRF, ppm					
Ni	1	2	2	5	4
Cr	4	3	2	2	2
Sc	2	0	2	1	1
V	4	3	5	1	3
Ba	1264	1234	1550	739	784
Rb	118	131	134	416	241
Sr	31	18	30	26	10
Zr	723	684	620	609	627
Y	111	67	97	108	104
Nb	43.1	42.7	38.7	40.2	41.4
Ga	24	22	25	23	25
Cu	7	2	4	3	4
Zn	172	124	165	157	157
Pb	22	27	22	24	25
La	76	50	69	74	74
Ce	136	124	141	151	153
Th	14	15	14	16	16
Nd	80	52	72	73	75
U	4	4	3	4	4

Table 10. XRF major and trace element compositions for green tuff samples

Sample ID	**CB-18-02**	**CB-19-10**	**CB-19-78b**	**CB-19-80b**	**CB-19-82**
Coordinates	43.488, -117.133	43.507, -117.159	43.510, -117.121	43.508, -117.168	43.507, -117.162
Sample Type	Green Tuff	Green Tuff	Green Tuff	Green Tuff	Green Tuff
XRF, normalized wt%					
SiO_2	71.26	74.78	74.72	74.15	77.09
TiO_2	0.39	0.30	0.31	0.38	0.22
Al_2O_3	14.12	12.11	12.60	12.87	12.23
FeO	4.06	3.78	3.02	3.45	2.09
MnO	0.26	0.02	0.02	0.02	0.01
MgO	0.43	0.21	0.33	0.74	0.44
CaO	0.77	1.19	0.96	2.34	1.70
Na_2O	1.72	2.88	1.81	1.72	2.22
K_2O	6.95	4.72	6.23	4.31	3.99
P_2O_5	0.03	0.02	0.02	0.03	0.01
XRF, ppm					
Ni	5	3	1	1	1
Cr	0	4	3	1	3
Sc	3	1	1	2	1
V	5	6	4	7	21
Ba	2354	1285	1146	1953	1152
Rb	142	125	166	117	106
Sr	90	41	100	162	170
Zr	635	622	614	640	600
Y	96	87	93	66	67
Nb	43.5	38.1	39.8	38.9	34.9
Ga	26	23	25	23	21
Cu	4	6	6	4	3
Zn	188	169	130	177	114
Pb	26	12	15	18	17
La	63	54	74	57	44
Ce	134	107	147	112	85
Th	14	13	14	12	15
Nd	70	57	73	61	43
U	3	5	4	3	3

Table 11. XRF major and trace element compositions for green tuff samples continued.

Sample ID	**CB-19-83**	**CB-19-86b**	**CB-19-92**	**CB-19-93**
Coordinates	43.496, -117.157	43.497, -117.160	43.495, -117.159	43.495, -117.156
Sample Type	Green Tuff	Green Tuff	Green Tuff	Green Tuff
XRF, normalized wt%				
SiO_2	71.30	74.45	75.30	76.80
TiO_2	0.54	0.32	0.36	0.32
Al_2O_3	15.21	12.30	12.72	11.46
FeO	1.89	3.35	2.31	2.85
MnO	0.01	0.05	0.02	0.04
MgO	0.12	0.37	0.33	0.18
CaO	1.95	1.34	1.71	0.68
Na_2O	3.08	3.94	2.96	3.26
K_2O	5.85	3.85	4.25	4.39
P_2O_5	0.03	0.02	0.02	0.02
XRF, ppm				
Ni	2	0	1	1
Cr	3	2	3	2
Sc	5	2	3	2
V	5	17	8	5
Ba	1778	1553	1299	2217
Rb	117	84	111	101
Sr	247	116	91	117
Zr	536	551	581	489
Y	69	85	86	71
Nb	36.4	35.3	36.1	31.0
Ga	35	21	22	18
Cu	2	4	4	4
Zn	39	143	161	158
Pb	20	17	21	17
La	55	61	70	50
Ce	108	122	136	99
Th	13	13	13	11
Nd	50	62	70	53
U	3	5	5	3

Inductively Coupled Plasma-Mass Spectrometry (ICP-MS) Data

Table 12. ICP-MS geochemical data for tuff of Succor Creek samples.

Sample ID	CB-18-05	CB-19-32	CB-19-34	CB-19-87	MS-11-15SCT
Coordinates	43.501, -117.138	43.498, -117.135	43.498, -117.135	43.495, -117.156	43.512, -117.123
Sample Type	Dike	Lava Flow	Lava Flow	Lava Flow	Welded glassy tuff
ICP-MS, ppm					
La	67.11	64.12	63.61	69.17	67.84
Ce	139.58	131.72	130.41	141.01	148.11
Pr	17.94	16.57	16.45	17.68	17.63
Nd	72.20	66.52	65.54	69.76	71.42
Sm	16.73	15.43	15.38	16.10	16.45
Eu	3.36	3.56	3.58	3.61	3.36
Gd	16.36	15.10	14.89	15.63	16.33
Tb	2.84	2.65	2.63	2.76	2.82
Dy	18.09	16.79	16.37	17.18	17.70
Ho	3.71	3.53	3.44	3.53	3.69
Er	10.52	9.77	9.58	9.85	10.39
Tm	1.59	1.44	1.45	1.49	1.54
Yb	10.03	9.03	8.99	9.33	9.76
Lu	1.65	1.44	1.40	1.45	1.62
Ba	1782	1760	1740	1782	1870
Th	14.16	14.21	14.19	15.18	14.41
Nb	43.12	35.22	34.97	38.96	41.26
Y	95.48	90.15	87.08	87.68	93.74
Hf	17.03	14.53	14.49	16.18	16.85
Ta	2.48	2.20	2.21	2.40	2.42
U	4.23	4.12	4.02	4.35	4.29
Pb	21.56	19.47	19.46	20.69	21.70
Rb	160.0	176.2	176.1	122.6	134.9
Cs	3.45	5.76	5.26	1.46	3.16
Sr	19	136	132	107	29
Sc	1.9	6.0	6.2	3.3	1.4
Zr	703	565	557	621	719

Table 13. ICP-MS geochemical data for tuff of Succor Creek samples continued.

Sample ID	MS-10-12SCT	MS-10-8SCT	MS-10-13SCT	MS-11-17SCT	MS-13-29
Coordinates	43.512, -117.123	43.512, -117.124	43.514, -117.125	43.515, -117.125	43.496, -117.154
Sample Type	Welded glassy tuff	Welded glassy tuff	Welded glassy tuff	Welded glassy tuff	Rhyolite lava
ICP-MS, ppm					
La	70.62	69.85	66.90	64.86	66.26
Ce	143.79	144.88	138.97	141.48	137.05
Pr	18.48	18.25	17.70	17.17	17.14
Nd	74.79	73.75	72.12	70.07	68.52
Sm	17.26	16.89	16.63	16.35	15.65
Eu	3.53	3.13	3.52	3.63	3.44
Gd	17.20	16.53	16.32	16.14	15.47
Tb	3.00	2.90	2.81	2.78	2.75
Dy	18.70	18.22	17.64	17.50	17.37
Ho	3.93	3.83	3.71	3.66	3.58
Er	10.89	10.64	10.28	10.17	9.98
Tm	1.61	1.57	1.54	1.51	1.49
Yb	10.35	10.19	10.05	9.81	9.26
Lu	1.67	1.62	1.64	1.63	1.47
Ba	1941	1663	1958	2111	1732
Th	14.14	14.78	13.98	13.57	14.51
Nb	40.71	42.71	42.03	42.09	37.28
Y	99.28	95.97	92.03	91.55	92.33
Hf	16.57	17.43	16.64	16.54	15.29
Ta	2.40	2.53	2.17	2.39	2.30
U	4.24	4.41	4.23	4.07	4.08
Pb	21.52	22.24	21.51	20.61	20.26
Rb	147.3	139.2	138.2	214.3	181.0
Cs	3.43	3.34	3.24	5.62	6.57
Sr	50	23	24	26	114
Sc	4.4	3.7	4.7	1.7	3.2
Zr	701	742	706	707	597

Table 14. ICP-MS geochemical data for mafic samples.

Sample ID	CB-19-63b	CB-19-71	CB-19-88	CB-19-77	CB-19-79	CB-18-06
Coordinates	43.510, -117.152	43.514, -117.139	43.497, -117.155	43.510, -117.123	43.509, -117.164	43.501, -117.138
Sample Type	Mafic	PG-like basalt	PG-like basalt	Mafic	Basalt Columns	Dike
ICP-MS, ppm						
La	24.75	10.01	5.93	23.83	25.38	25.53
Ce	51.82	22.02	13.68	48.50	55.06	52.13
Pr	6.81	2.98	2.03	6.37	7.46	6.72
Nd	28.62	13.43	9.36	26.53	32.13	27.55
Sm	6.73	3.64	2.74	6.09	7.35	6.33
Eu	2.07	1.26	1.13	1.89	2.32	1.84
Gd	6.26	4.14	3.19	5.91	7.59	5.73
Tb	1.02	0.73	0.57	0.95	1.21	0.97
Dy	6.08	4.60	3.70	5.98	7.16	6.02
Ho	1.23	0.97	0.78	1.24	1.47	1.23
Er	3.37	2.68	2.14	3.41	4.14	3.46
Tm	0.49	0.39	0.32	0.50	0.64	0.52
Yb	3.04	2.46	1.98	3.26	3.95	3.32
Lu	0.49	0.39	0.32	0.52	0.62	0.51
Ba	832	223	138	891	806	1000
Th	2.03	0.84	0.40	2.66	1.83	3.19
Nb	8.84	7.40	3.21	8.92	10.73	9.90
Y	31.66	24.63	20.15	33.21	40.17	31.94
Hf	3.47	2.23	1.44	3.76	4.40	4.14
Ta	0.48	0.47	0.19	0.49	0.59	0.59
U	0.78	0.28	0.13	0.86	0.71	1.39
Pb	7.06	2.47	1.37	8.62	6.14	9.20
Rb	22.5	4.4	8.6	19.3	26.0	20.8
Cs	1.22	0.20	0.83	0.33	0.43	0.27
Sr	573	230	303	482	465	458
Sc	24.6	37.8	30.6	23.7	28.9	20.2
Zr	130	84	53	143	175	160

Table 15. ICP-MS geochemical data for unwelded top ignimbrite.

Sample ID	CB-19-50	CB-19-53	CB-19-54	CB-19-72
Coordinates	43.531, -117.144	43.530, -117.144	43.530, -117.144	43.513, -117.133
Sample Type	Lonesome Tuff	Lonesome Tuff	Lonesome Tuff	Lonesome Tuff
ICP-MS, ppm				
La	82.84	48.94	27.59	82.48
Ce	161.45	94.84	53.91	155.62
Pr	17.61	10.59	7.26	17.25
Nd	61.87	37.46	28.88	60.14
Sm	11.65	7.46	6.39	11.87
Eu	0.60	0.69	1.42	1.30
Gd	9.51	6.46	5.87	10.40
Tb	1.61	1.13	0.98	1.80
Dy	9.71	6.90	5.99	11.02
Ho	1.91	1.42	1.27	2.23
Er	5.23	4.03	3.50	6.10
Tm	0.79	0.61	0.54	0.91
Yb	4.94	3.92	3.47	5.71
Lu	0.75	0.61	0.54	0.87
Ba	214	488	369	995
Th	25.63	16.79	6.93	32.94
Nb	33.71	23.05	14.18	40.62
Y	48.92	37.66	32.49	58.89
Hf	9.84	8.64	5.97	13.30
Ta	2.12	1.58	0.95	3.08
U	5.12	4.42	3.10	8.45
Pb	27.75	19.31	11.03	26.91
Rb	135.6	117.4	60.8	164.0
Cs	3.37	3.30	2.43	6.30
Sr	51	90	200	75
Sc	4.1	5.8	13.9	4.0
Zr	326	303	232	496

Table 16. ICP-MS geochemical data for Old McIntyre Samples.

Sample ID	CB-19-44	CB-19-65	CB-20-04	OMCI1	EJ-12-11	EJ-12-12
Coordinates	43.488, -117.136	43.513, -117.155	43.505, -117.166		43.518, -117.152	43.521, -117.152
Sample Type	Vitrophyre	Vitrophyre	Vitrophyre			
ICP-MS, ppm						
La	68.41	76.19	69.94	69.39	80.88	71.54
Ce	141.96	156.68	144.89	136.80	164.39	149.47
Pr	17.97	19.62	18.34	18.43	19.96	18.80
Nd	72.07	77.51	73.28	72.56	79.14	75.14
Sm	16.83	17.92	16.35	16.23	17.57	17.35
Eu	2.97	2.59	2.95	2.39	2.65	3.04
Gd	16.22	17.48	16.08	15.37	16.86	17.18
Tb	2.87	3.07	2.83	2.72	2.93	2.99
Dy	18.33	19.40	16.78	17.38	18.24	18.79
Ho	3.78	4.06	3.56	3.64	3.80	3.91
Er	10.62	11.33	10.07	10.38	10.49	10.92
Tm	1.60	1.69	1.61	1.54	1.54	1.63
Yb	10.29	10.57	10.23	9.84	9.57	10.50
Lu	1.62	1.64	1.62	1.52	1.49	1.65
Ba	1330	1152	1645	1218	1284	1457
Th	15.21	16.68	14.95	16.62	15.06	15.48
Nb	43.87	42.23	42.41	42.04	40.61	43.94
Y	96.11	105.55	97.30	88.88	94.80	97.97
Hf	17.70	17.66	17.51	17.17	15.85	18.10
Ta	2.61	2.63	2.58	2.67	2.41	2.62
U	4.49	4.87	4.34	3.84	4.18	4.34
Pb	21.89	24.17	22.76	20.04	32.39	22.98
Rb	199.0	159.3	152.4	137.6	144.4	160.0
Cs	5.94	4.09	3.84	2.18	2.12	9.41
Sr	16	19	23	27	25	37
Sc	1.4	0.8	1.1	0.6	0.6	0.9
Zr	724	690	709	700	631	744

Table 17. ICP-MS geochemical data for Young McIntyre Samples.

Sample ID	MS-18-08	YMCI1	EJ-12-14	MS-13-24b
Coordinates	43.490, -117.134		43.471, -117.124	43.422, -117.134
Sample Type	Vitrophyre	devitrified	Vitrophyre	Vitrophyre
ICP-MS, ppm				
La	65.58	61.82	64.49	65.93
Ce	132.06	125.64	129.69	134.46
Pr	15.80	17.68	15.60	15.86
Nd	59.20	67.34	58.58	59.58
Sm	12.21	14.70	13.01	12.99
Eu	0.51	0.55	0.50	0.56
Gd	12.15	14.07	12.73	12.39
Tb	2.20	2.57	2.35	2.32
Dy	13.87	16.80	15.16	15.04
Ho	3.03	3.59	3.23	3.21
Er	8.88	10.26	9.30	9.08
Tm	1.46	1.56	1.41	1.42
Yb	9.05	9.94	9.02	9.03
Lu	1.41	1.57	1.41	1.45
Ba	256	260	251	268
Th	13.26	14.22	13.43	13.39
Nb	36.18	39.88	36.44	36.23
Y	85.67	93.80	85.74	85.13
Hf	9.89	10.47	9.62	10.12
Ta	2.29	2.48	2.30	2.33
U	4.00	4.41	4.08	4.04
Pb	20.14	15.47	19.65	19.56
Rb	129.7	161.8	142.6	126.3
Cs	3.48	1.52	3.48	3.06
Sr	23	22	24	25
Sc	1.4	1.6	1.4	1.6
Zr	303	320	296	318

Table 18. ICP-MS geochemical data for tuff of Leslie Gulch samples.

Sample ID	CB-19-67	MS-10-6LGT	MS-12-41	MS-17-15	MS-18-07
Coordinates	43.513, -117.155	43.550, -117.103	43.314, -117.219	43.299, -117.271	43.297, -117.263
Sample Type					
ICP-MS, ppm					
La	78.07	51.89	69.05	76.46	77.05
Ce	142.47	125.64	140.29	155.59	156.95
Pr	20.69	14.11	18.09	19.50	19.62
Nd	83.05	55.51	72.37	77.04	76.48
Sm	19.63	12.76	16.44	17.17	17.44
Eu	3.48	2.47	3.16	1.96	1.94
Gd	19.66	11.69	16.22	17.33	17.11
Tb	3.50	2.10	2.81	3.04	3.02
Dy	22.25	13.20	17.77	19.52	19.46
Ho	4.58	2.76	3.68	4.12	4.00
Er	12.68	7.73	10.15	11.44	11.41
Tm	1.91	1.16	1.51	1.69	1.72
Yb	11.65	7.67	9.57	10.61	10.66
Lu	1.83	1.22	1.51	1.65	1.57
Ba	1287	1279	1563	753	802
Th	14.93	14.81	14.81	15.92	16.10
Nb	42.74	41.66	38.81	38.95	39.60
Y	111.13	64.67	93.52	107.46	104.07
Hf	17.49	17.42	16.08	16.58	16.62
Ta	2.54	2.50	2.33	2.51	2.55
U	4.18	4.18	3.94	4.55	4.64
Pb	22.17	26.71	21.10	23.18	23.74
Rb	116.4	133.2	132.5	412.3	240.2
Cs	10.25	2.15	1.34	14.21	4.41
Sr	32	19	34	26	11
Sc	1.2	3.4	1.3	0.0	0.9
Zr	715	730	632	610	616

Table 19. ICP-MS geochemical data for green tuff samples.

Sample ID	CB-18-02	CB-19-10	CB-19-78b	CB-19-80b	CB-19-82
Coordinates	43.488, -117.133	43.507, -117.159	43.510, -117.121	43.508, -117.168	43.507, -117.162
Sample Type	Green Tuff	Green Tuff	Green Tuff	Green Tuff	Green Tuff
ICP-MS, ppm					
La	69.77	56.64	76.43	60.34	45.11
Ce	138.99	113.67	154.26	119.69	92.06
Pr	17.95	15.29	19.19	15.92	11.26
Nd	72.15	60.77	76.83	63.16	44.97
Sm	16.60	14.58	17.58	14.09	10.53
Eu	4.74	2.61	3.59	3.59	1.43
Gd	17.01	13.90	16.36	12.81	10.36
Tb	2.94	2.65	2.74	2.16	1.85
Dy	18.35	17.33	17.16	13.59	12.39
Ho	3.81	3.63	3.72	2.78	2.64
Er	10.44	10.31	10.65	7.76	7.74
Tm	1.60	1.56	1.60	1.19	1.23
Yb	9.99	10.06	10.02	7.64	7.84
Lu	1.59	1.55	1.57	1.21	1.22
Ba	2418	1317	1178	1994	1173
Th	14.03	13.72	14.74	12.73	15.58
Nb	42.48	37.91	39.56	38.73	34.51
Y	96.72	88.63	94.23	66.42	65.94
Hf	16.00	15.77	15.86	15.31	15.86
Ta	2.47	2.31	2.42	2.25	2.45
U	4.20	5.03	3.96	3.27	2.89
Pb	26.99	11.28	14.93	17.39	16.31
Rb	143.0	125.0	165.5	116.2	104.1
Cs	1.93	4.10	4.13	5.40	4.22
Sr	93	42	100	158	165
Sc	2.1	1.2	1.3	1.7	1.1
Zr	638	633	619	642	593

Table 20. ICP-MS geochemical data for green tuff samples continued.

Sample ID	CB-19-83	CB-19-86b	CB-19-92	CB-19-93
Coordinates	43.496, -117.157	43.497, -117.160	43.495, -117.159	43.495, -117.156
Sample Type	Green Tuff	Green Tuff	Green Tuff	Green Tuff
ICP-MS, ppm				
La	56.74	62.45	73.07	52.78
Ce	112.27	126.66	142.02	105.48
Pr	13.19	16.31	18.09	13.94
Nd	50.84	65.07	73.21	56.63
Sm	11.50	14.84	16.87	13.02
Eu	5.26	3.39	3.16	3.94
Gd	11.07	14.66	16.46	12.58
Tb	1.98	2.57	2.73	2.28
Dy	12.49	16.33	16.83	14.45
Ho	2.67	3.46	3.41	3.03
Er	7.58	9.50	9.13	8.32
Tm	1.15	1.43	1.30	1.23
Yb	7.21	8.91	8.30	7.94
Lu	1.11	1.40	1.27	1.30
Ba	1814	1568	1328	2308
Th	12.97	13.05	13.97	11.17
Nb	36.15	34.76	36.05	31.71
Y	69.41	84.21	88.85	73.68
Hf	13.91	13.96	15.17	12.60
Ta	2.16	2.16	2.26	1.91
U	3.58	5.22	4.51	3.45
Pb	20.02	17.23	20.80	17.28
Rb	116.2	82.3	111.8	102.6
Cs	18.52	1.69	3.16	3.57
Sr	243	112	93	119
Sc	4.8	1.5	2.3	1.9
Zr	536	546	588	499

Appendix D: Additional Feldspar Plots

CB-18-01 Feldspar

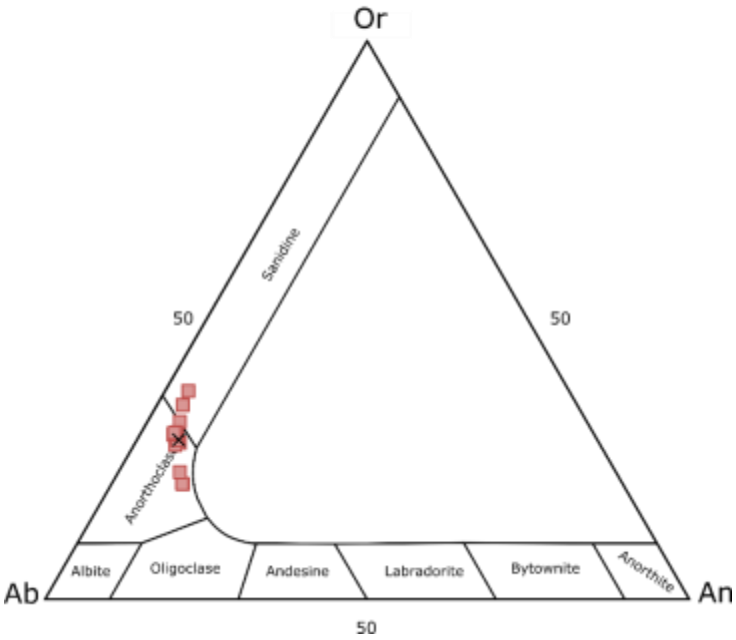

CB-18-02 Feldspar

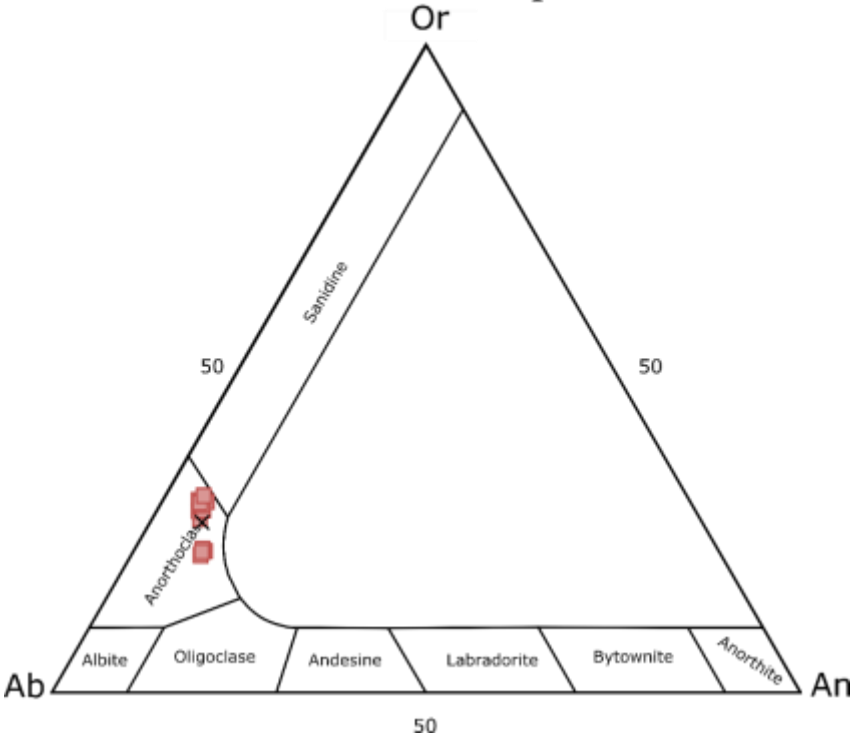

CB-18-03 Feldspar

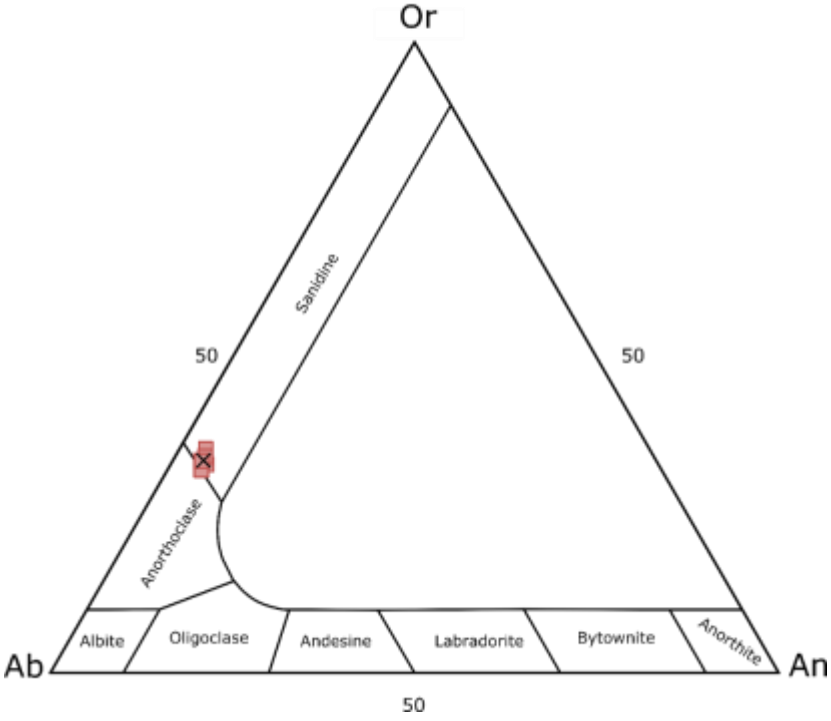

CB-19-37 Feldspar

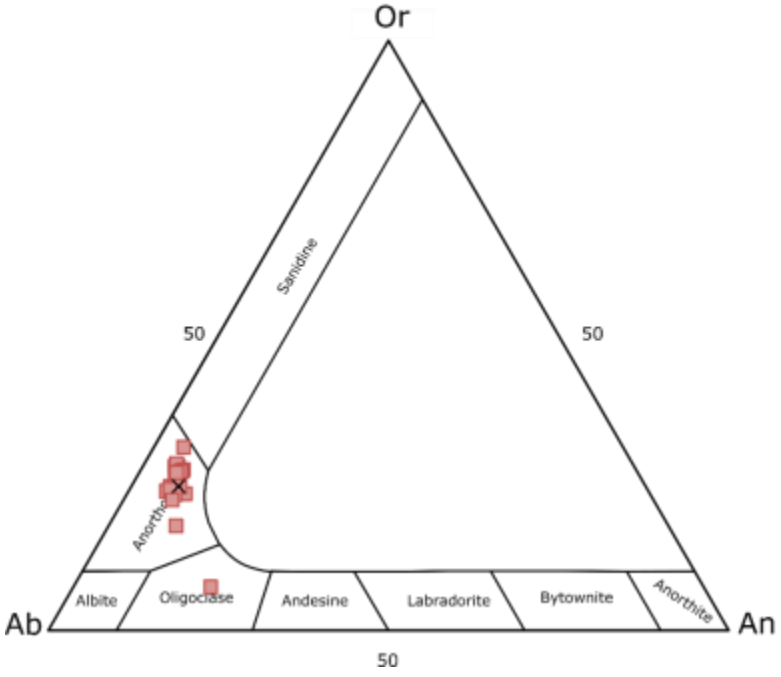

CB-19-44 Feldspar

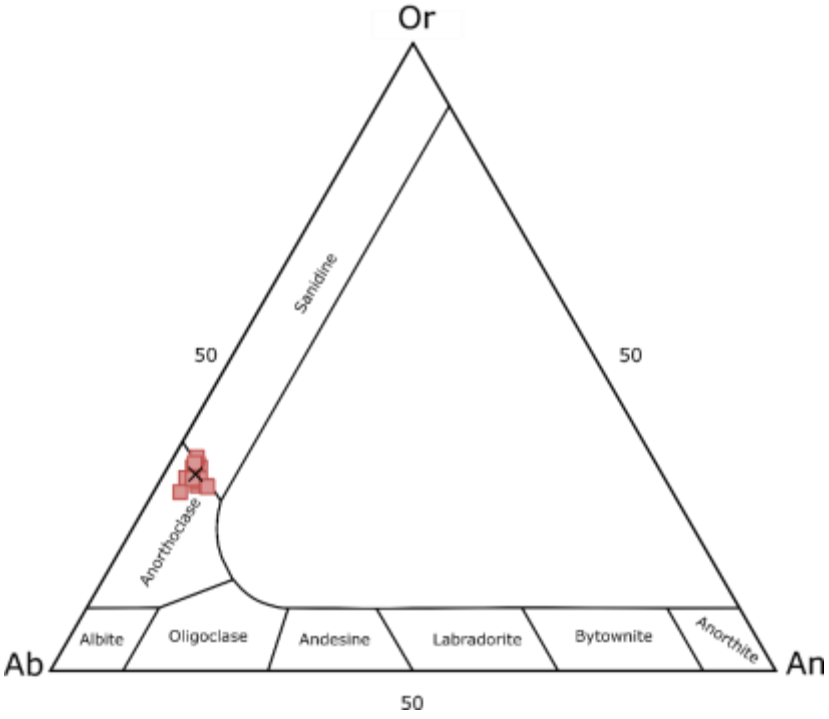

CB-19-65 Feldspar

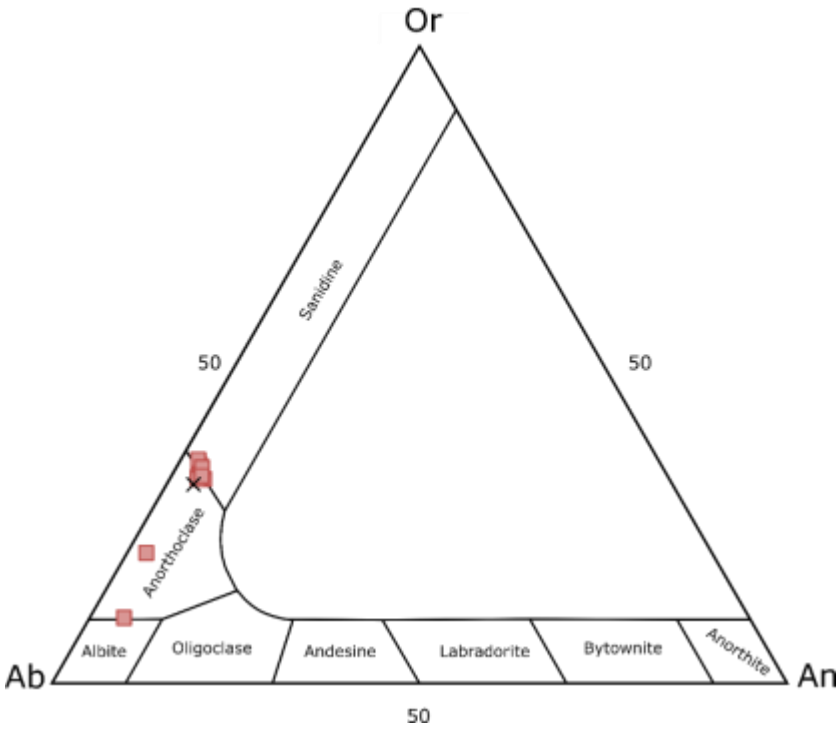

MS-10-6LGT Feldspar

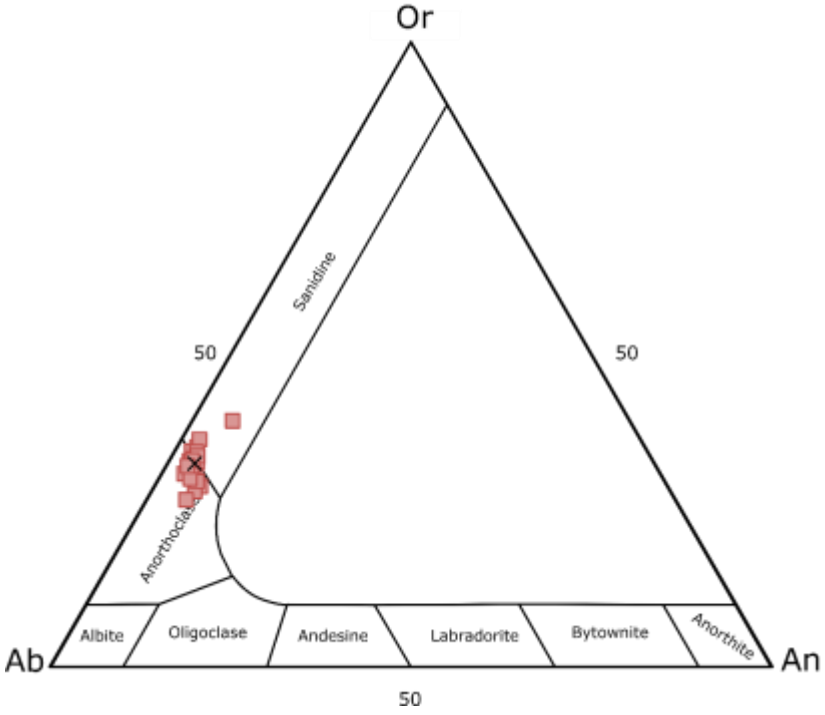

MS-10-15 Feldspar

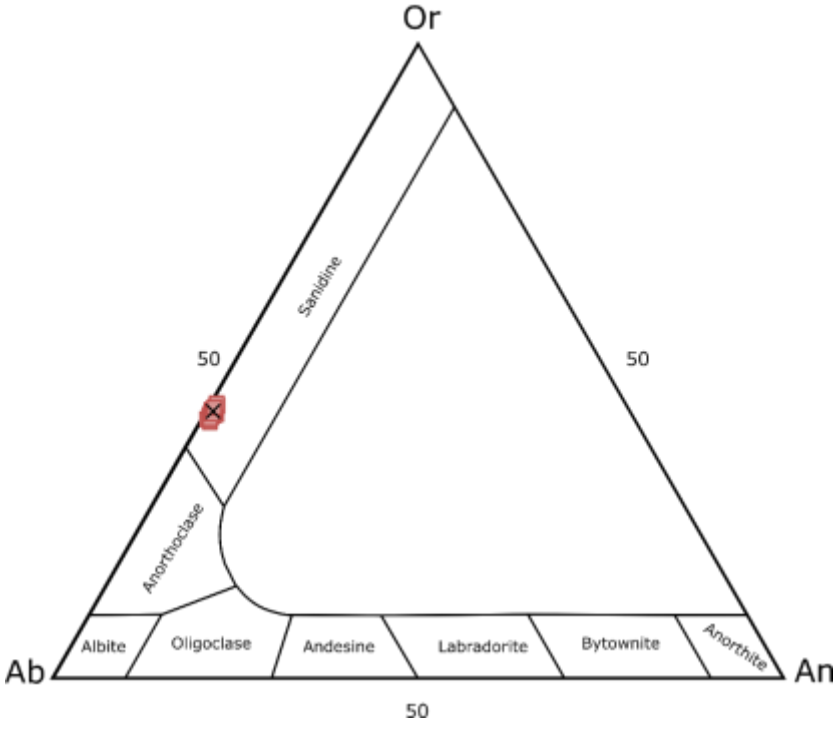

MS-11-15SCT Feldspar

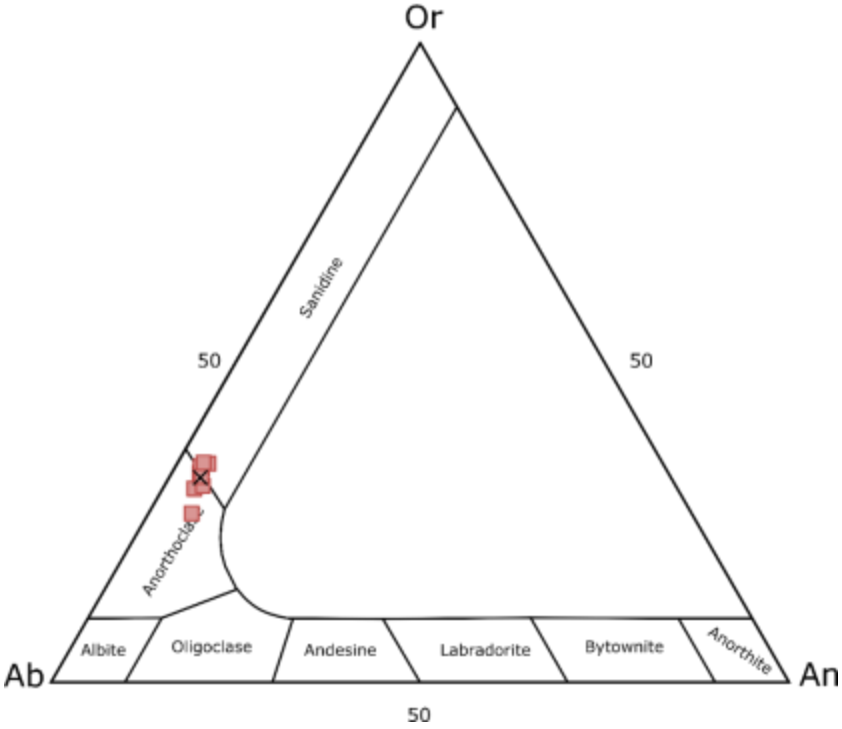

MS-11-17SCT Feldspar

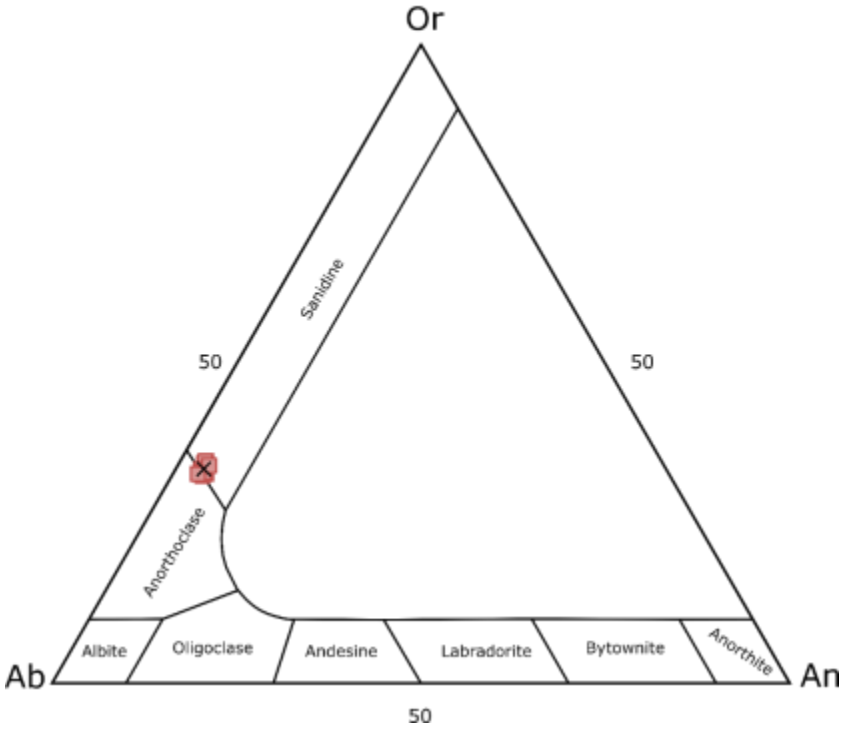

MS-12-39 Feldspar

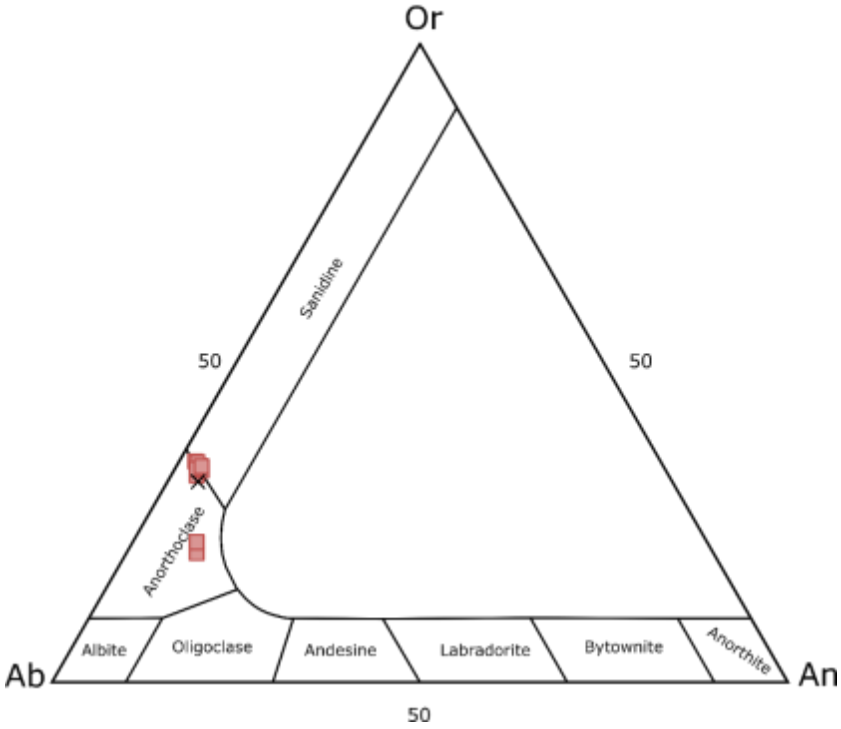

MS-12-39c Feldspar

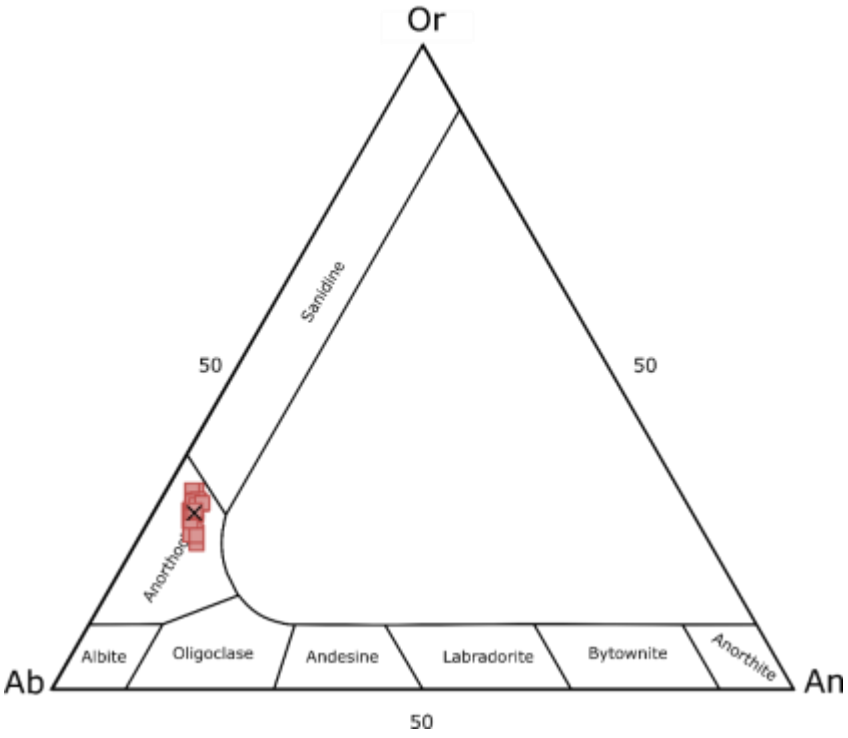

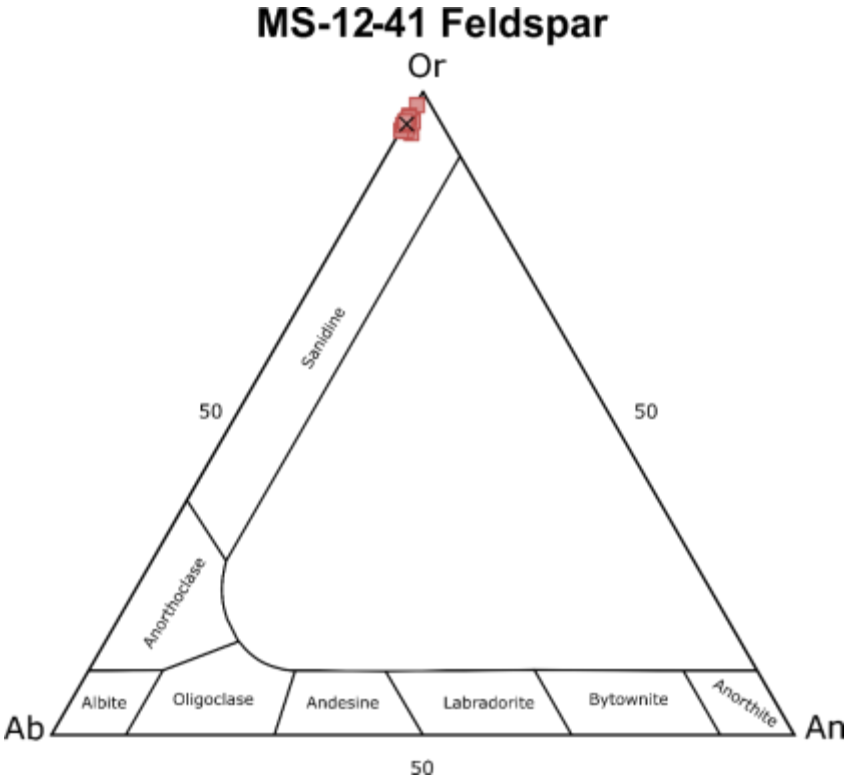
MS-12-41 Feldspar
Or
Sanidine
50
50
Anorthoclase
Albite
Oligoclase
Andesine
Labradorite
Bytownite
Anorthite
Ab
An
50

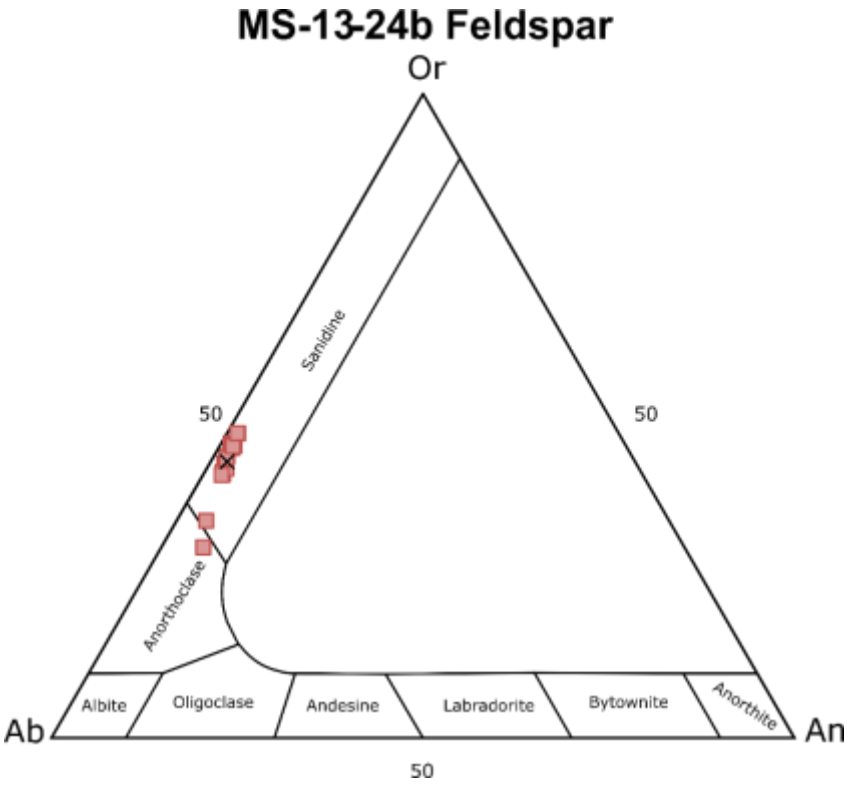
MS-13-24b Feldspar
Or
Sanidine
50
50
Anorthoclase
Albite
Oligoclase
Andesine
Labradorite
Bytownite
Anorthite
Ab
An
50

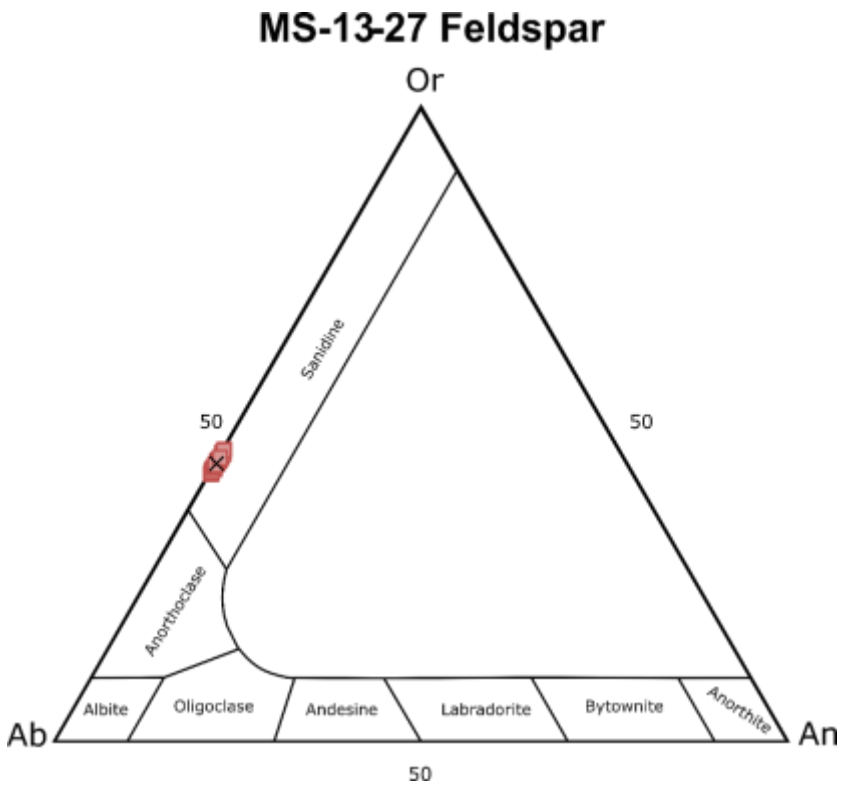
MS-13-27 Feldspar
Or
Sanidine
50
50
Anorthoclase
Albite
Oligoclase
Andesine
Labradorite
Bytownite
Anorthite
Ab
An
50

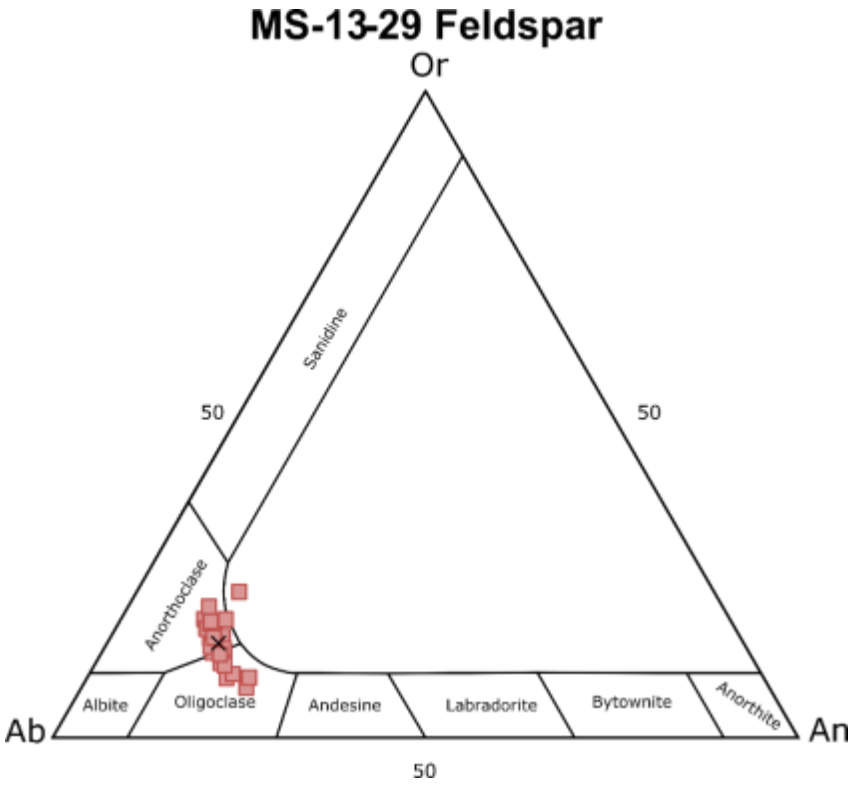
MS-13-29 Feldspar
Or
Sanidine
50
50
Anorthoclase
Albite
Oligoclase
Andesine
Labradorite
Bytownite
Anorthite
Ab
An
50

TF152EH Feldspar

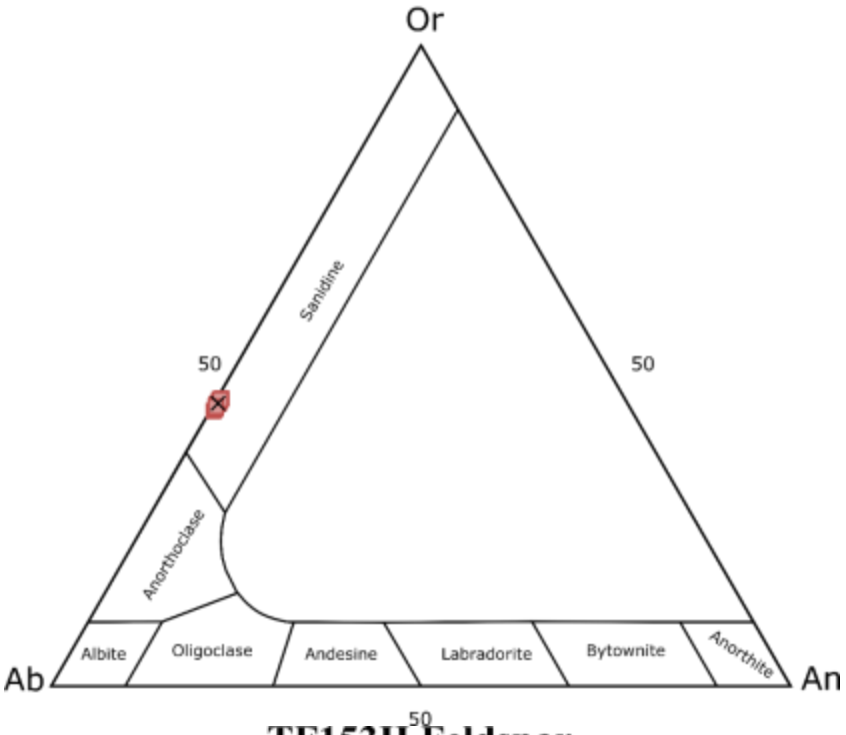

TF153H Feldspar

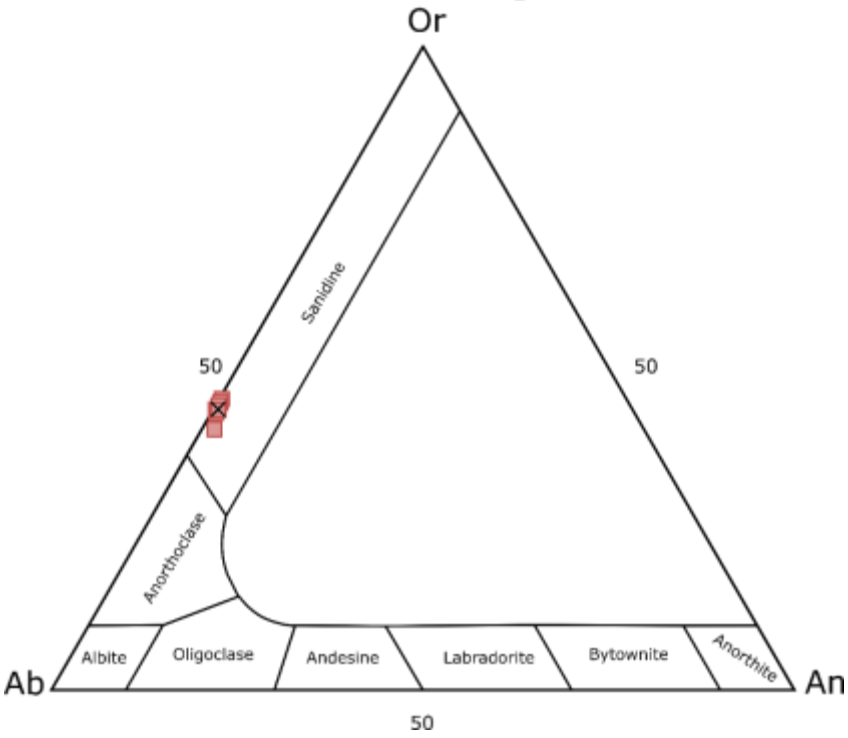

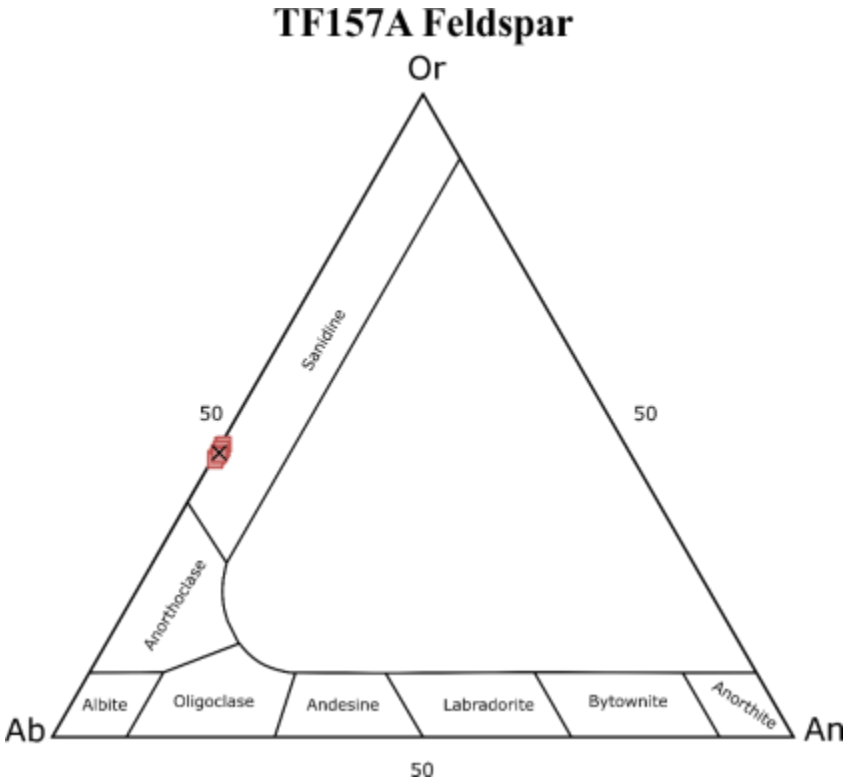
TF157A Feldspar
Or
Ab
An
50
50
50
Sanidine
Anorthoclase
Albite
Oligoclase
Andesine
Labradorite
Bytownite
Anorthite

Appendix E: Additional Pyroxene Plots

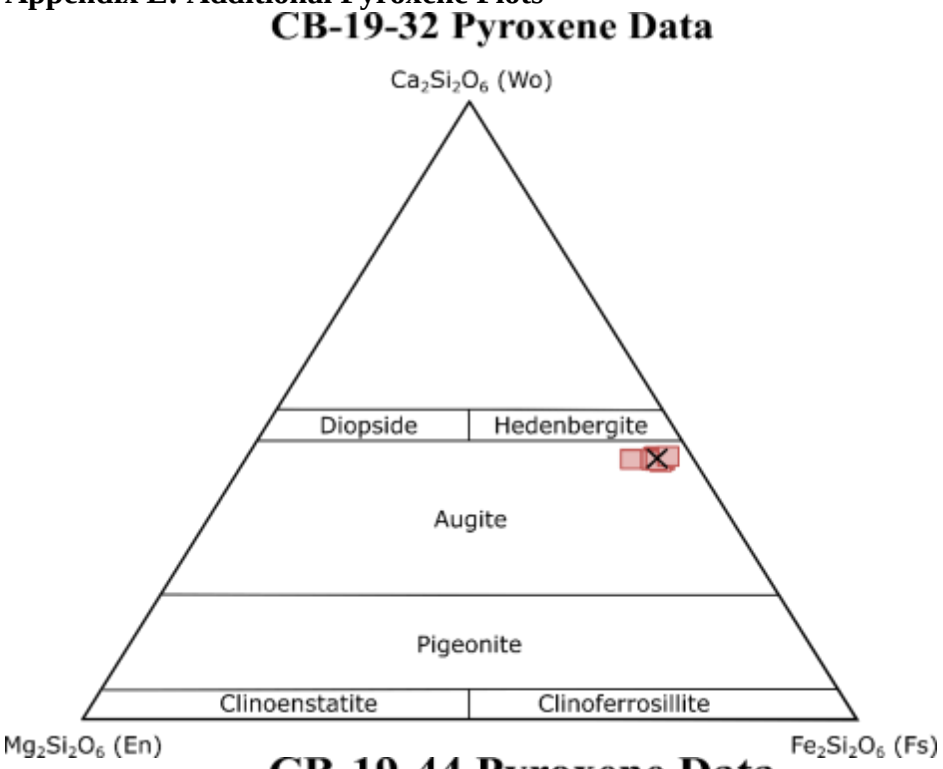

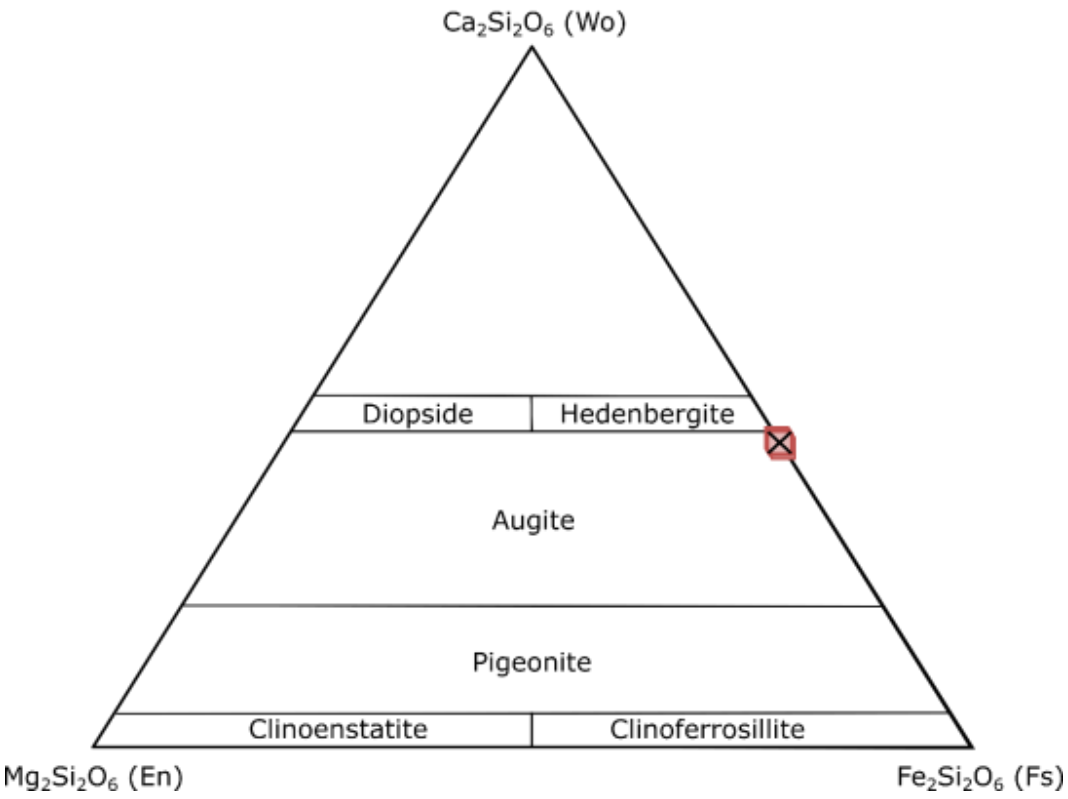

CB-19-65 Pyroxene Data

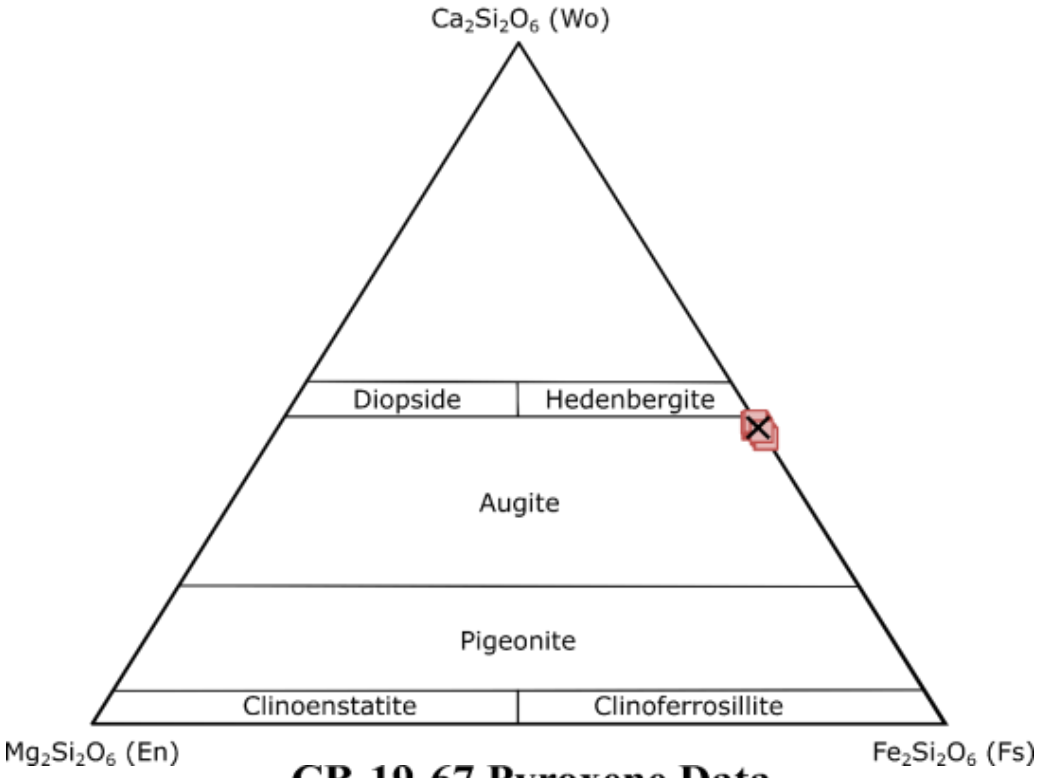

CB-19-67 Pyroxene Data

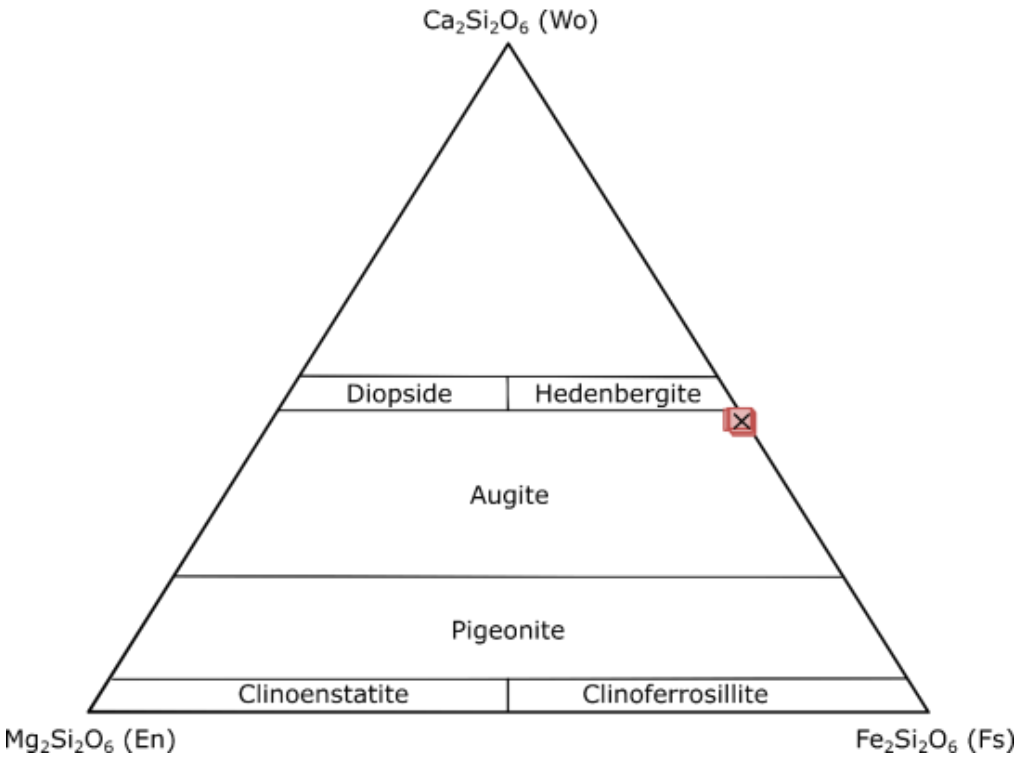

MS-11-15SCT Pyroxene Data

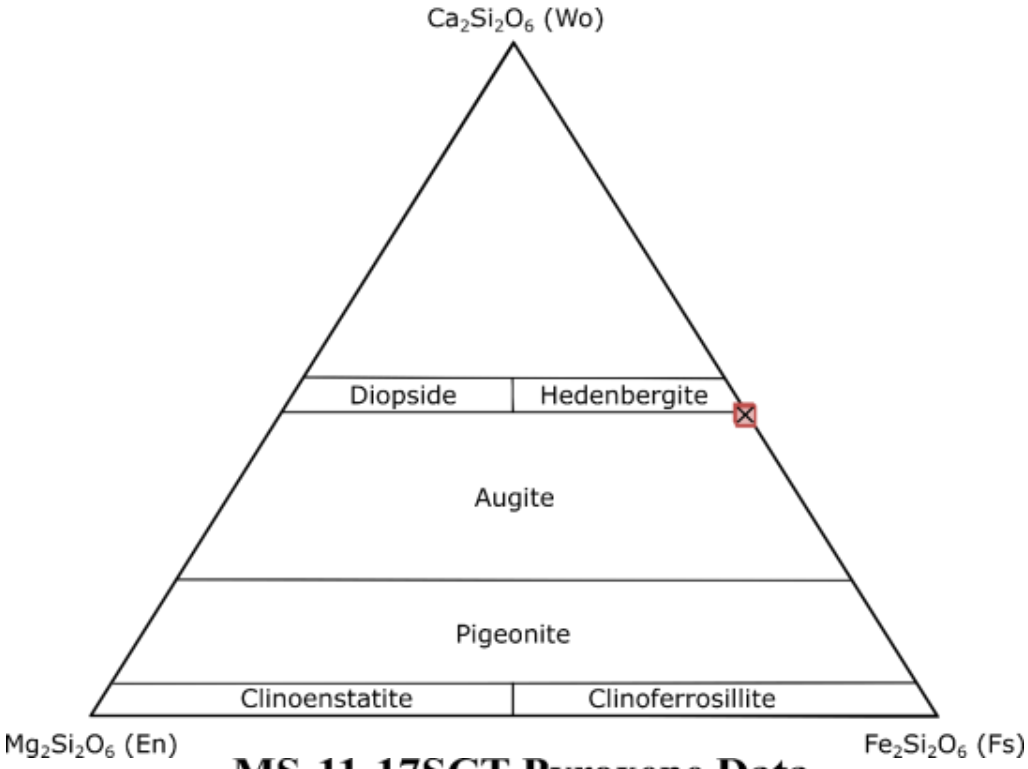

MS-11-17SCT Pyroxene Data

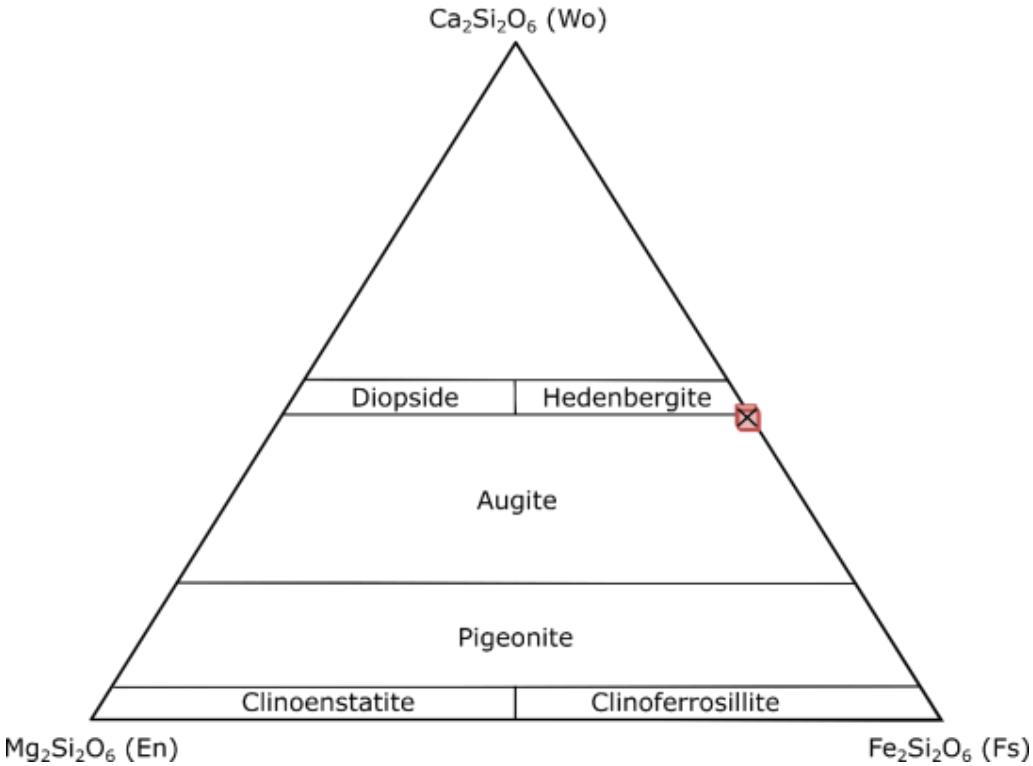

MS-13-24b Pyroxene Data

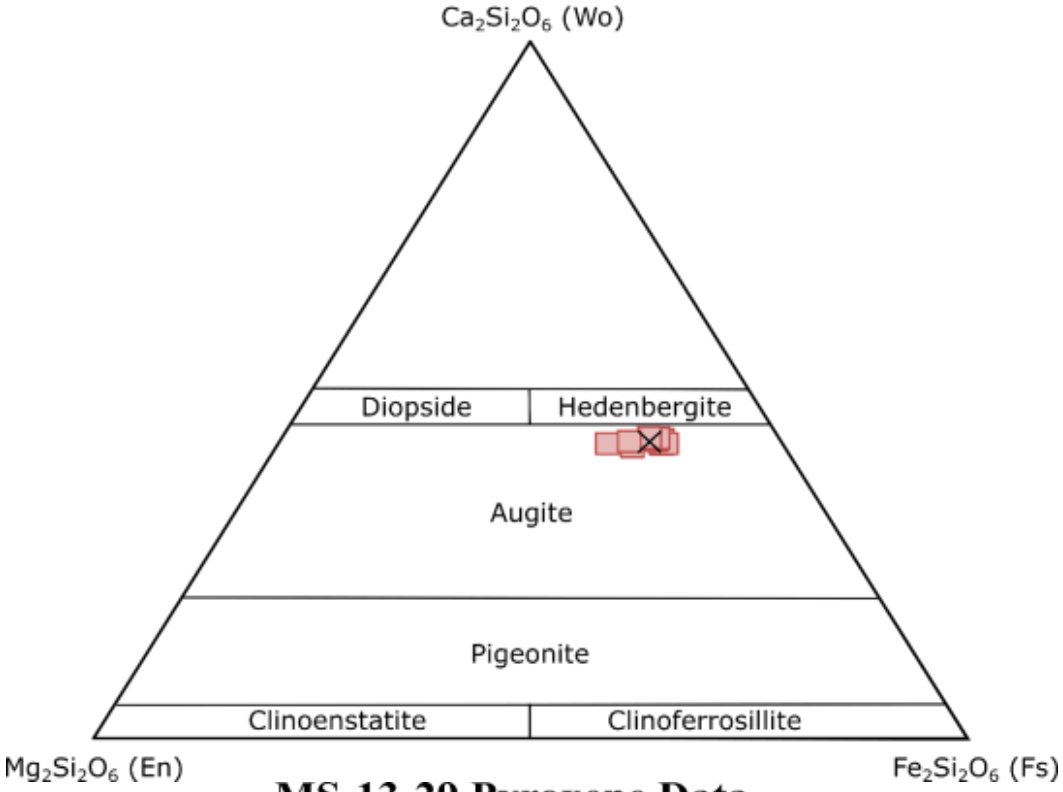

MS-13-29 Pyroxene Data

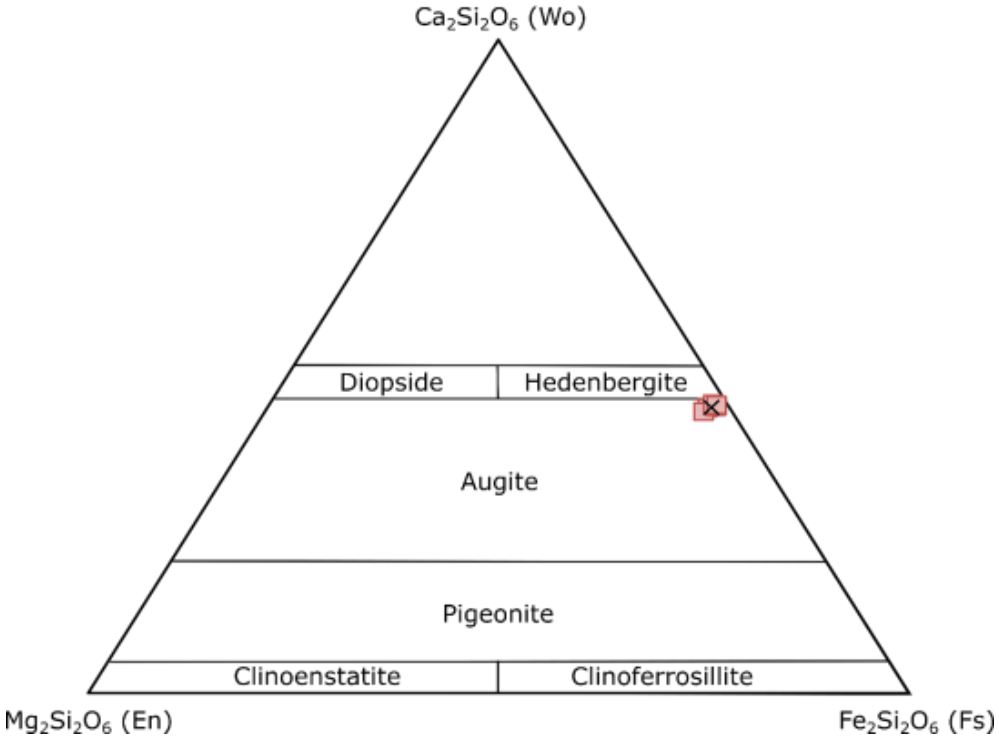

TF152EH Pyroxene Data

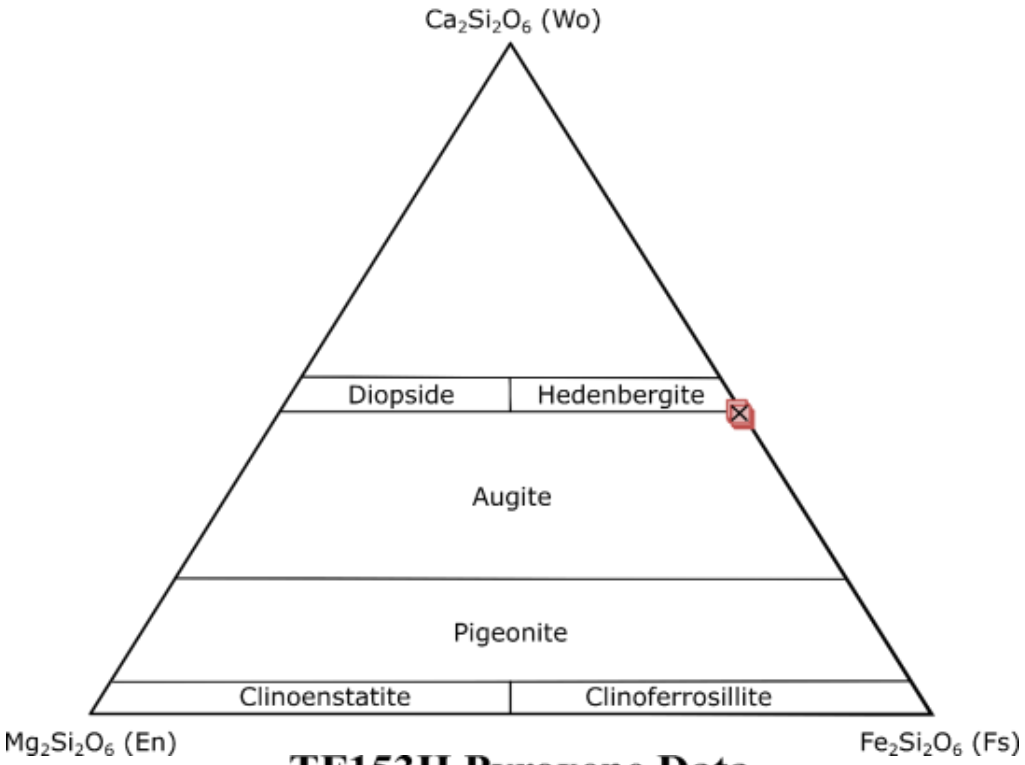

TF153H Pyroxene Data

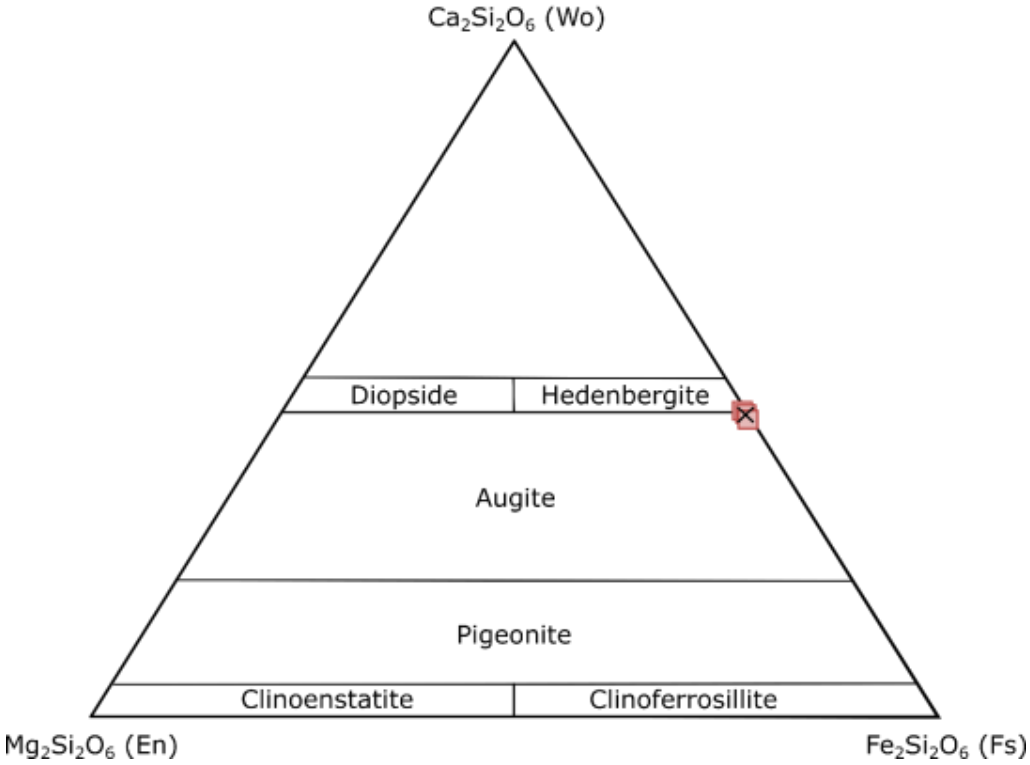

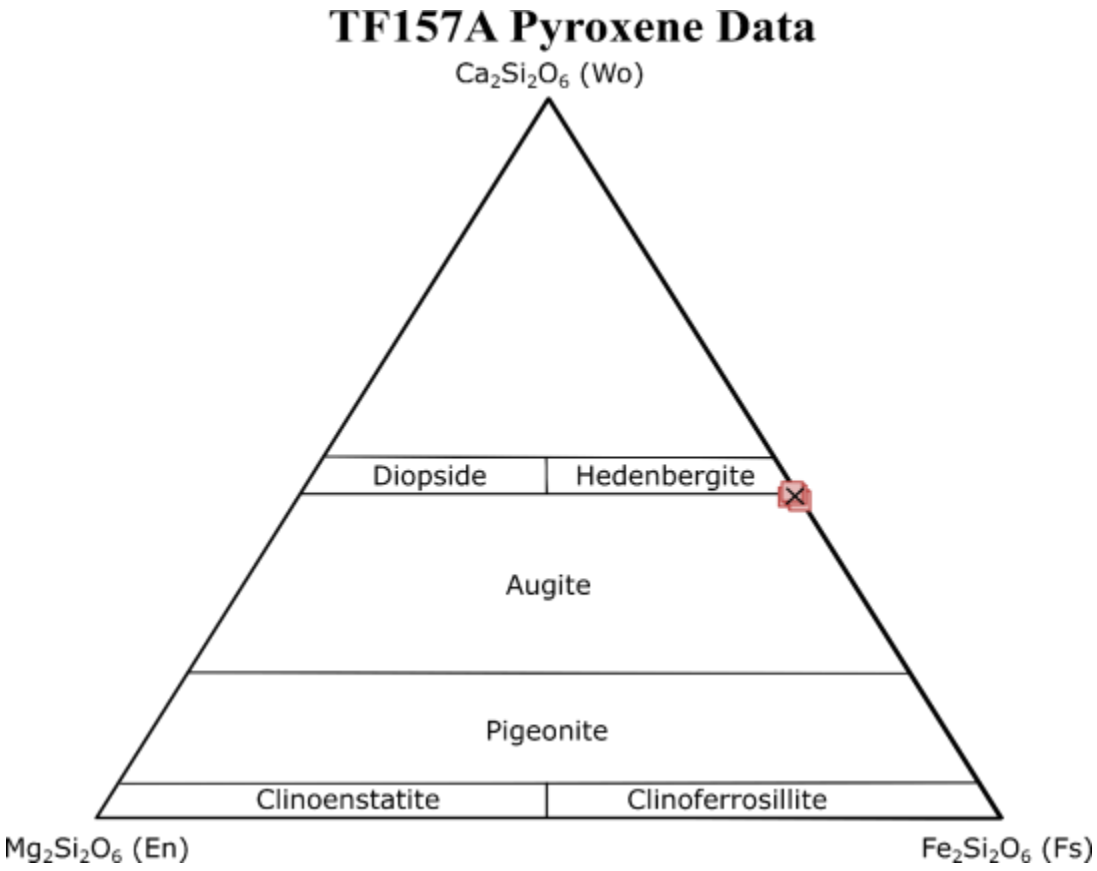
TF157A Pyroxene Data
$Ca_2Si_2O_6$ (Wo)
Diopside
Hedenbergite
Augite
Pigeonite
Clinoenstatite
Clinoferrosillite
$Mg_2Si_2O_6$ (En)
$Fe_2Si_2O_6$ (Fs)

Appendix F: Sample Location Map

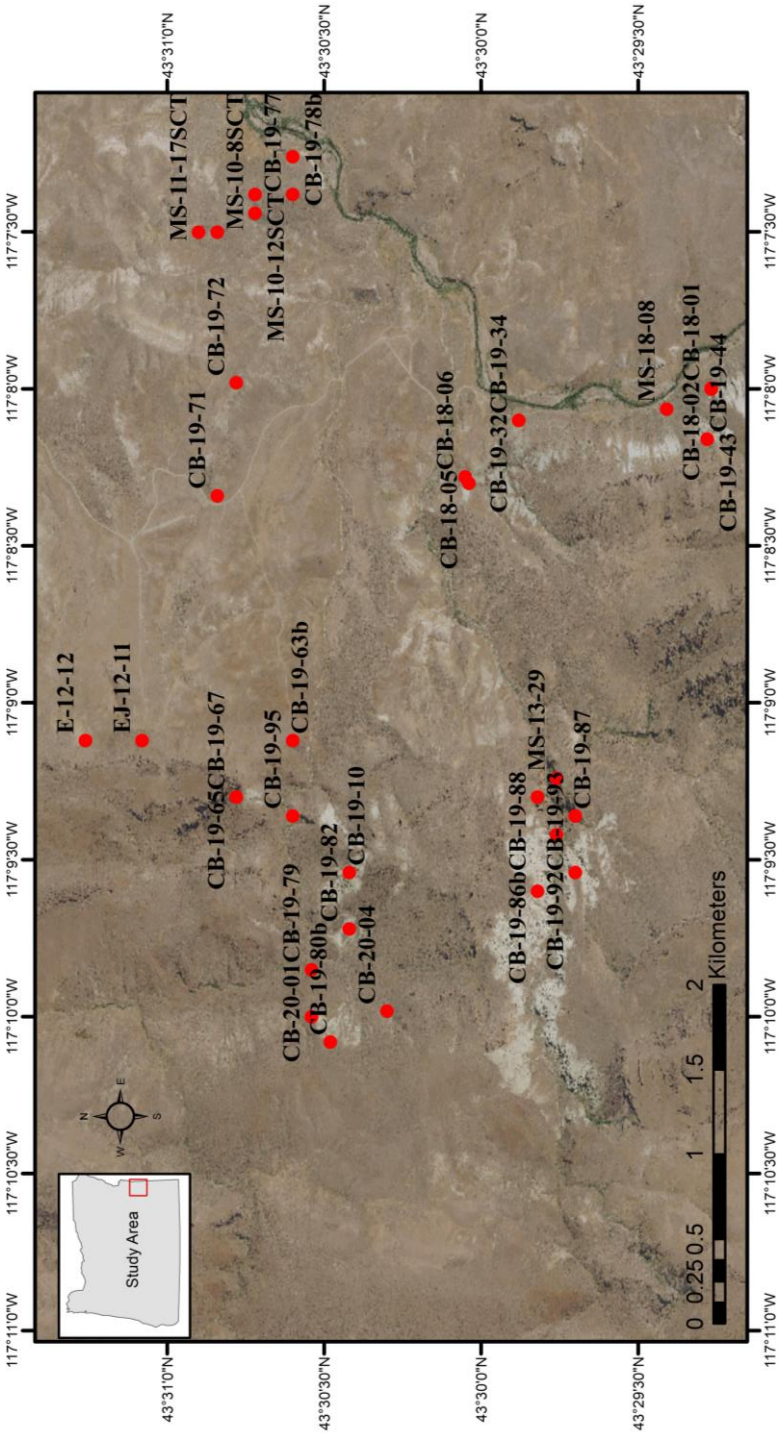

Figure 102. Study area sample locations.